universität wien

MAGISTERARBEIT

Titel der Magisterarbeit

Fluid-rock interaction in a low-angle normal fault

(Kythnos, Western Cyclades, Greece)

Verfasserin

Gabriele Laner, Bakk.

Angestrebter akademischer Grad

Magistra rerum naturalis (Mag.rer.nat)

Matrikel-Nummer: 0301890

Studienkennzahl lt. Studienblatt: A 066 815

Studienrichtung lt. Studienblatt: Erdwissenschaften

Betreuer: Univ. Prof. Mag. Dr. Bernhard Grasemann

Wien, Jänner 2009

ACKNOWLEDGEMENTS

First of all I want to thank my supervisor, Prof. Dr. Bernhard Grasemann for the possibility to do this work, his support and expertise and all the knowledge he got across to me.
A special thank also to my co-advisor, Dr. Mike Edwards, for all his help to get ready for the field trip, his support in the field and for helping me to arrange myself with the English language and for providing me with music!

Very sincere thanks to my friend and trusted colleague Iris Lenauer, who accompanied me since the first day of my studies. Thanks for all the fun we had, for the strong technical and emotional support and above all for sustaining my caprices and pessimism over all these years.

I also want to say great thanks to Christoph Iglseder for his help and motivation in the field as well as to the complete ACCEL-Team, especially to Dr. Kostas Petrakakis, Klaus Voit, Moni Müller and Andras Zamoly.
Furthermore I want to thank Dr. Hugh Rice for convincing me by his lecture to stop my studies of Biotechnology in order to switch to the Geology, thus preventing me from cloning mice.

A great thank goes to Dr. Martin Thöni for helping me with the analyses and interpretations concerning the radiogenic isotopes. Also a warm thank to Monika Horschinegg, who carried out all my Sr-analyses, for always finding time to explain and show me technical specifications.

Furthermore I would like to appreciate Dr. Dieter Mader, for his great help and patience to carry out hundreds of isotope analyses and for providing me with information and literature on stable isotopes. A special thank goes to Michel Bestmann for producing new ideas concerning stable isotopes.

In addition, I want to thank all members of the former Geochemistry Department, especially Dr. HH Weinke and Dr. Willfried Körner, who took care to me over the first years of my studies.

Really warm thanks go to my family for their unremitting support and help in every respect and for teaching me the truly important things of life. A special thank is due to my “little” sister Maria, always on the spot if all else fails and to my best friend Rita Trost, who really lives up to her´s name!

Finally: Thank you Richi!

CONTENTS

ABSTRACT

Fluid-rock interaction in a low-angle normal fault (Kythnos, Western Cyclades, Greece)

The island of Kythnos belongs to the western Cyclades of Greece. It is part of the Attic-Cycladic-Crystalline Complex which represents a polymetamorphic terrane. It was subjected to Eocene high-pressure-metamorphism under eclogite- to blueschist-facies conditions, overprinted by Oligocene-Miocene greenschist-facies metamorphism and shows evidence for several postmetamorphic brittle deformation events.

This work together with recent structural investigations show the existence of a hitherto unrecognised large-scale ductile-brittle shear zone in the southernmost part of Kythnos Island, which is probably due to Miocene extension in the Aegean region. The shear zone consists of two distinct horizons of extremely fine grained, calcitic marble ultramylonites and ultracataclasites. The main SW-dipping, rather low-angle normal fault, separates the Qtz-feldspar protocataclasites on top from the greenschist-marble unit below. Within the greenschist-facies rocks that build up the footwall of the shear zone, there are some lenses of metagabbros which show relicts of their original magmatic fabric. They form relative rigid blocks and are coated with Srp-Tlc-schists, positioned in the core of a km-scale recumbent fold.
Structural investigations show evidence for an earlier phase of tight to isoclinal folding with subhorizontal axial planes and a later upright folding with nearly vertical axial planes and also NNE-SSW striking fold axes. Our field observations show that mineral lineations and partly stretching lineations in all lithologies trend NE-SW. Ductile as well as all brittle/ductile shear sense indicators consistently show a top to SW directed movement. Due to ongoing extension, rocks were later on subjected to brittle high angle normal faulting and fracturing.

Cross cutting relationships, orientation and chemistry of conjugate brittle vein-systems allow us to separate four different generations of extension gashes filled with Cal, Qtz or iron minerals. Stable isotopes of carbon and oxygen, measured in the mylonitic marbles, the marble-ultramylonites of the shear zone and in the calcitic extension gashes, all give evidence of a strong interaction with fluids in the shear zone. Variation in isotope ratios allows us the discrimination of three deformation events and implies a transition from a ductile, closed system to an opened regime with infiltration of surface waters.
$^{87}Sr/^{86}Sr$-ratios of marbles and calcitic vein-fillings show quite dramatic fluctuations compared to current seawater data.

ZUSAMMENFASSUNG

Fluid-Gesteins-Interaktion im Bereich einer Low-Angle Abschiebung (Kythnos, Westliche Kykladen, Griechenland)

Die Insel Kythnos gehört zu den Westlichen Kykladen Griechenlands. Sie ist Teil des Attisch-Kykladischen Kristallinkomplexes, einem polymetamorphen Terrane. Die Gesteine von Kythnos unterlagen einer eozänen Hochdruck-Metamorphose unter Blauschiefer-faziellen Bedingungen und wurden im Oligozän-Miozän grünschiefer-faziell überprägt. Es gibt zudem auch Anzeichen für mehrere postmetamorphe spröde Deformationsereignisse.

Jüngste strukturelle Untersuchungen zeigten im südlichsten Bereich der Insel eine bisher noch unbekannte, große spröd-duktile Scherzone. Wahrscheinlich wurde diese aufgrund der Extension des Ägäischen Raumes im Miozän ausgebildet. Die Scherzone besteht aus zwei unterschiedlichen Horizonten von extrem feinkörnigen, kalzitischen Marmor-Ultramyloniten und Ultrakataklasisten. Die vorwiegend flach nach SW einfallende Scherzone trennt die Qtz-Feldspat-Protokataklasite im Hangenden von der Grünschiefer-Marmor Einheit im Liegenden. Innerhalb der Grünschiefer befinden sich einige Metagabbro-Linsen, die zum Teil noch Relikte ihrer ursprünglichen magmatischen Struktur aufweisen. Diese sind von Srp-Tlc-Schiefern umhüllt und bilden relativ rigide Blöcke im Zentrum einer großen Liegend-Falte. Untersuchungen im Gelände zeigten eine frühere Faltung mit subhorizontalen Axialebenen und einer späteren aufrechten Faltung mit nahezu vertikalen Axialebenen, beide mit NNE-SSW gerichtete Faltenachsen. Minerallineationen und Streckungslineare aller Lithologien streichen NE-SW. Sowohl duktile als auch spröd-duktile Schersinn-Indikatoren zeigen einheitlich Top-nach-SW gerichtete Bewegungen. Aufgrund anhaltender Extension im Ägäischen Raum kam es im Weiteren zur Ausbildung von relativ steilen, spröden Abschiebungen und zahlreichen Extensionsspalten.

Aufgrund von Überschneidungskriterien, der Orientierung und der chemischen Zusammensetzung von konjugierten, spröden Kluftsystemen konnten vier unterschiedliche Generationen von Extensionsspalten unterschieden werden. Die Analyse der stabilen Isotope von den verschiedenen Marmoren und Cal-gefüllten Extensionsspalten deutet auf eine starke Beeinflussung der Gesteine durch Fluide hin. Die Variation in den stabilen Isotopenverhältnissen ermöglicht grundsätzlich die Unterscheidung von drei Deformationsereignissen und zeigt den Übergang von einem geschlossenen, duktilen System zu einem relativ offenen, spröden Regime mit Infiltration von Oberflächenwässern.
Die Analyse der $^{87}Sr/^{86}Sr$-Verhältnisse in Marmoren und kalzitischen Spaltenfüllungen zeigt starke Schwankungen und deutliche Unterschiede zur derzeitigen Sr-Isotopie des Meerwassers.

INTRODUCTION

1.1. Aims of the diploma thesis

The aims of our field works on the island of Kythnos is the investigation of a hitherto unrecognised large-scale ductile-brittle shear zone in the southernmost part of the island to give us information about the geodynamic history in this region. Therefore detailed structural and lithological mapping in the field of this shear zone was required. This includes the macroscopic and microscopic characterization of the various lithologies and the generation of a lithostratigraphic chart as well as a detailed study of ductile, ductile-brittle and brittle deformation features. Building on the only existing geological map of Kythnos of De Smeth (1975), a new geological map of our research area in south Kythnos was generated.

In addition, analyses of crosscutting relationships and orientations of extension gashes together with stable isotope-ratios of oxygen and carbon of the mylonitic marbles and calcitic vein cements in the shear zone help to separate different generations of extension gashes and thus distinguish and discriminate brittle deformation events.

The analysis of the radiogenic isotopes of strontium of different marble units gives key information about age, impact of terrestric sediments and fluid-rock interactions.

1.2. Geographic overview

The Aegean Sea is an arm of the Mediterranean Sea in the southeast of Europe between Greece and Turkey. It is connected to the Black Sea through the Dardanelles Strait and the Marmara Sea by the Bosporus. The Aegean Sea includes numerous islands which are subdivided into seven groups (from north to south): the Northestern Aegean Islands, Sporades, Euboea, Argo-Saronic Islands, Cyclades, Dodecanese and Crete.

The Cyclades comprise about 220 islands. Most of the smaller ones are not inhabited. The climate is of Mediterranean type with dry and hot summers but mild and wet winters. The soils are not very fertile so vegetation is rather sparse.

Figure 1: Geographic overview of Greece and Aegean Sea with Kythnos Island marked in red (source: http://www.lib.utexas.edu/maps/europe/greece_rel96.jpg).

Kythnos is a small island in the Western Cyclades between Kea in the North and Serifos in the south. Its geographic coordinates are 37°23N24°25E. The island has a length of about 17 km and reaches a maximum width of 8 km. Its area is roughly 100 km^2. In the northern part of Kythnos there are two topographic ridges. One in the east with Profitas Ilias (336 m) and the other along the western coast with Petra (297 m) and Kakavolo (355 m). To the south of the village of Driopis a third mountain chain strikes NNE-SSW and reaches a maximum hight of 317 m (Carl, 1993). Kythnos has about 1500 permanent inhabitants. First colonizations can be traced back to the 8th millenium B.C., which is the oldest known inhabitation in the Cycladic islands (www.kythnos.gr).

Figure 2: Schematic map of Kythnos Island (source: www.sailingissues.com)

1.3. The ACCEL project

The project ACCEL (Aegean Core Complexes along an Extended Lithosphere) was granted in 2005 by the FWF, the Austrian Science Foundation. The principal investigators are Bernhard Grasemann and Konstantin Petrakakis. The aim of this project is the geodynamic investigation of the Western Cyclades, focussing on the islands of Kea, Kythnos and Serifos. Various disciplines of geoscienes undertaken by the Structural Processes Group and the Department of Lithospheric Research of the University of Vienna as well as by some international collaboration should provide a comprehensive West Cycladic database. Together with the body of acquired knowledge on the Eastern Cyclades, this should help to explain the geodynamic history of the Aegean region.

1.4. Previous geological works

Concerning geology, the island of Kythnos has not achieved much attention in the past. The first island wide mapping was carried out by De Smeth, resulting in the geological map of Kythnos Island, published in 1975 by the Greek National Institute of Geological and Mineral Researches. In 1993, in the course of two diploma theses, a detailed petrographic description of northern and southern parts of the island was conducted by Carl (1993) and Bartsch (1993). One year later Schliestedt et al. (1994) described the P-T-path of the greenshist-facies rocks of Kythnos Island. Chrysanthaki and Baltatzis (2003) concentrated on the geochemical composition of Fe-Mn-metasediments from the Panagia Kanala and Episkopi area. Finally the structural evolution of Kythnos Island was investigated by Keiter et al. (2008).
Results of scientific investigation on Kythnos, carried out by the ACCEL Team of the University of Vienna, were presented in the year 2008 with the following posters:

G. Mörtl, B. Grasemann, I. Lenauer, M. Edwards, C. Iglseder, M. Thöni, D. Mader (2008): Fluid-rock interaction in a low-angle-normal fault (Kythnos, Western Cyclades, Greece).- Geophysical Research Abstracts, Vol. 10, EGU2008-A-04585.

I. Lenauer, G. Mörtl, C. Iglseder, B. Grasemann, M. Edwards (2008): Field evidence for a major normal fault on Kythnos Island (Western Cyclades, Greece).- Geophysical Research Abstracts, Vol. 10, EGU2008-A-03218.

I. Lenauer, G. Mörtl, B. Grasemann and C. Iglseder (2008): Structural investigations along a low-angle-normal fault zone (Kythnos, Greece). YORSGET 2008, Oviedo, Spain.

2. GEOLOGICAL OVERVIEW OF GREECE AND THE EASTERN MEDITERRANEAN

For a better understanding of the geology and geodynamics of Kythnos Island and the whole Aegean region, I want to give a short geological overview of Greece and the Eastern Mediterranean at the beginnging. Information was taken from Aubouin (1959), Dürr et al. (1978), Dermitzakis (1984), Jacobshagen (1986), Ring et al. (1999), Piper & Pe-Piper (2002), Iglseder (2005), Rambousek (2007), Voit (2008).
In the following, rock-forming minerals are termed by symbols according to Kretz (1983).

2.1. Geologic overview of Greece

The Hellenide orogen covers the major part of Greece. It is part of the Alpine-Himalaya-belt and forms an arc ranging from the Balkan Peninsula over the Greek mainland and the Aegean Sea to Southwest Anatolia. The present structure of the Hellenides was caused by four orogenic cycles (Jacobshagen, 1986):

a) The *Cimmerian cycle*, with its maximum during Dogger, was limited to the inner parts of the Varda Zone and the Circum-Rhodope Belt.
b) The *Eohellenic stage* from late Jurassic to early Cretaceous was caused by the closing of the Almopias Ocean in the Varda Zone due to subduction beneath the Paikon island arc in the East along with the deformation of the Circum-Rhodope Belt. Furthermore, parts of the Pindos Ocean were subjected to a relative westward subduction under the spreading ridge. These sections were later obducted in the region of the Pelagonian margin and thus build up the ophiolitic Eohellenic nappe (Piper & Pe-Piper, 2002).
c) The *Mesohellenic cycle,* with its culmination in the Eocene, resulted from the re-widening of the Pindos Ocean associated with sea floor spreading in the Cretaceous and the contemporaneous building of oceanic crust by pull-apart basins in the Varda zone. These processes end, after the consumption of the Varda and Pindos Ocean, with the collision of continental fragments of Apulia and Pelagonia and the Rhodope Massif (Piper & Pe-Piper, 2002). The metamorphic blueshist-complexes, ranging from Thessaly to the Cyclades, arose from this collision. They underwent high-temperature metamorphism during exhumation in the early Miocene.
d) During the *Neohellenic phase*, from late Oligocene to early Miocene, mainly the external Hellenides were affected by shortening.

2.2. Tectono-metamorphic and Tectono-stratigraphic units of Greece

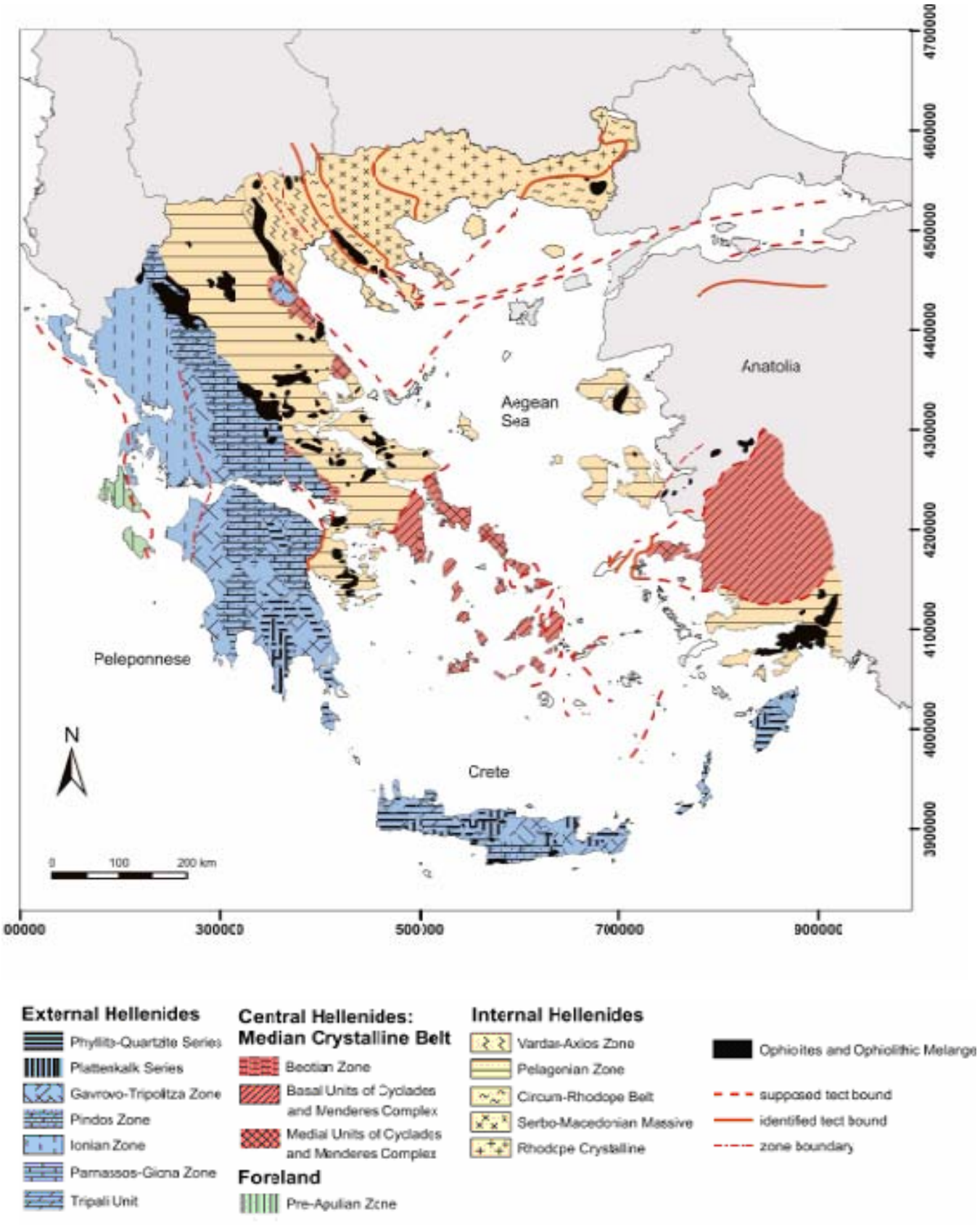

Figure 3: Geological map of Greece (Voit, 2008 after Jacobshagen, 1986)

The Hellenides are built up by a complex nappe pile. The usual classification into tectono-stratigraphic zones (isopic zones) was replaced by a tectonic subdivision based on nappe sequences (Jacobshagen, 1986). The reason for this new concept was the complex napping and the large thrust displacement to the north.
According to Jacobshagen (1986), the Hellenide orogen consists of three main units with the Extern Hellenides in the west, the Central Hellenides and the Internal Hellenides to the east. A similar classification was made by Aubouin (1959).
The foreland, however, which is build up by the Pre-Apulian Zone is not included into this scheme.

2.2.1. The Pre-Apulian Zone

The Pre-Apulian Zone (Aubouin 1959), is limited to only some areas at the western coast of Greece. These are the islands of Paxos und Anti-Paxos, the headland of southwest Lefkas and major parts of Kefallinia and Zakinthos (Jacobshagen 1986). It is interpreted as eastern margin of the Apulian plate and thus the foreland of Hellenide orogen. It consists of basically unmetamorphosed mesozoic marine carbonates which are overlain by neogene, also marine, clastic sediments.

2.2.2. The Extern Hellenides

The Extern Hellenides consist of the Phyllite-Quartzite series, the Plattenkalk series, the Ionian and Gavrovo-Tripolitza zone, the Pindos zone, the Tripali unit and the Pamassos-Giona zone (Figure 3)
The Plattenkalk series is found on the Peloponnesus, Crete and the Dodecanese (Astypalea, Karpatho, and Rhodos (Dermitzakis, 1984). It is built of a series of shale and sandstones alternating with dolomites at the base which are overlain by a thick marble sequence. To the top the marbles partially alter with quartzitic layers and are covered, finally, by meta-flysch-sediments (Plattenkalkflysch).
The Phyllite-Quartzite series, which overthrusts the Plattenkalk unit, is mainly built of phyllites, micaschists, quartzites and meta-conglomerates which were subjected to high-pressure metamorphism during the Lower Miocene.
The sediments of the Ionian zone were deposited in a subsiding trough with Triassic breccias and evaporites at the base and, due to subsequent deepening, neritic limestone and dolomites followed by black shales, platy limestone and cherts, ending with pelagic limestones and carbonate breccias.
The Gavrovo-Tripolitza zone, however, represents a carbonate platform and comprises metaclastits, carbonate rocks, evaporites and metavolcanics.

The Pindos unit was deposited in a deep basin and thus consists, from substratum to top, of shales and sandstones, platy limestones with cherts, a Radioloarite formation, connected with pillow lavas and tuffs, and a platy limestone formation.
The Pamassos-Giona unit is mainly built of sediments of a subsiding basin. It comprises oolithic limestones alternating with bauxite horizons, sand- and mudstones (Dermitzakis, 1984; Jacobshagen, 1986).

2.2.3. The Central Hellenides

The Central Hellenides are built of the Beotian zone, the Attic-Cycladic Crystalline and tectonic the windows at Olympos, Ossa and Almyrapotamos.

The Beotian zone is exposed discontinuously from northern Greece to the Arolis peninsula of the Pellopennesus. This clastic formation, the so-called Beotian flysch, is composed of pelites, limestone intercalations, sandstones and conglomerates from the more eastern regions (Dermitzakis, 1984).
The Attic-Cycladic Complex is an alpidic complex which is composed of numerous tectonic units, mainly of Mesosoic age, which only appear in fragments. The Crystalline Complex is located underneath the non-metamorphic Pelagonian nappes in south-eastern Euboea and Attica and extends toward east over the Cycladic archipelago through the western part of the Menderes Complex to Anatolia. The complex is a result of the continent-continent collision during the Mesohellenic orogenesis caused by the convergence of the African and the Eurasian plate (Jacobshagen, 1986).
The Attic-Cycladic complex is subdivided into the Basal Units, the Intermediate Units, the Upper and Uppermost Units, the Ophiolites and the Mesohellenic molasse (Jacobshagen, 1986).

The *Basal Units* expose pre-alpine continental basement (M0) on Ios, Sikinos and Naxos. These rocks consist of metasediments and orthogneisses and can be well compared with the core of the Menderes Complex in the southwest of Anatolia. Thick Cycladic marble formations with metabauxite horizons overlay the basement rocks and presumably represent a carbonate platform with sequences from Upper Triassic to Cretaceous. The Basal Units can be found within the Menders Massiv, the Central Cyclades and the Central Aegean region. The rocks show evidence for a high P/T-metamorphism which can be related to late Eocene (M1) and Miocene granitic intrusions (M2) with the formation of migmatites and contact-aureoles (Dürr et al., 1978).

The *Intermediate Units* superpose the Basal Units. They consist of thinner marbles, manganese bearing metapelites, metavolcanics and metasediments of flysch and wildflysch character. Metamorphic slices of ophiolites show the imprint of Eocene high-pressure metamorphism (M1). The high-pressure rocks (blueshists) of the Intermediate Units were overprinted by greenschist-

facies metamorphism (M2) due to exhumation in the late Oligocene to Miocene. This was caused by large extensions of the Aegean crust and the formation of metamorphic core complexes.

The rocks of the *Upper Units* are unaffected, or only little affected, by metamorphism in the Eocene. They separate the non-metamorphic Pelagonian units in the west from the highly metamorphic rocks of the Attic Cycladic Complex in the east. Thereby they form the hanging wall of the metamorphic core complexes in the Cyclades. On top of the Central Cyclades, relicts of the Uppermost Units can be found (e.g. on Mykonos, Naxos and Erimonisia). They are not affected by Tertiary metamorphism.
Ophiolites are exposed on Paros, Naxos and Erimonisia. The detritus from these and similar Pelagonian and Eohellenic units makes up the conglomerates and sandstones of the *Mesohellenic molasse* (Jacobshagen, 1986).

Pan-Aegean stretching and exhumation of the crust were accompanied by the intrusion of I-type granitoides and contact-metamorphism (M3) from Middle to Late Miocene. Since the volcanic arc-formation, accompanied by volcanic and subvolcanic activity (e.g. Santorini), further alteration of rocks was caused by fluids (M4).

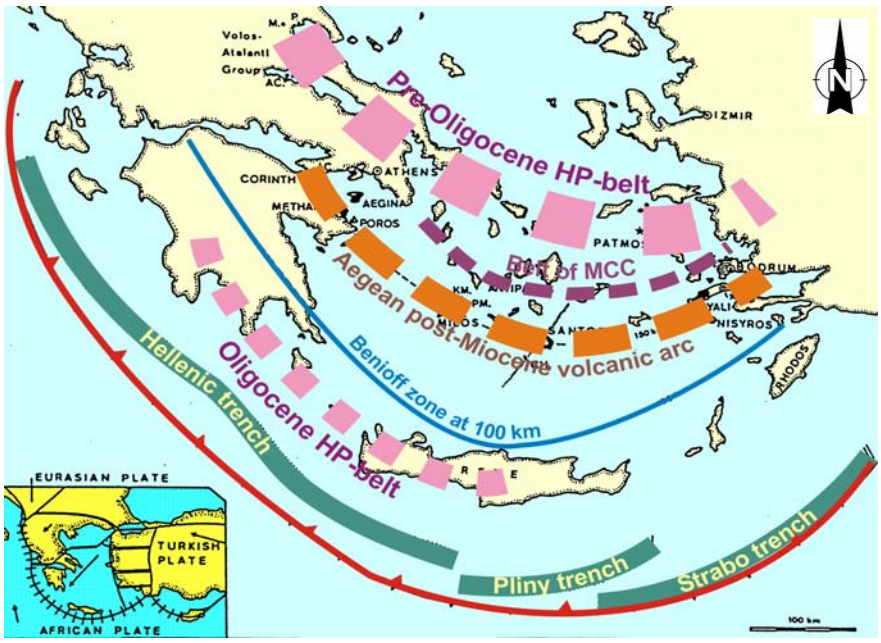

Figure 4: Geological settings in the Aegean Sea (Ring et al. 1999)

2.2.4. The Internal Hellenides

The Internal Hellenides comprise the Vardar-Axios Zone, the Pelagonian Zone, the Circum-Rhodope Belt, the Serbo-Macedonian Massive and the Rhodope Crystalline.

The *Vardar-Axios Zone* is a highly complex geotectonic unit between the Serbo-Mecedonian massif and the Pelagonian Zone. According to paleography and structural characteristics, five subunits can be established: the Almopias, Paikon and Guevguelije unit, the Stip-Axios massif and the Circum Rhodope Belt.
The development of the Vardar Zone started in the Permian with the formation of a proto-Vardar furrow at the western margin of the Serbo-Macedonian Massif. Further openings during the Lower and Middle Jurassic produce oceanic crust. In the Upper Jurassic, this furrow was closed and incorporated into the Serbo-Macedonian continental slab. A new continental margin was formed west of the Guevguelije and Paikon units. In the Almopias unit, new oceanic crust was built which was then, during the Lower Cretaceous, obducted onto the Pelagonian foreland. In the Upper Maestrichtian, a continental flysch trough was formed in the region of the Almopias, Paikon and Pelagonian units (Jacobshagen, 1986).

The metamorphic area of north-eastern Greece can be divided into two parts which are built up by Palaeozoic or Precambrian series. This is the Serbo-Macedoninan Massif in the West and the Rila-Rhodope-Massif in the East. The *Serbo-Macedonian Massif*, located on the central Balkan Peninsula, bears two different metamorphic sequences. A lower series of Bt-gneiss, lenses of amphibolite and marble and an upper series of micagneiss, micaschist, amphibolite, metagabbro and ophiolite. This – altogether - Precambrian crystalline basement is covered by Mesozoic sediments and penetrated by Mesozoic granitoid intrusions. Towards the east it is overthrust onto the Rila-Rhodope Massif.
The ca. E-W striking *Rhodope-Crystalline* is located in the north of Greece along the border to Bulgaria. It consists of gneisses, schists, amphibolites and marbles.

The *Circum–Rhodope Belt* surrounds the Serbo-Macedonian and the Rila-Rhodope Massif in the south. The western part of this belt can be attributed to the Vardar Zone. The eastern parts, around Thrakia, are built up by greenschists, conglomerates, sandstones, slates and limestones.

3. TECTONICS AND GEODYNAMICS OF GREECE

3.1. Geodynamic evolution during Neogene and Quarternary

The last orogenic imprint occurred during the Cenozoic, in which the last rock deformation took place in the Internal Hellenides in Eocene and final folding in the External Hellenides in Lower Miocene. These periods were followed by the uplift of mountain ranges and the subsidence of basins. Beside eustatic changes, the interplay of uplifting and subsidence, erosion and sedimentation caused a tectonic fragmentation of the Aegean region and thus rapid changes in paleogeography (Jacobshagen, 1986). The major transverse fault zones of the Hellenides originated in the Cenozoic, probably due to the bending of the Hellenic arc. In general the neotectonic deformation of the Upper Cenozoic period is affected by extension over the whole Aegean region, which is caused, according to Jacobshagen (1986), by a South Aegean "mantle dome". Compressional regimes are limited to the submarine Eastern Mediterranean ridge and some external islands.

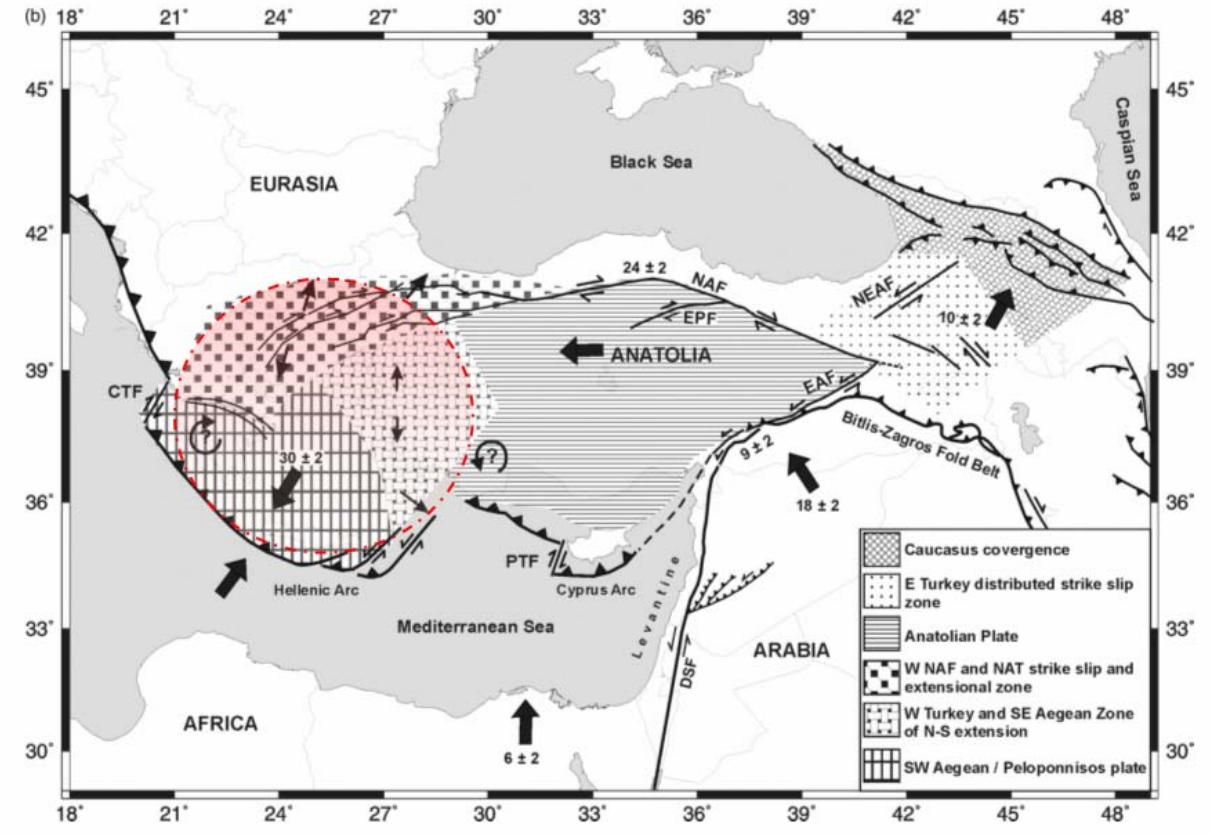

Figure 5: Schematic map of the principal tectonic settings in the Eastern Mediterranean. Hatching shows areas of coherent motion and zones of distributed deformation. Large arrows designate generalized regional motion (in mm/a) from Taymaz et al. (2007) modified after McClusky et al. (2000 and 2003). Area marked in red shows extensional regime in the Aegean region.

The Aegean region consists of four tectonic plates. These are Eurasia in the north, Africa in the southwest and Arabia and Anatolia in the east. In figure 5 the relative motions of plates and along their boundaries in the Eastern Mediterranean are shown. The African plate moves about 6±2 mm/a towards north relative to fixed Eurasia, where it is subducted beneath the European plate. This convergence of the African and European mega-plates basically caused the formation of the Hellenides during the Mesozoic and Cenozoic period. In the southeast, the Arabian plate is partitioned from the African plate by rifting along the Red Sea and the Dead Sea Fault (DSF). The Arabian plate is moving 18±2 mm/a to the northwest. This is reciprocated by the westward extrusion of Anatolia along the North Anatolian Fault (NAF) and East Anatolian Fault (EAF) and leads to a convergence among NW-Greece and Apulia. Meanwhile southward movement of the Aegean region with a velocity of 30±2 mm/a (McClusky et al., 2000, 2003) means that altogether the Aegean is dominated by local E-W-shortening and widespread N-S-directed extension.

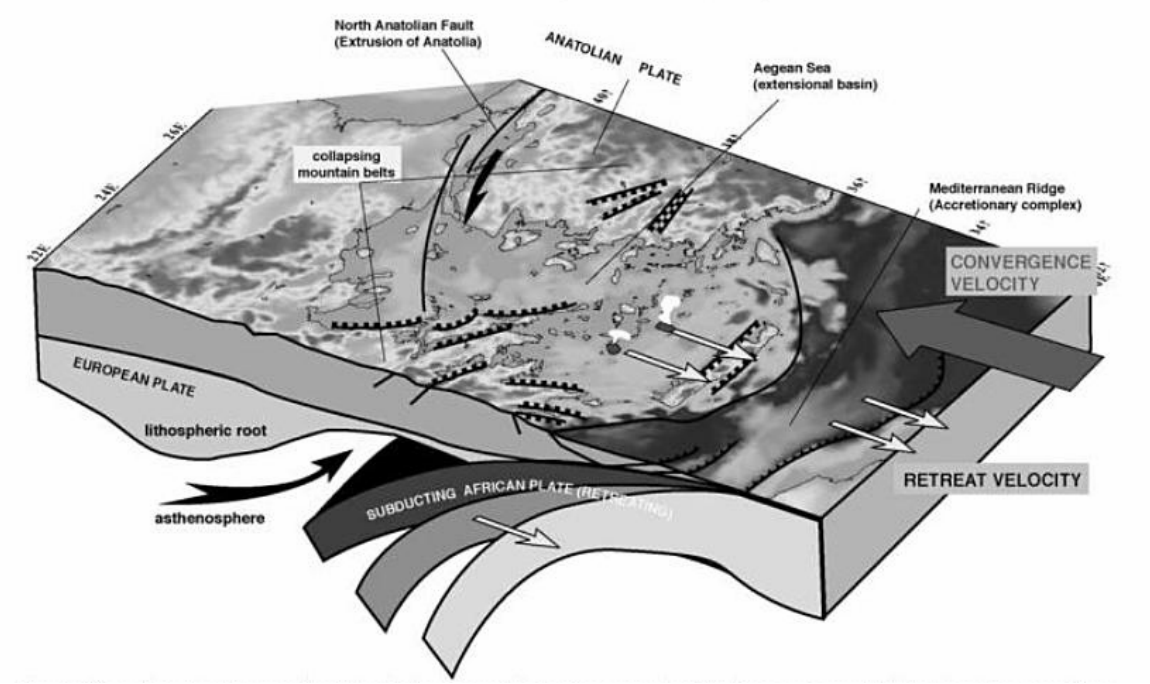

Figure 6: Three-dimensional illustration of the Aegean Sea showing the subduction of the Hellenic arc combined with back arc extension in the Aegean Sea and slab retreat (Jolivet et al., 2004).

The centre of extension is located in the back-arc-zone to the north of the Hellenic subduction zone. According to Jolivet and Faccenna (2000) and Edwards & Grasemann (in press), the extensional regime is caused by the southward movement of the subduction zone due to an increase of slab retreat and the slowing down of the African plate motion through first collisions between Africa and Eurasia (figure 6). Post-orogenic extension in the Aegean region have led to a strong thinning of the crust and the generation of metamorphic core complexes, which define a steep gradient of finite extension between continental Greece and the centre of the Cyclades, with a likely maximum below the island of Naxos (Jolivet et al., 2004). Two classes of doming

have been proposed by Jolivet et al. (2004) for in the Aegean region (see figure 7) based upon the presence or absence of lower crust material and the island-geometry, concerning the domal long axis compared to the stretching lineation. They found out that, in principal, domes have a prevailing lineation, either quite parallel or quite normal to the domal long axis. The first type, then, termed “a-type” domes, is elongated in line with the direction of extension. Extension is here accompanied by amphibolite-facies recrystallization and partial melting. The “b-type”-domes show a gentle doming of the foliation normal to the direction of stretching-lineation. The island of Tinos and Andros, for example are b-type whereas Kea, Kythnos and Serifos would be a-type. But this classification seems not to be universally true as Kea and Kythnos do not bear lower crust material (see Edwards & Grasemann, in press). Extension, however, is mostly associated with greenschist-facies recrystallization. Jolivet et al. (2004) argue that the a-type domes have been formed later with a maximum of extension in the centre of back arc region. More recently extension has re-located to the Gulf of Corinth. In the central Aegean region, however, extension is no longer active or at last very slow (McClusky et al., 2000; Jolivet et al., 2004) and aseismic.

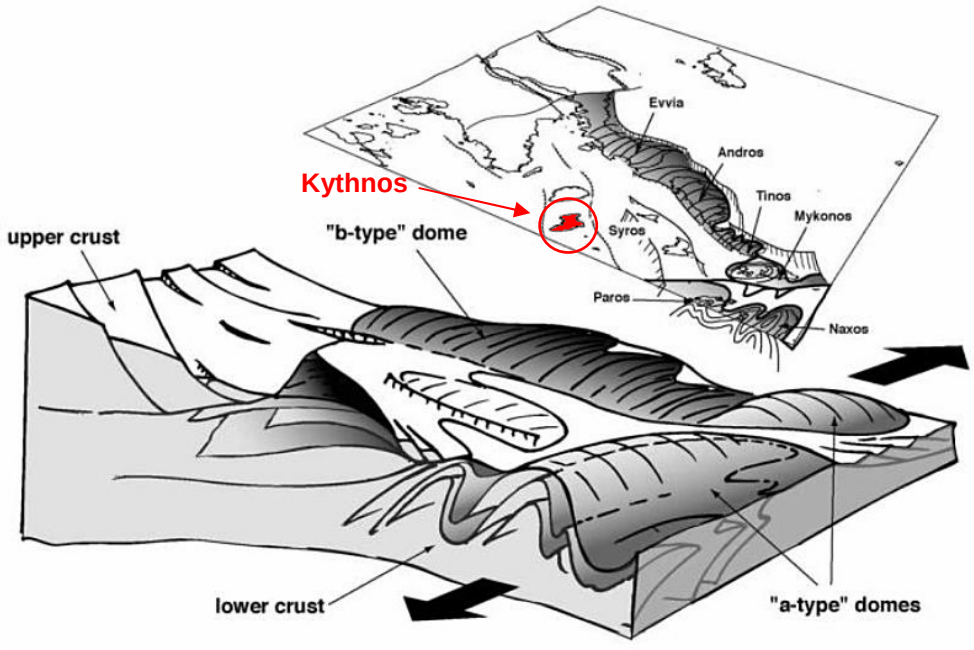

Figure 7: Types of metamorphic domes within the Cyclades of the Aegean Sea (after Jolivet et al., 2004), modified. A-type domes are parallel to the direction of lineation whereas b-type domes are arranged normal to streching- lineation. The island of Kythnos is marked in red.

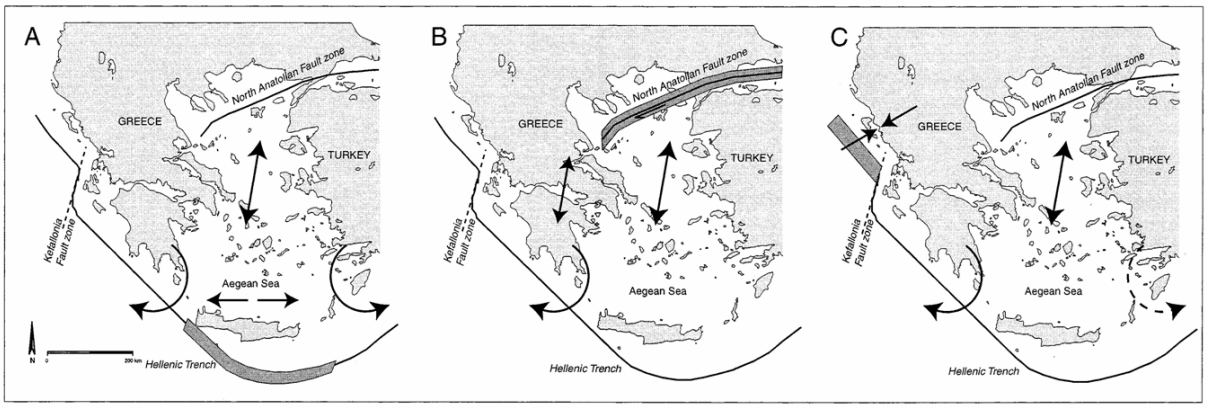

Figure 8: Three geodynamic models for the Aegean region based on paleomagnetic data (Duermeijer et al., 2000).

Duermeijer et al. (2000) evaluated the three proposed models for the tectonic evolution in the Aegean region considering their new paleomagnetic data. The first model (see figure 8A) attributes the arc-parallel extension in the southern Hellenic arc to an increase in resistance within the subduction zone. This is probably caused by the first collisions with the African continental lithosphere. Furthermore this leads to a clockwise rotation of the Peloponnesus and an anticlockwise rotation of the eastern arc segment.

The second scenario (see figure 8B) is the propagation of the westward moving Anatolian plate along the North Anatolian fault system due to the beginning of fast extension in the Gulf of Corinth (Armijo et al., 1996). This causes a clockwise rotation of the Peloponnesus.

The third model concentrates on plate boundaries to the northwest of Greece. Presently, the subduction of the African plate underneath the Aegean terminates in the area of the Ionian-islands. Here the convergence is blocked and energy is concentrated only on a small region, the Kefallonia fault zone. This transition from oceanic subduction to continental collision again causes the clockwise rotation of the western arc segment (Duermeijer et al. 2000).

3.2. Seismicity of the Aegean region

The Aegean region is a geodynamically still very active part of the Alpine-Himalayan orogenic system and shows the highest seismic activities of the Mediterranean. As demonstrated in figure 9, the highest activities appear along the Hellenic arc, from the Ionian Islands to the Peloponnesus, Crete, Karpathos, Rhodos and the southwest of Anatolia. The maxima are reached around the islands of Rhodos, Karpathos and Kos. In the area of the North Aegean trough, at the western parts of the North Anatolian fault, another zone of high seismic activities is established. The central Aegean Sea, however, represent an almost aseismic region (Papazachos, 1973; Jackson et al., 1992; Van Hinsbergen et al., 2005).

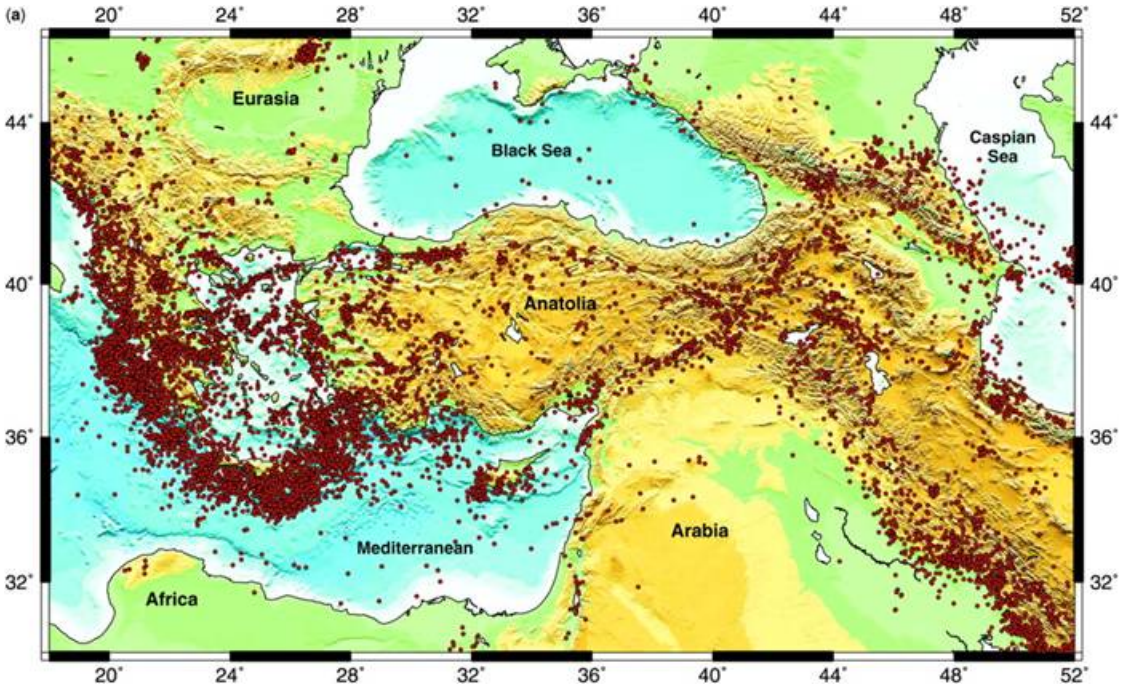

Figure 9: Seismicity of the Eastern Mediterranean region and surroundings: Dots indicate location of hypocenters with magnitude > 3; Taymaz et al. (2007).

The fault plane solutions in figure 10 show compressional stresses in the external parts of the Hellenic arc. The Aegean region represents an extensional regime while dextral movement can be observed along the North Anatolian fault (Jacobshagen, 1986).

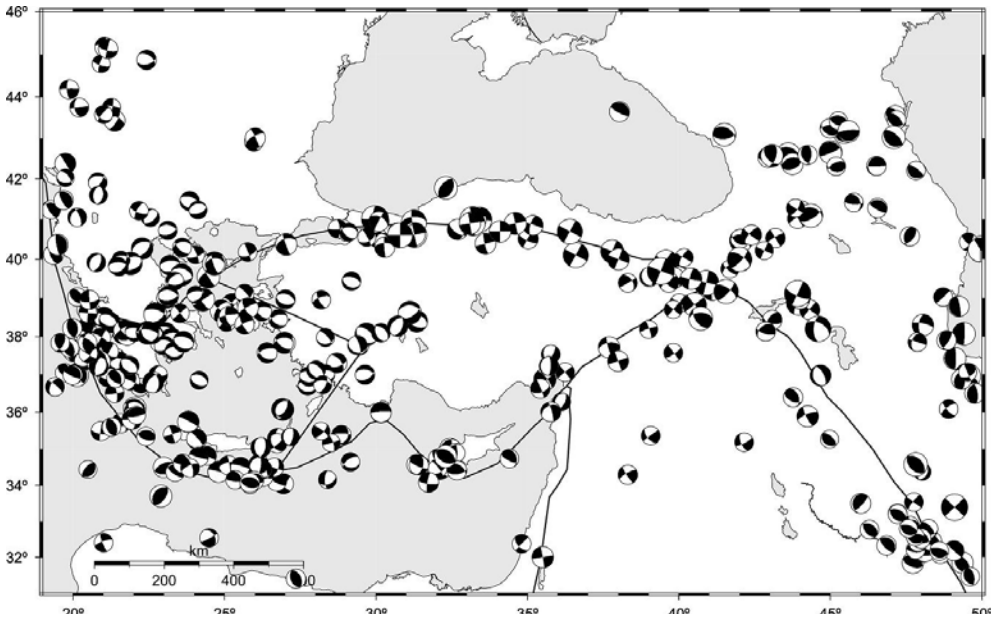

Figure 10: Focal mechanisms for large (M>6) and shallow (<50 km) earthquakes (McClusky et al, 2003).

Figure 11 shows three vertical sections of the Aegean region with hypocenters of earthquakes below the crust/mantle boundary and their regional positions.

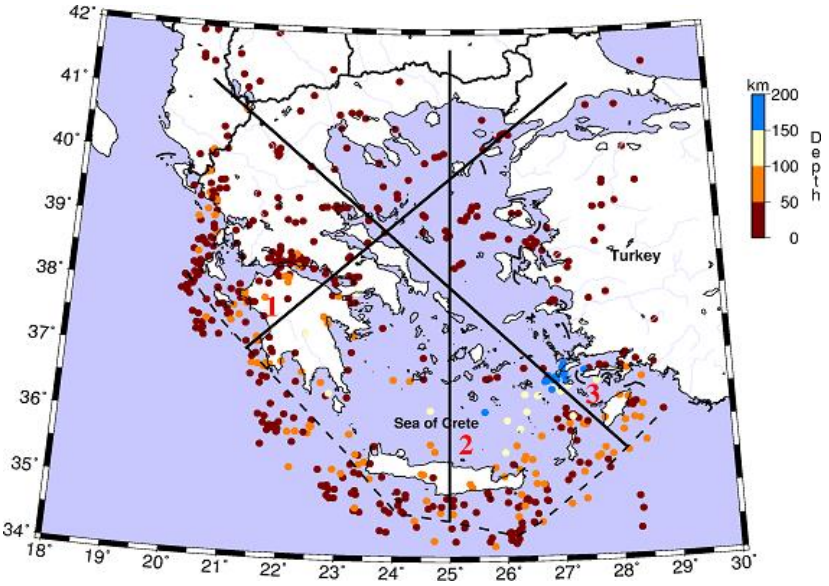

Figure 11: Hypocenters of earthquakes in the Aegean region (Sodoudi, 2000).

Using hypocentres plotted on a profile, the depth of hypocentres and therefore the Benioff-zone was detected. In general, the depths of hypocenters increase from the Hellenic arc towards the Aegean Sea. This testifies to a Benioff-zone which plunges beneath the European continent. But as shown in figure 12 the position and the angle of plunge of the Benioff-zone is not consistent over the Hellenic subduction zone. From SW toward SE the dip of the slab increases. The deepest hypocenters are located beneath the Aegean volcanic arc, especially around the Dodecanese islands in the southeast. Seismic and gravity investigations also offered that the continental crust in the Aegean region only has a thickness of about 20 km (Endrun et al., 2005) whereas in the western parts of Greece and the Peloponnesus the crust reaches thicknesses of some 45 km.

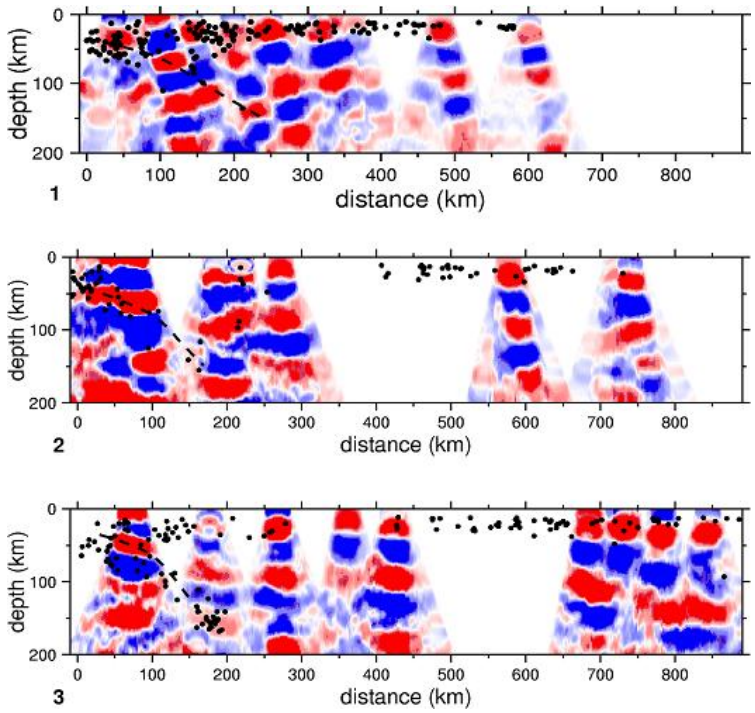

Figure 12: Seismic tomograms with earthquake hypocenters for three cross sections in the Aegean region show the trend of the Hellenic slab (Sodoudi, 2000).

Metamorphic Core Complexes

Many islands of the Cyclades like Ios, Naxos but also Kea and Serifos feature oval domes with a penetrative ca. NNE–SSW striking stretching lineation. They are defined Metamorphic Core Complexes (MCCs) similar to those in the North American Cordillera (Lister et al., 1986).
Metamorphic Core Complexes are exposures of the middle or lower crust as a result of major continental extension. Typical for MCCs is a decollement and/or steep metamorphic gradient between basement terrane and cover. So high-grade metamorphic rocks, which show ductile deformation, are exposed below mylonitic shear zones (detachment faults), while the low to non-metamorphic rocks of the hanging wall feature brittle or ductile-brittle deformation (Coney, 1980; Lister & Davis, 1989). Characteristic for the hanging wall are cataclasites. Thus exhumation along these large-scale extensional shear zones is acting from ductile to brittle conditions. The exposure of rocks from several km depths to surface results in an initial production of heat which leads to a thermal doming, hence the typical antiformal shapes of MCCs.

Figure 13 below shows the three theoretical possible models for MCCs which are the Pure-shear, the Wernicke and the Delamination model. Alternatively, on the basis of geometry and kinematics, two end-member models can be established. The Symmetrical MCC is bounded by two low-angle shear zones, dipping into opposite directions with antithetic kinematics. The asymmetrical MCCs are bounded by only one low-angle normal fault. MCCs in nature are thought to be a mix of these models, evolved through time.

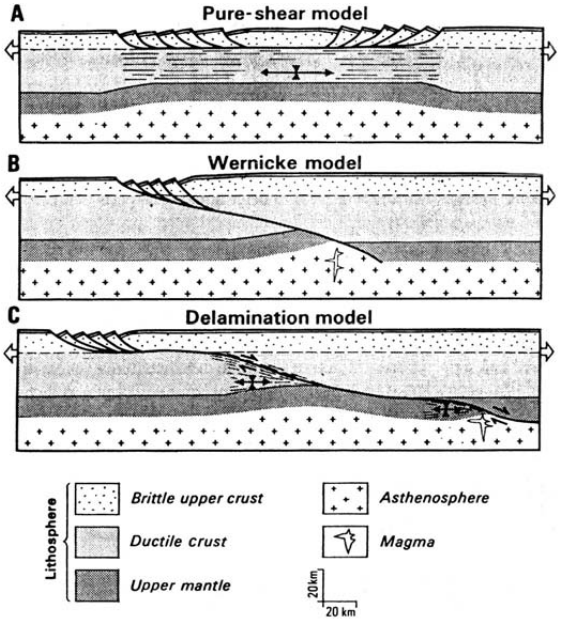

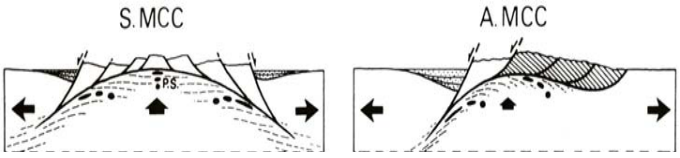

Figure 13: Left: Schematic diagram of the three possible end-member models for continental extension with formation of Metamorphic core complexes: Pure-shear model, Wernicke model and Delamination model (Lister et al., 1986). Right: End-member geometries of MCCs. (a) Symmetrical MCC (b) Asymmetrical MCC (after Malavieille, 1993).

4. GEOLOGY AND STRUCTURAL GEOLOGY OF KYTHNOS

4.1. General information & previous geological works

The island of Kythnos belongs to the Western Cyclades, so it is part of the Attic-Cycladic Crystalline Complex. It is situated around 100 km southeast-ward of Athens. Up to now it has achieved little attention. The geological mapping (see figure 14) of De Smeth (1975) established four major rock units: Ab-schists, greenschists, marbles and a metagabbro unit, which was expected in the lowermost structural position (Schliestedt et al., 1994). However, Schliestedt et al. (1994) suggested this metagrabbro unit to be a remnant of ophiolite nappes belonging to the Upper Tectnonic Unit, bearing mineral relicts of Eocene high-pressure-metamorphism (M1) in porphyroblastic Ab and Ep. The existence of such M1-remnants on Kythnos Island was already suggested by van der Maar & Jansen in 1983. The main rocks of Kythnos are Ab-Chl-micashists and greenshists (Ep-Zo-schists) which are intercalated with two kinds of marble layers. Furthermore there are, according to the geological map of De Smeth (1975), rare occurrences of metagabbros near Kanala, Flabouria and in Aghios Dimitrios. Chrysanthaki & Baltatzis (2003) also described outcrops of fe-mn-metasediments. The rocks of Kythnos show a strong greenschist-facies overprint (M2) but relicts of high-pressure minerals also testify to a M1-impact. So the island can be attributed to the Cycladic Lower Unit (Okrusch & Bröcker, 1990). Keiter et al. (2008) distinguished three ductile compressive deformation events and at least one brittle faulting stage after the tectono-metamorphic evolution. The youngest structures are normal faults, which resulted from a predominant NE-SW extension, that goes with the overall stress-velocity field of present day crustal motion in the Aegean (Keiter et al., 2008; McClusky et al., 2000).

Figure 14: Geological map of Kythnos, 1:50 000 (De Smeth, 1975) with research area marked in red and sections A, B and C; modified.

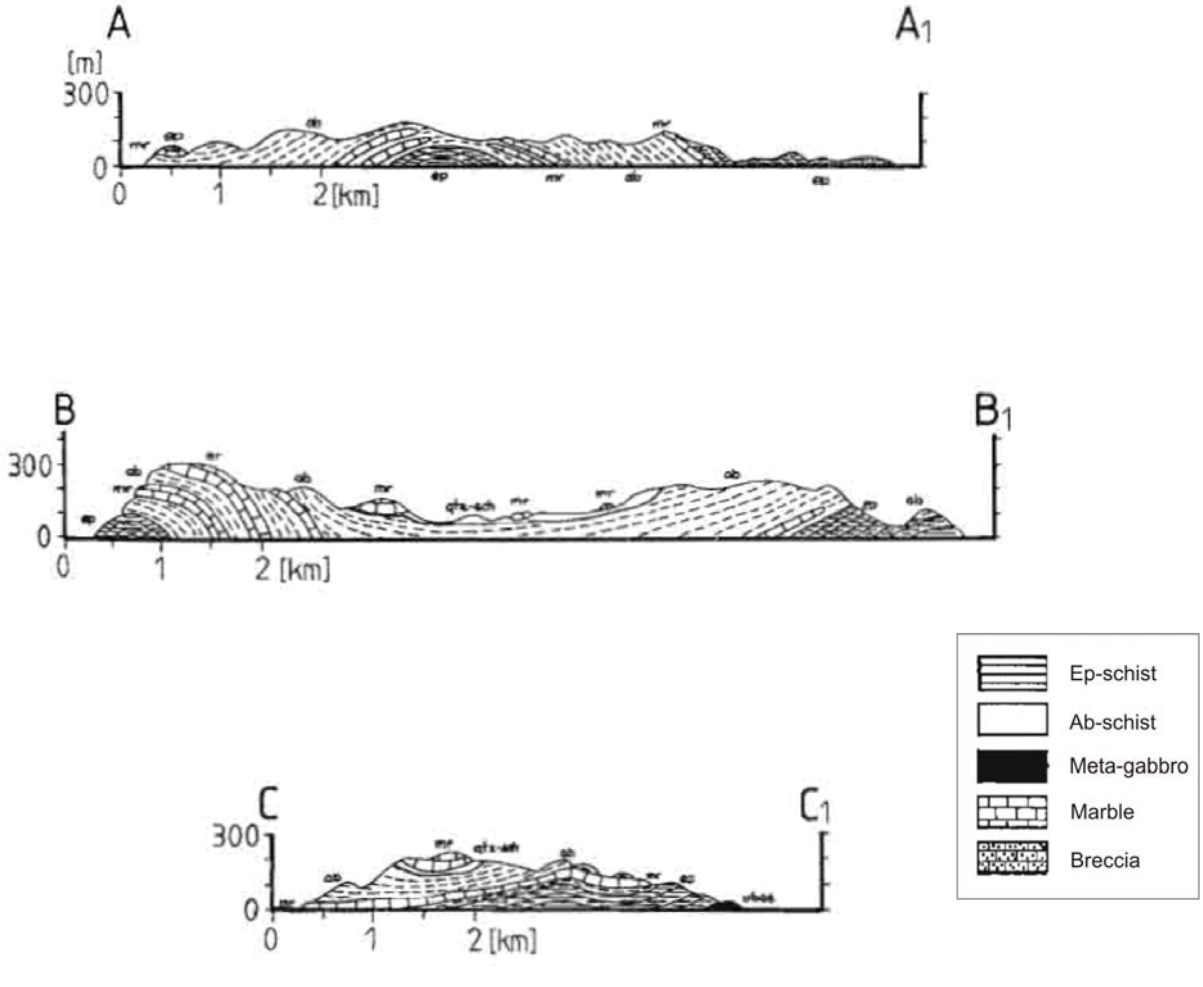

Figure 15: Geologic profiles of section A, B and C, modified after De Smeth (1975).

According to the sections of De Smeth (see figure 15) there are two km-scale antiforms govern fabric in the north of Kythnos. Section A, which runs NE-SW, shows a fold with a WNW-ESE-striking fold axis. The profile in B, pointing from NW to SE, displays a major fold in the north-western mountain ridge, whose axis strikes NNE-SSW. The third section (C), ranging from the western coast to the bay of Kanala in the east, represents a roughly NNE-SSW-striking antiform.

4.2. Mapping area

Figure 14 shows the geological map of Kythnos from De Smeth (1975). Our field work concentrate on the southernmost part of the island around the small village Aghios Dimitrios (see figure 16 and 17) which is situated about 7 km SSW-wards from the port of Merichas.

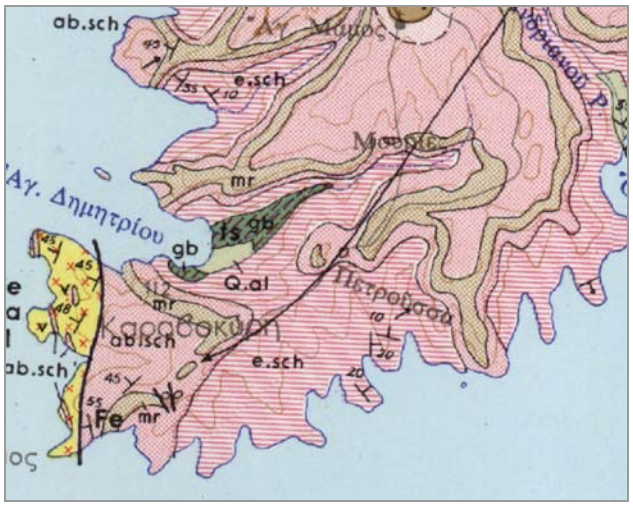

Figure 16: Zoom to the research area from geological map of Kythnos (De Smeth, 1975). Lithologies are specified in figure 14.

Figure 17: Satellite picture of the mapping area section (GoogleEarth 2007).

As already mentioned, the predominant rock types of our research area are Ab-schists, greenschists, marbles and a small metagabbro lense cropping out in the NE of Aghios Dimitrios. De Smeth described the rocks of the south-westernmost part of Kythnos as carbonized volcanites, exotic and separated from the schists and marble layers by a remarkable fault. There are also a few occurrences of hydrothermal deposits, especially iron, developed as Hem, Brt (De Smeth, 1975) and mn-bearing metasediments (Chrysanthaki & Baltatzis, 2003). Veins of pure Tur and Qtz-Cal-bearing have been observed by Chrysanthaki & Baltatzis (2003) in Grt-bearing Am-schists in more northern parts of Kythnos, close to the bay of Kanala.

Figure 18: Aghios Dimitrios, view to the assumed “volcanic” rocks in the SW of Kythnos.

The figure 19 below shows the schematic stratigraphic column of all lithologic units on Kythnos from De Smeth (1975). At the base, De Smeth proposes the meta-ultrabasites. As will be presented in the following chapters, we are in complete agreement with his point of view. The hanging wall of the meta-gabbro unit is build up by Ep-schist, Ab-schist and marbles of variable thicknesses. The marbles are partially associated with quartzites (Carl, 1993).

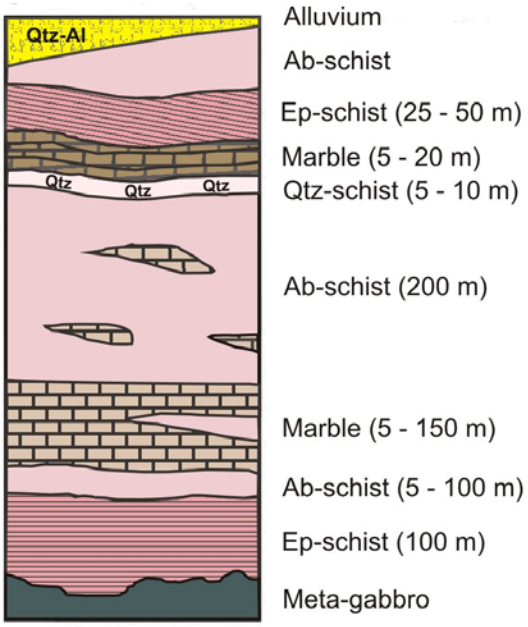

Figure 19: Schematic stratigraphic column, redrawn after De Smeth (1975). Note that the metagabbro unit (here specified as meta-ultrabasites) is expected at the base.

4.3. Lithostratigraphy and lithologies of Kythnos Island

4.3.1. Greenschist

The dominant lithology on Kythnos Island is greenschist. Mineralogically the greenschists mainly consist of Chl, Ser, Act, Ep, Ab and Qtz as well as Cal. In terms of macroscopic criteria, two different types of greenschists can be distinguished. There is a very fine grained, highly foliated rock containing large amounts of phyllosilicates and is therefore termed phyllite, or indeed phyllonite, where single micas are not distinguishable without microscope. The second type is rather coarse grained, with crystals of mm-scale, and massive, with less phyllosilicates but large Ep crystals and Ab “blastesis” causing a kind of “grainy”-structure (see figure 20 and 21). In general, the more massive greenschists consist of larger amounts of Qtz and feldspar, leading to an overall brighter outcrop colour.

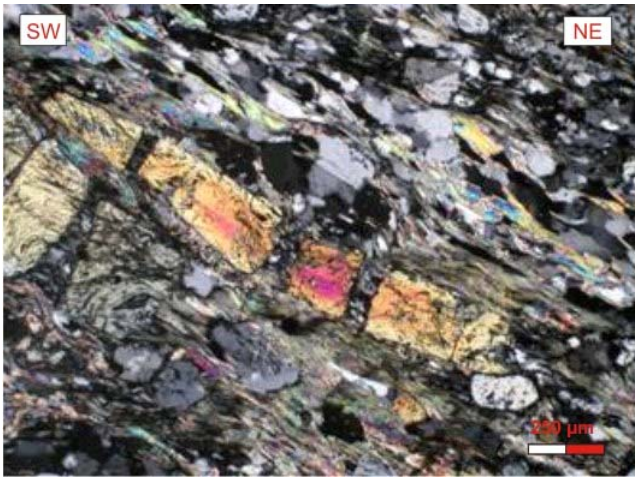

Figure 20: Photo of a thin section shows the characteristic mineral assembly of greenschists: Qzt, Chl, Ser, Act, Ep, Ab and Cal; crossed Nichols.

Figure 21: Intensively folded and partly hydrothermal overprinted greenschists with Qtz and Cal-veins, which are folded too.

4.3.2. Metabasite

The metabasites are concentrated within a few isolated lenses within the greenschists, cropping out near to Kanala, Flabouria and Aghios Dimitrios (De Smeth, 1975). In the case of south-Kythnos, the metabasic rocks are coated by Srp-Tlc-schists.

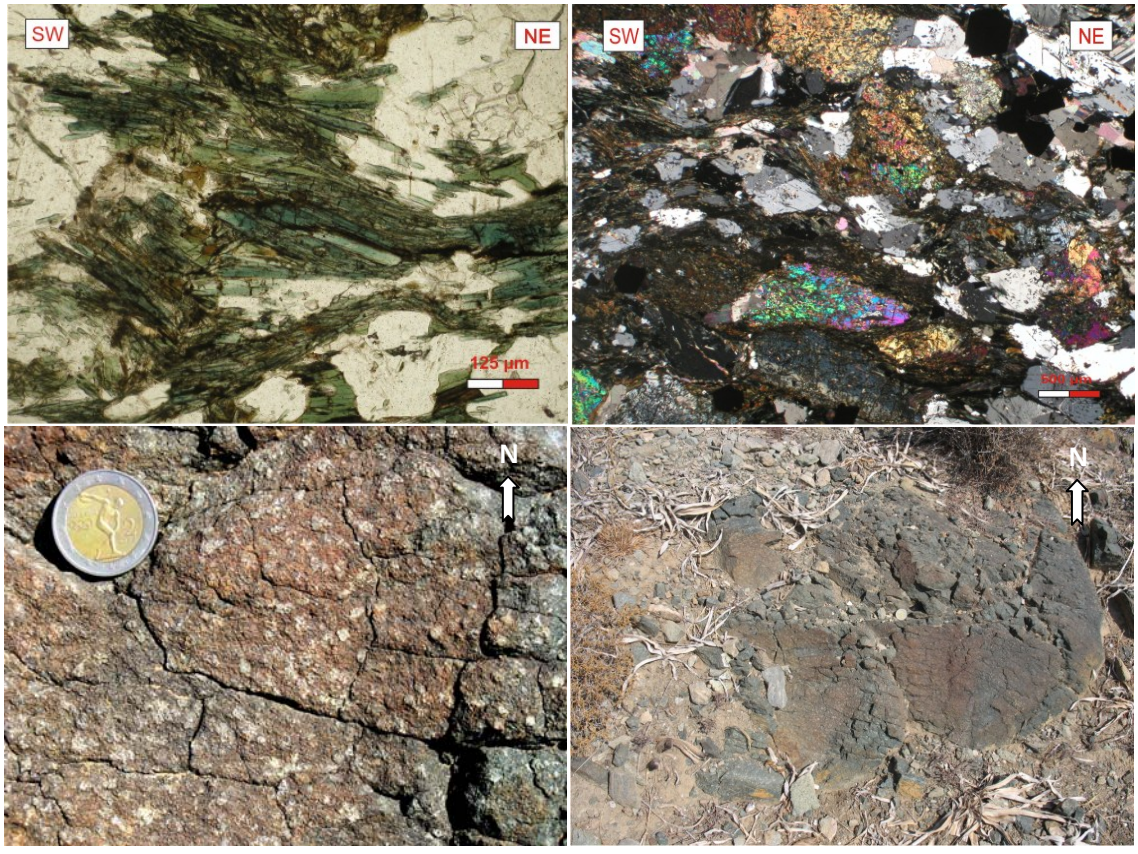

Figure 22: Top left: Thin section of metabasic rock with Am. Top right: Thin section of metabasic rock, crossed Nichols. Down to the left and right: metabasic rocks with relicts of an original magmatic fabric.

In general, the metabasites are rather massive without noticeable lineation, foliation or any evidence for deformation-events. Qtz-gashes are absent, but veins of feldspar and Cal are present. Partially, they still show relicts of their primordinal magmatic fabric. Their mineralogy comprises Am (Gln), Px, Chl, Mgh, Ab and Cal (see figure 22).

4.3.3. Srp-Tlc-Schist

These rocks principally consist of Srp, Tlc and the asbestos minerals Ctl and Atg. As already mentioned before, they envelope the metamorphic gabbroic rocks lenses cropping out at Aghios Dimitrios. As Tlc-layers are very soft and low-frictional, deformation is facilitated at such horizons.

Figure 23: Srp-Tlc-schist, which are susceptible to erosion because of their low rigidity.

4.3.4. Fe-Mn-Medasediments & Tur-Ep-Gneiss

The Fe-Mn-metasediments on the island of Kythnos have been described by Chrysanthaki and Baltatzis (2003). In the area of Aghios Dimitrios especially, Am-Ab-Mag-gneisses were found, consisting of Sps, Mag, Rbk, Qtz, Ab, Ms, Chl and minor amounts of Tnt, titano-Mag, Ap and Rt (Lenauer, 2008). Perpendicular to the crenulation, also a lineation, defined by the orientation of Am-needles, was observed. This lineation, slightly dipping towards NE with an angle of 10°, might be a relict of the M1-HP-deformation. The gneisses show a mylonitic foliation, especially in the darker layers, which are rich in Mag (figure 24).

As well as the Fe-Mn-metasediments, the Tur-Ep-gneisses are positioned within the greenschists, in the hanging wall of the metabasites. We identified these only in one smaller outcrop in the north of Aghios Dimitrios. The rocks are foliated and show a lineation, caused by the preferential orientation of Tur crystals in SE-NW direction. The rocks consist of Tur, Ep, Mag, Qtz, Act, Ms and Chl (figure 25).

Detailed geochemical and petrological investigations on Fe-Mn-metasediments, Tur-Ep-gneisses and metabasic rocks were carried out by Iris Lenauer (2009).

Figure 24: Fe-Mn-metasediments in the north of Aghios Dimitrios. Rocks are clearly foliated and show a layering due to variation between Qtz- and Mag-rich sections.

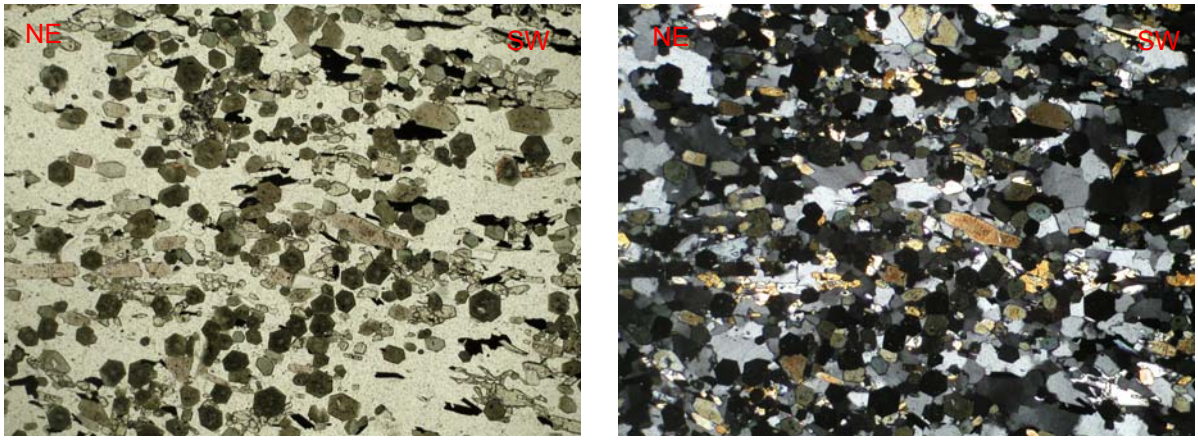

Figure 25: Photo of a thin section of a Tur-Ep-gneiss, viewed with crossed Nichols on the right.

4.3.5. Ab-Chl-Ser-Schist

The Ab-Chl-Ser-schists overlay the Ab-gneisses and are partly found on top of the marble-ultramylonites. Their mineralogical composition is made up of Qtz, Ab, Chl, Ser and also Cal. They show intensive foliation in thinsection, defined by Chl and Ser. Lineation dips towards NE at very low angles. This rock is dominated by structures like SC- and SC´-fabrics (see figure 26), kink bands and isoclinal folding as well as brittle veins filled with Cal, Qtz or carbonatic Fe-mineralizations. Thin sections also showed large feldspar-clasts with deformations twins (see figure 26).

Figure 26: Left: Ab-Ser-Chl-schist with brittle high angle fault, overlain by Ep-schist (top right). Top right: Thin section of Ab-Ser-Chl-schist shows large Ab-blasts with deformation-twinning. Down right: Thin section of Ab-Ser-Chl-schist with SC-fabric, indicating to a top-to-S kinematic.

4.3.6. Ab-Gneiss

Ab-gneisses comprise layers of several meters and are mostly accompanied by grey-blue marbles. They consist of Qtz, Ab, Chl, Cal and Ms.The rocks were subjected to intensive deformation resulting in tight to isoclinal folding of all orders (figure 27). They sometimes form boudins in the subjacent marble layer. The Ab-gneisses show foliation by preferential orientation of phyllosilicates. Beds are dipping towards WNW, NW and SE at low angle, resulting in an antiform. Lineation is directed to NE respective NNE at low angle too.

Figure 27: Ab-gneiss with subhorizontal tight folding (left). Thin section of Ab-gneiss (right), crossed Nichols.

4.3.7. Impure Marble

A layer of impure marbles of at least 5 meters, which can also be decribed as carbonatic-gneisses, forms the boundary between the Ab-Chl-Ser-schists in the footwall and the ultramylonitic marbles in the centre of the shear zone. In mineralogic context, this lithology mainly consists of fine grained and layered respectively foliated Cal, Qtz, Ab and Chl. The generally greyish-brown carbonate-gneisses partly contain Fe-oxides leading to red discolorations.

4.3.8. Marble-Mylonite

The grey to blue-coloured marble-mylonites are often accompanied by a layer of Ab-gneisses in the hanging wall. As the marble-units are, in comparison to the schists, relatively resistant to weathering, they form prominent ranges in the almost relatively smooth landscape. De Smeth (1975) distinguished two types of marbles: a grey-blue marble-unit and yellow marbles comprising also Qtz and Ms. In our research area, only the very fine-grained grey-blue marbles occur. They mainly dip to NW or to the WNW in the western part of the island and toward SE on the eastern sides, both at low angles. Marble layers have thicknesses up to 5 meters and show intense folding on all orders, forming an overall km-scale recumbent fold. Qtz-clasts act as shear sense indicators, like the σ-clasts shown in figure 46, demonstrating a top-to-SW directed movement. Lineations on foliation planes dip NNE at low angles. Rotate Qtz-boudins also verify the top-to-SW directed movement. Thin sections of these marbles show large variations in grain size, with an unequally developed mylonitic foliation as well as micro fractures filled with Cal and minor amounts of Qtz and Ser. The average grain size lies between 50 and 100 µm. Large Cal crystals of up to 500 µm or more, exhibit heavily twinning as a result of deformation in lower temperature ranges (Passchier & Trouw, 2005).

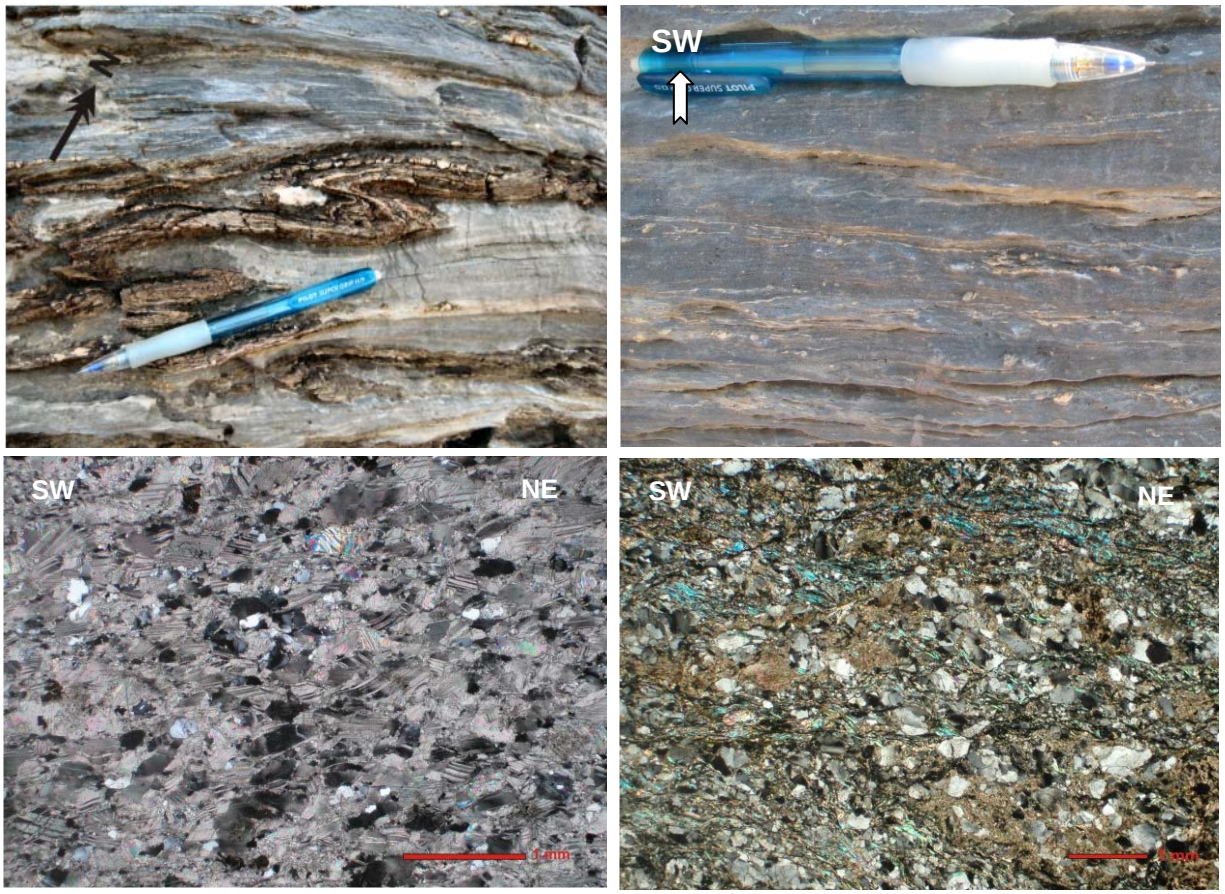

Figure 28: Top left: Mylonitic marble with folded gneiss layer and calcitic veins. Top right: Mylonitic, fine grained marble. Down left: Thin section of relative pure, calcitic marble-mylonite, crossed Nichols. Larger Cal-crystals show deformation twinning. Down right: Thin section of impure marble-mylonite with Qtz components and Ser; crossed Nichols.

4.3.9. Ultramylonitic Marble

The ultramylonitic marbles are positioned in the footwall to the cataclasites. They show a distinct layering by colour, varying from red to yellow and white or to grey and blue. Generally two different types of marble ultramylonites can be distinguished. The first type is rather steeply dipping, approximately with 50 ° SW and of red and yellow colours (see figure 29). These marbles are positioned just on top of the carbonate-gneisses. Marble ultramylonites in the outermost southwest of the island are shallow dipping and are mainly grey, blueish or white coloured. As will be discussed in below, they also exhibit some differences in isotopic characteristics.

Both marble-ultramylonites are extremely fine grained with grain sizes of ca. 10 µm or partly below the resolution of the optical microscope. In thin section, fine µm-layers of different grain size or colour can be distinguished. The marbles are made up almost exclusively by Cal with only a few clasts of Qtz with grain sizes between 50 and 200 µm. Partly the Qtz clasts are broken up

(figure 30) indicating to very high differential stress conditions that is consistant with the fine recrystallized grain size of the marbles. Thin sections of the marble-ultramylonites partly comprise micro veins, filled with, compared to the rest, coarser grained Cal (figure 30 and 45). They all indicate a top-to-SW displacement-direction. The ultramylonites also comprise several larger Cal-porphyroclasts of some 500 µm, which can give, as shown in figure 45, information about the shear sense. Large Cal-crystals exhibit deformation twins which are mostly tabular or wedge-shaped.

In general, the highly strained massive marble-ultramylonites only show a few veins, whereas the blue-grey marbles in the footwall are rich in extension gashes filled with Cal. Parts of the ultramylonite, especially in the very south of the marble-ultramylonite-unit, underwent a subsequent hydrothermal overprint by fluids which were rich in Fe. Veins filled with carbonatic Fe-mineralizations penetrate both marbles and the cataclasites in the hanging wall, whereas all the former developed Cal-veins end at the contact to the cataclasites.

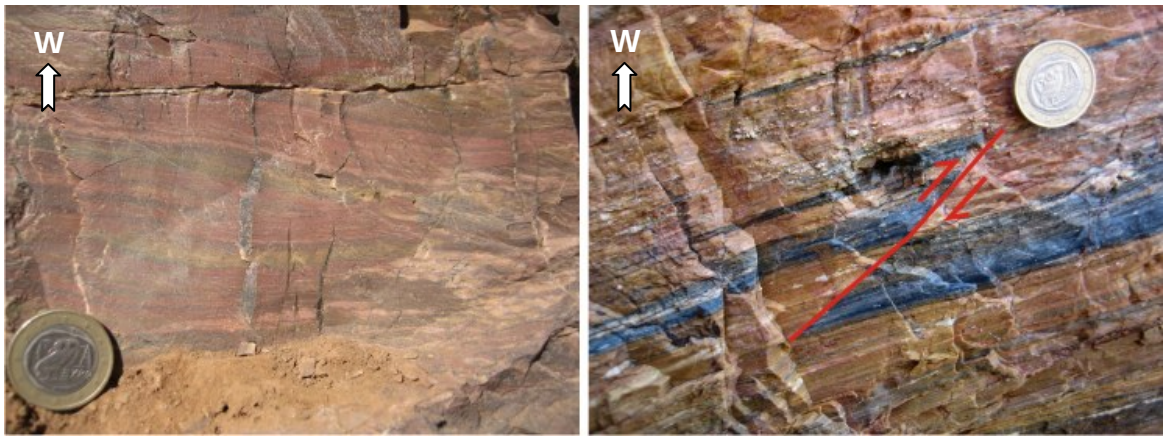

Figure 29: Ultramylonitic marbles with thrust fault, top-to-N, on the right.

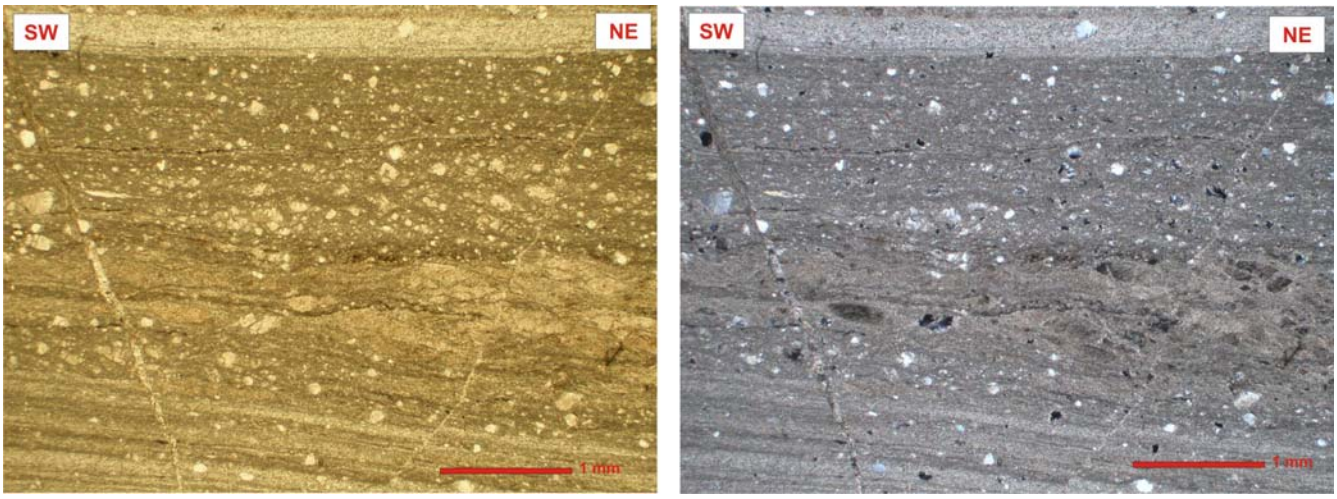

Figure 30: Thin section of a highly strained marble (crossed Nichols on the right) showing distinct mylonitic layering. High differential stresses have caused extreme reductions in grain size of Cal and the partly breaking up of Qtz clasts. Late, brittle conjugated system of veins, filled with Cal cements, penetrate the ultramylonites.

4.3.10. Ultracataclasite

The major shear zone comprises, besides the marble-ultramylonites in lower parts, also a thin layer of fine grained cataclasites of a few decimetres. Near the ultramylonitic marble-unit, the cataclasites consist mainly of internal fractured marble components. With increasing distance from shear zone, the Qtz and gneiss amount increases. Cataclasites are, in general, defined by the presence of less than 30 vol-% fragments in a fine grained matrix. The cohesive nature of the rock is due to precipitation of crystals from a fluid (Passchier & Trouw, 2005). As minerals are partly fringed by Cal or show secondary generated Fe-oxides, participating fluids must have been rich in Fe and carbonates (figure 32). The cataclasites exhibit random fabric with subrounded marble and Qtz components of variable sizes. Qtz grains are mostly polycrystalline and, as well as the marble and gneiss fragments, often cracked and subsequently healed (figure 31). Due to the fact that components are internally broken and of µm-size, this rock might be termed ultracataclasite.

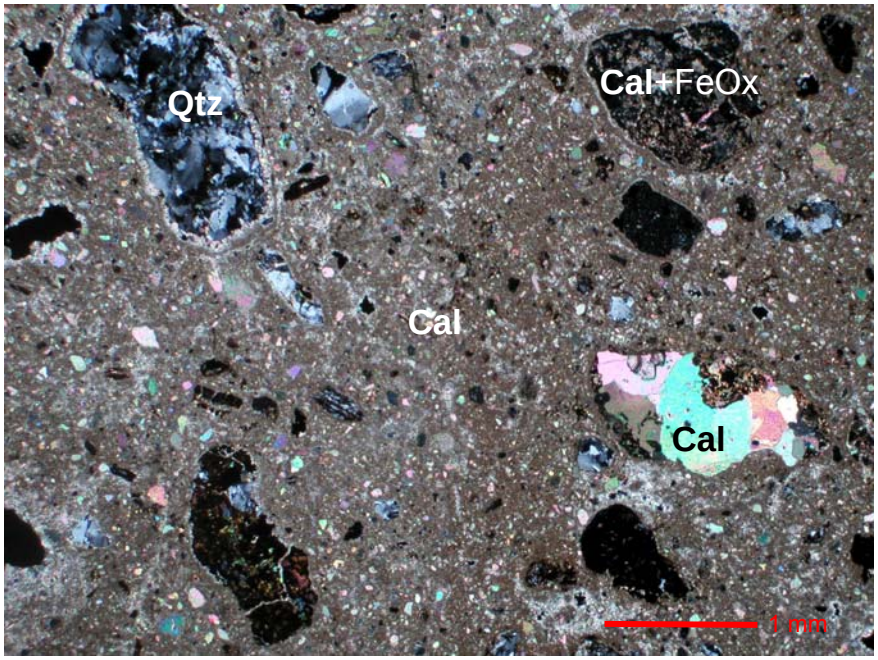

Figure 31: Thin section of ultracataclasite, crossed Nichols, with extremely fine grained calcitic matrix and large components of polycrystalline Qtz and partly altered Cal.

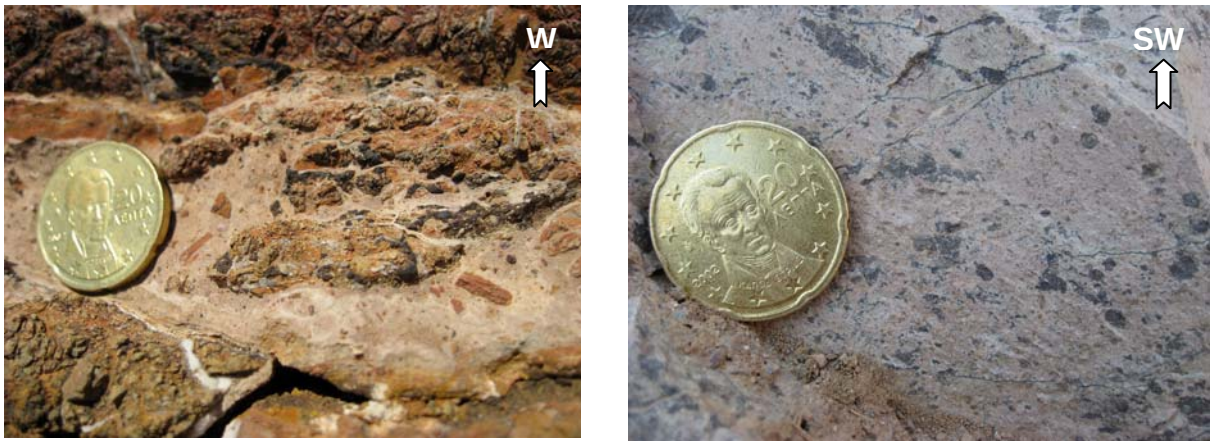

Figure 32: Hydrothermal highly altered ultracataclastic marble (left); Right: Massive ultracataclasite, consisting mainly of marble components.

4.3.11. Quartzite

The uppermost unit in the south-western end of the island was originally described by De Smeth (1975) as carbonized volcanic rock. According to our field observations, we are in disagreement with him. We found out that the rocks mainly consist of strongly brecciated Qtz, with some amounts of Cal and also Ms (figure 33). The deformation fabric can be specified overall as protocataclastic. The rocks show a strong hydrothermal overprint with partial accumulations of Fe-oxides and/or carbonates. Quartzites show different intensities of fracturing, therefore they must have been subjected to variable grades of deformation. Carbonates show indication of partial dissolution. In thin section, the Qtz of the more massive areas show a polygonal fabric with triple junctions between Qtz grains which infer, that the rock was subjected to static recrystallization. This strongly contrasts with the massive greenschist facies overprint in the footwall.

Figure 33: Hydrothermal altered and highly brecciated quartzite on the left. Thin section of massive quartzite on the right shows tripe junctions with angles of approximately 60°, which results from static recrystallization-processes.

Lithostratigraphy of research area:

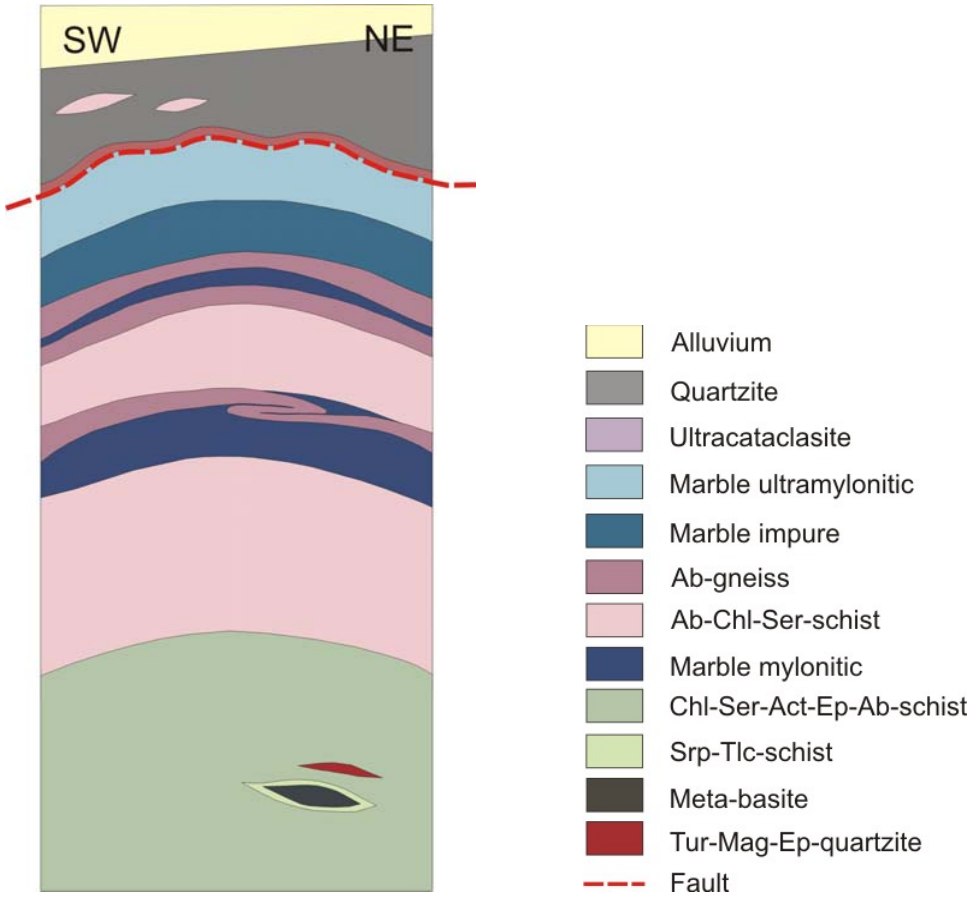

Figure 34: Schematic lithostratigraphic column of S-Kythnos.

4.4. Deformation and Kinematics

4.4.1. Ductile Deformation

4.4.1.1. Foliation

In general, foliation is defined by (1) local variation in grain size and/or (2) by mineralogical composition, due to the preferred orientation of elongated minerals or platy minerals like chlorite, biotite and mica or (3) by planar discontinuities like microfractures.
The rocks of south-Kythnos form a major anticline. The schists show prominent foliation planes, which are, in the northern parts of our study area, shallow dipping towards NE and NNE. In the southernmost areas, however, foliation is dipping toward the SSW, locally at steeper angle. The main foliation, formed under peak metamorphic circumstances (M1), was later on deformed by folding or mylonitization of the earlier fabrics under retrograde metamorphic conditions (M2). Only in some mylonitic metabasites, such relicts of the earlier HP-M1-deformation stage were found.
In the marble-mylonites and –ultramylonites foliation is defined by fine, penetrative layers of different colour or extremely small grain size. Foliation in the marble ultramylonites, which only occurs in the southernmost parts of Kythnos, is dipping more steeply towards SW.

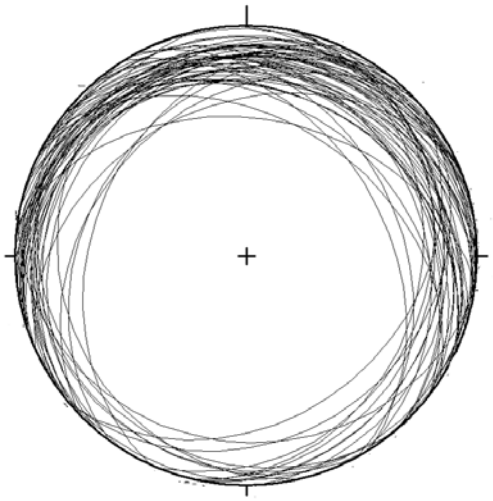

Figure 35: Left: Mylonitic foliation in marbles. Right: Schmidt plot shows, that foliation planes mainly dip to the NW, N and NE at rather low angles.

4.4.1.2. Lineation

A lineation is defined, according to Passchier & Trouw (2005) as any linear feature that occurs penetratively in a rock. This is caused by the parallel orientation of single, elongated crystals or the shape preferred orientation of elongated aggregates. A prominent mineral-(stretching)

lineation was found in all schists and also in the marble-ultramylonites. The metabasites however show only slight lineation by crenulation and the preferred orientation of Am. Am-needles are arranged almost normal to the crenulation lineations. This might be a relict of the argued M1-deformation, dipping almost subhorizontal towards NNW, altough the metabasites only may be rigidly transported or rotated.

In general, lineation in S-Kythnos mostly dips NE with about 20°. On those foliation planes which are dipping to SW, lineation is directed towards SSW.

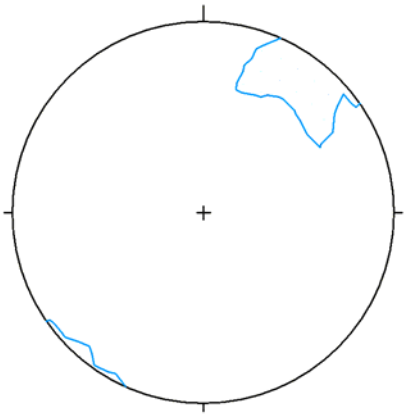

Figure 36: Contour Plot (5%); lineation shows a max. NE-SW- direction.

4.4.1.3. Folding

According to our observations, Kythnos was affected by at least two different phases of folding. The dominant internal structure in marbles and schists is a tight to isoclinal folding (D1) with subhorizontal axial planes and NE-SW trending fold axis with SW vergence (figure 37). This folding has caused the development of a penetrative schistosity, with mica and Chl orientated parallel to the axial plane of the folds. A subordinate isoclinal folding, with fold axis striking NW-SE but also subhorizontal axial planes was observed (figure 41). This earlier folding stage generates hundreds of meter to km-scale recumbend folds, which are confirmed by a multiplicity of second order Z-, S- and M-folds. These are especially well developed in the Ab-gneisses.

In a later deformation phase (D2), Kythnos was affected by folding due to strong shortening perpendicular to the stretching lineation, as a consequence of the incipient N-S-extension in the Aegean Sea. This caused the large scale, upright to slightly vergent open fold and the overall dome-shaped style of the island. Fold planes are nearly vertical and fold axis are striking NNE-SSW, dipping more steeply to the south in the southernmost parts of the island (figure 40 and 41). In the more competent and relative thin marble layers with thicknesses of only a few meters, this N-S extension and E-W directed compression has caused detached buckle folding. The extremely fine grained and layered marble-ultramylonites in the hanging wall show formation of box folds and fault bend folds in dm-scale (figure 38).

Figure 37: Former subhorizontal isoclinal folds of a gneiss layer within the marble unit, stretched and sheared as a result of the later N-S extensional regime.

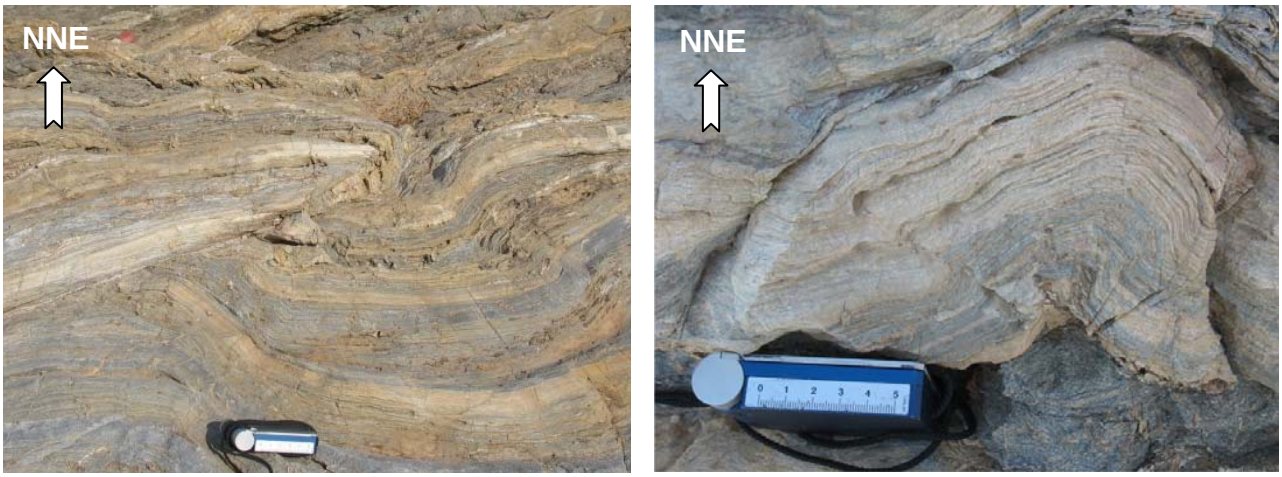

Figure 38: Left: fault bend fold in ultramylonitic marble. Right: box fold within marble-ultramylonites, testifying to an E-W shortening (D2).

Refolding in between type 2 and type 3 of the folds classification of Ramsay (1967) (see figure 39) are common structures on Kythnos Island. The refolded patterns have subhorizontal axial planes overprinted by subvertical axial planes and two generations of fold axes which are about 10 - 30 ° to each other.

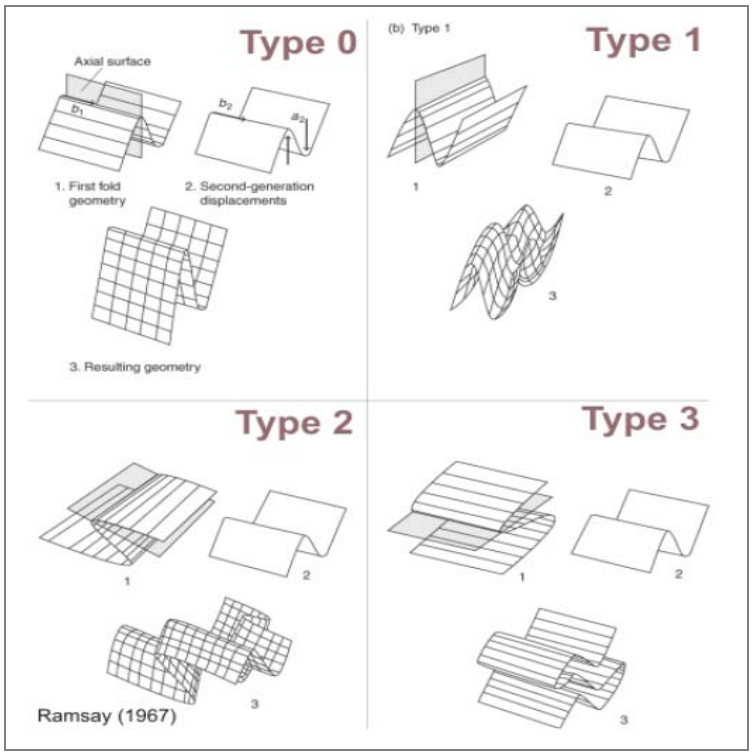

Figure 39: Refold pattern, endmembers (after Ramsay, 1967). Type 0 has parallel axial surfaces and parallel fold axis. Type 1 develops, if fold axis of the two deformations are perpendicular but axial planes are parallel. Type 2 has both axis and axial planes normal to each other. Type 3 has parallel fold axis with axial planes perpendicular to each other.

Figure 40: Large recumbend fold with subhorizontal axial plane (D1), overprinted by a second deformation phase with a subvertical axial plane (D2). Fold axis of D1 and D2 are nearly parallel.

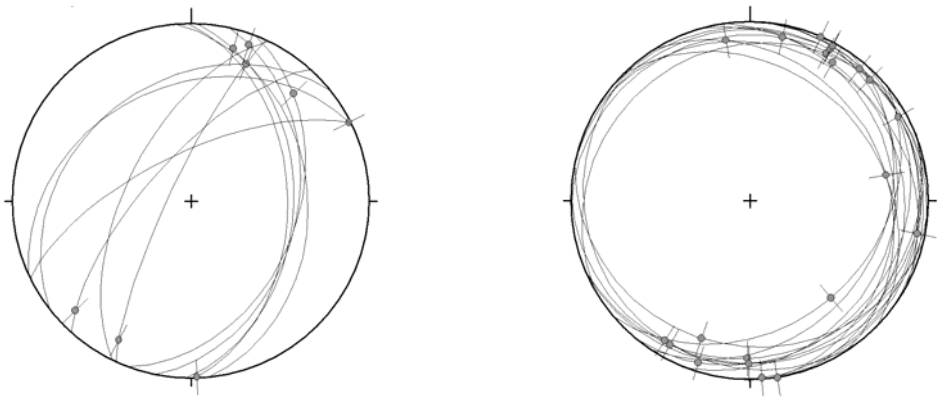

Figure 41: Schmidt plots show two different kinds of folding: an upright folding with fold axes dipping at low angles towards NNE and SSW (left) and an subhorizontal isoclinal folding with fold axes also shallowing dipping towards NNE and SSW (right).

Figure 42: Early type 1 Qtz-vein deformed by isoclinal folding (D1).

4.4.1.4. Boudinage

Marbles show domino type Qtz-boudins which are positioned parallel to the mylonitic foliation. Due to rotation of the boudins in direction of movement, top to S kinematics was identified (figure 43). Prior Qtz-veins in the marbles are therefore highly deformed and partly boudinaged. Also boudins or pinch and swell structures of gneisses are common within the marble-mylonites. They all indicate to a SW-NE extension.

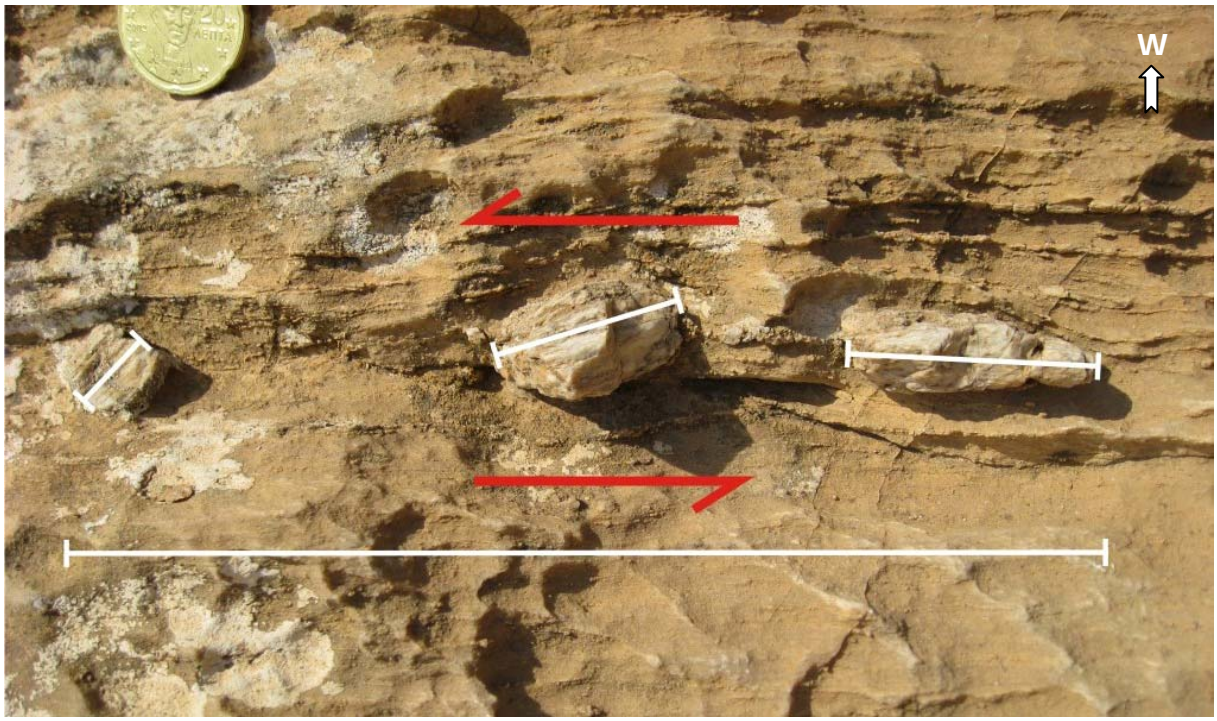

Figure 43: Rotated Qtz-boudins in mylonitic marble show top to S directed movement.

By measurement of the total lengths of the Qtz-boudins (original length l_0) and the present length of the layer (l), the elongation (e) can be calculated as followed: $e = (l - l_0)/l_0$.
For the example shown in figure 43, an elongation of 0.99 was calculated (l_0 = 6.8 cm; l = 13.5 cm; → e = 0.99). This means, the layer was stretched by approximately the double length.

4.4.1.5. Ultramylonitic marble shear zone

The major shear zone in the southernmost part of Kythnos Island comprises a ca. 5 meter thick marble-ultramylonite layer with a layer of ultracataclasites of several decimetres on the top. This shear zone separates the greenschists and Ab-gneisses and schist in the substratum from the quartzites in the hanging wall.

Figure 44: Mylonitic foliation in the extremely fine grained marble mylonites

The marble-ultramylonites show extremely fine reduction in the grain size down to 10 µm or even smaller. I interpret this as dynamically recrystallized grains in a deforming material as a function of differential stress. The differential stress in an active ductile shear zone increases with decreasing temperatures. The marbles are calcitic througout and show mylonitic foliation due to layering with variable grain size or colour (figure 44 and figure 45). Shear sense indicators like δ-clasts (figure 45) or crosscutting relationships and offsets, caused by micro faults and veins show consistent top to SW kinematics.

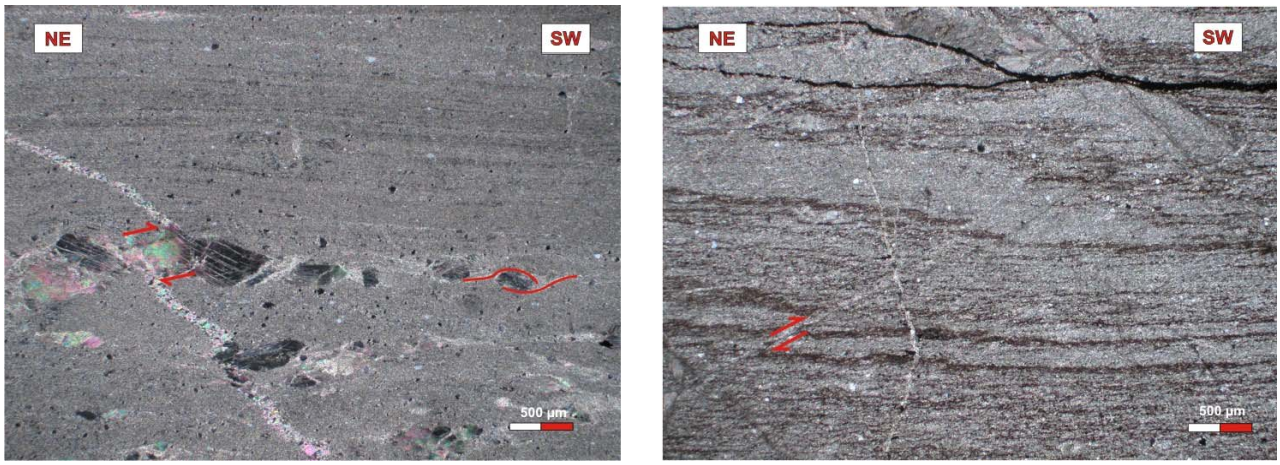

Figure 45: Thin sections of ultramylonic marbles. δ-clast and thrust faults indicate to a top-to-SW directed movement.

4.4.1.6. Crystal deformation & shear sense indicators

Within the marble mylonites and ultramylonites, several porphyroclasts of Qtz, gneiss or Cal point to a SW directed movement (figure 45 and 46). Mica fish in greenschists and Ab-Chl-schists also indicate a consistent top to SW kinematics.

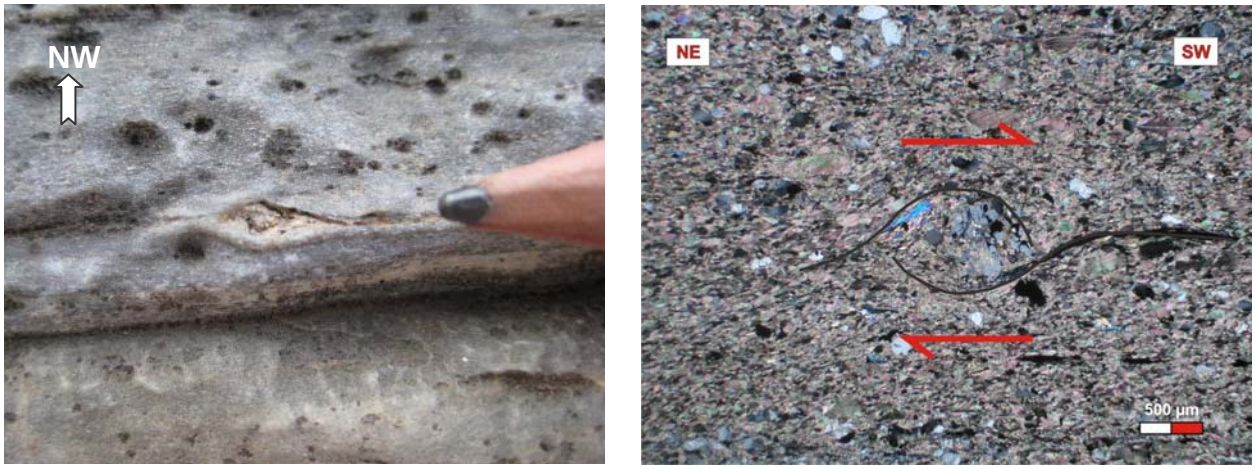

Figure 46: Qtz σ-clast in marble mylonite on the left and δ-clast within a marble shown on the right point to a top to SW directed kinematic.

4.4.2. Brittle-ductile Deformation

4.4.2.1. SC and SCC´ fabric

The mica-preferred orientation as well as the compositional layering is partly transacted by sets of subparallel minor shear zones. These smaller shear zones are called shear bands. Two types of shear bands can be distinguished (Passchier & Trouw, 2005): the SC-type and the SC´ or SCC´-

type. In SC-type shear bands, the C-planes (C stands for the French word “cisaillement”) are parallel to the shear zone boundaries. The S-planes (“schistosite” planes) dip against direction of shear. The direction of maximum shortening is normal to the S-planes.
In SC´-type shear bands, the C-planes dip at low angle (15 – 35°) into shear direction (Passchier & Trouw, 2005). This type mainly develops in strongly foliated phyllonites. At the transition to layers which are more weakly foliated, I observed that the shear bands end.

Figure 47: Large scale SC-fabric indicating to a top-to-SW-shear direction.

Figure 48: Top to SW directed movement in a shear band with SCC´-fabric.

Shear bands in the Ab-Chl-schists show a top to SW directed movement (figure 47 and 48). S-planes have developed from former veins, which were subjected to intensive deformation at high strain (figure 48).

4.4.2.2. Flanking structures

Flanking structures are deflections of initially planar markers around a central discontinuity in flowing media (Paschier, 2001; Grasemann et al., 2004). They develop if a transecting element, like a vein for example, is present in the host rock, which causes heterogeneous deformation in the immediate vicinity. If the transecting element is rheologically softer than the host element, a shear zone is developing with synthetic displacement (s-type flanking structure) or antithetic displacement (a-type flanking structure). S-type flanking folds develop along co-shearing contractional slip surfaces, whereas a-type flanking folds develp along counter-shearing contractional slip surfaces (Grasemann et al., 2003; Exner et al., 2004; Wiesmayr & Grasemann, 2005;). On Kythnos Island, flanking structures mostly occur in mylonitic marbles and the Ab-gneisses (figure 49).

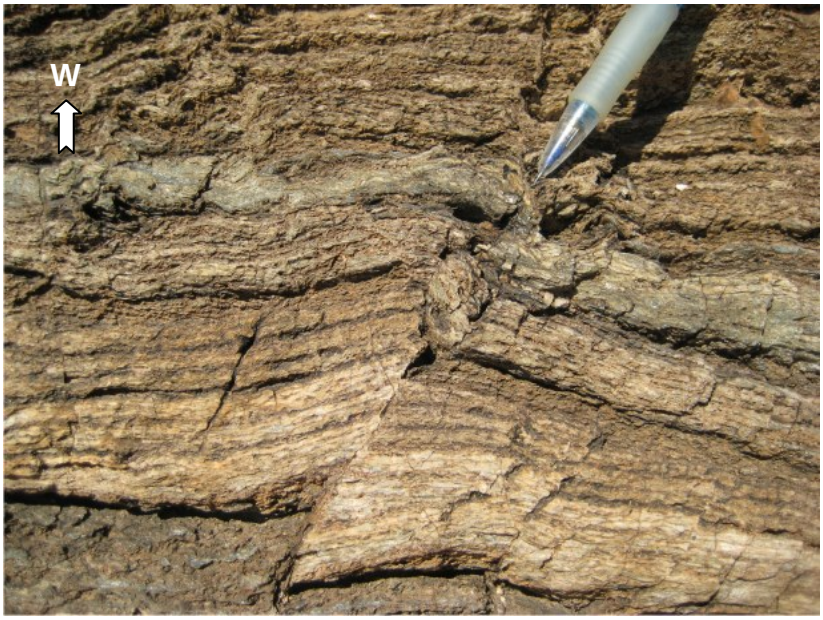

Figure 49: A-type flanking structure in Ab-gneiss shows sinistral (antithetic) shear sense.

4.4.3. Brittle Deformation

Structures, developed during the later brittle deformation phases, can be found in all lithologies of Kythnos. By way of cross cutting relationships, orientation and geochemistry the different generations of brittle extension gashes are distinguishable.

4.4.3.1. Normal faults

N-S directed extension results in a conjugated set of mostly high-angle normal faults which strike through the lower angle ultramylonitic shear zone. Ongoing extension causes the rotation of prior

normal fault to lower angles (figure 50 and 51). Especially within the quartzites in the southernmost part of the island, the intensive brittle faulting caused a strong fracturing of rocks, eventually leading to cataclasis.

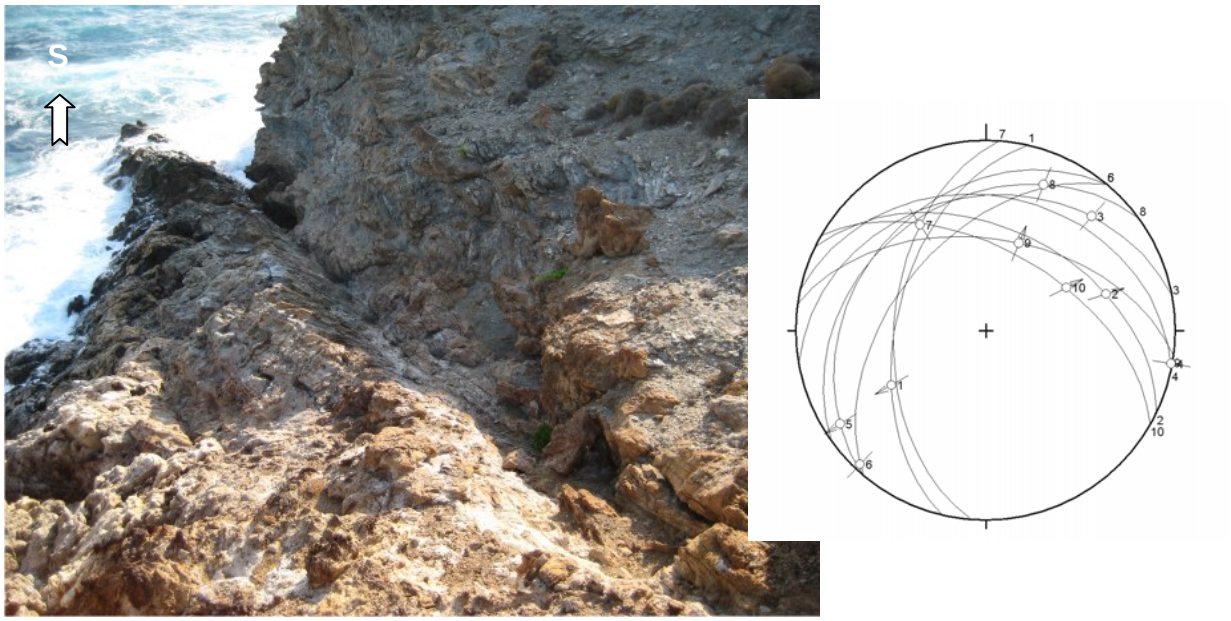

Figure 50: Left: Major normal fault, top to SW. Right: Angelier plot of conjugate brittle normal faults dipping towards SW and NE at moderate angles, indicating to NW-SW extension.

Figure 51: Major normal fault with top-to-S kinematic.

Figure 52: Set of brittle high-angle normal faults.

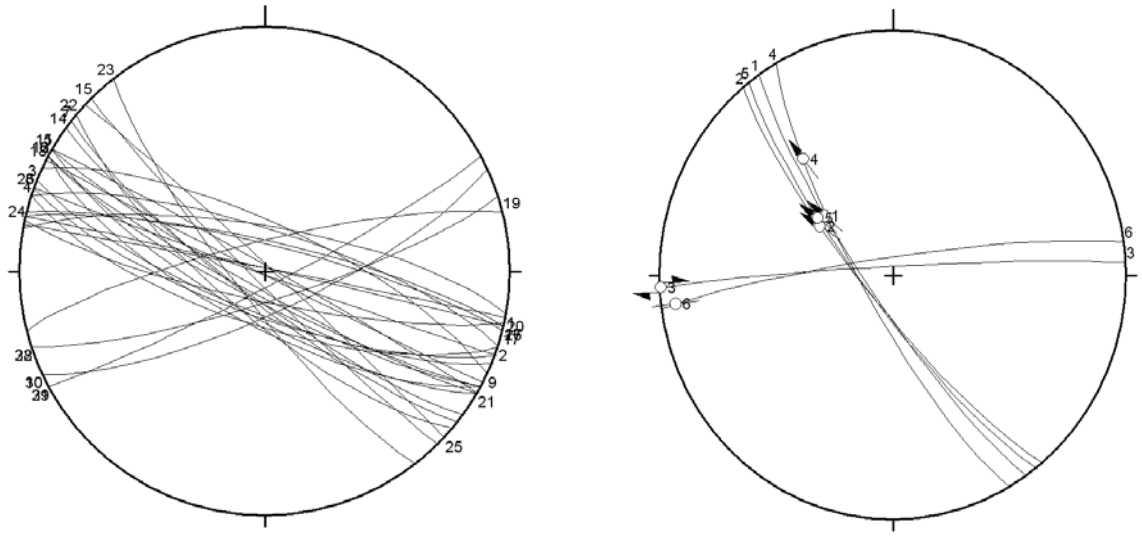

Figure 53: Left: Schmidt plot of conjugated high-angle faults mainly striking NW-SE with a secondary NE-SW direction. Right: Angelier plot of high-angle normal faults, mainly striking NW-SE but also in E-W direction. Both indicate to NW-SW extension.

4.4.3.2. Veins

The latest stage of brittle extension causes the evolution of a complex system of extension gashes and joints. Veins are filled with Qtz, white Cal, red coloured, Fe-bearing carbonates or hydrothermal Fe and Brt mineralizations. Due to their orientations and crosscutting relationships and also their vein-fillings, four distinct generations of extension gashes are distinguishable in the field (figure 56). The oldest generation of veins comprise Qtz and white Cal cements. Most of these veins are already rotated nearly parallel to the foliation, dipping north at very low angles. They show ductile deformation, e.g. folding and, especially for the more competent Qtz occurences, boudinage. In highly deformed rocks, the type 1 generation veins are principally confined to the hinge area of folds. The conjugated system of the type 2 veins is generally steeper dipping towards the S or ENE. These are predominantly filled with Cal, whereas the carbonates are sometimes coloured red because of the influence of Fe-oxides and –hydroxides. Very similar to the type 2 veins is the third generation of extension gashes. These are also steeper dipping and form conjugate sets which are striking NE-SW and NW-SE, crosscutting the type 2 veins. Concerning the geochemical composition, there are no significant differences, so these two types have probably formed from similar fluids or from fluids with similar origins. Both type 2 and type 3 partly show ductile deformations, so there must have been either a regime with appropriate temperatures allowing the Cal to react ductilely, or a correspondingly low strain rate.
The final stages of fracturing form very prominent structures, especially in the southernmost part of the island. Further NE-SW directed extension in the Aegean region causes the development of a complex system of conjugate high-angle faults. These are nearly vertical, striking NW-SE. This is caused by the NE-SW extension ($\sigma 3$), leading to a maximum shortening ($\sigma 1$) in the NW-SE direction. The type 4 extension gashes are filled with Cal or Qtz, which show a strong hydrothermal overprint. These veins therefore often comprise Fe-mineralizations and Brt. Most probably they form mode I opening joints (figure 54 and 55), locally including several generations of fillings, in view of the fact that most have been reactivated occasionally. The late high-angle joints and gashes penetrate the overall sequence of lithologies.

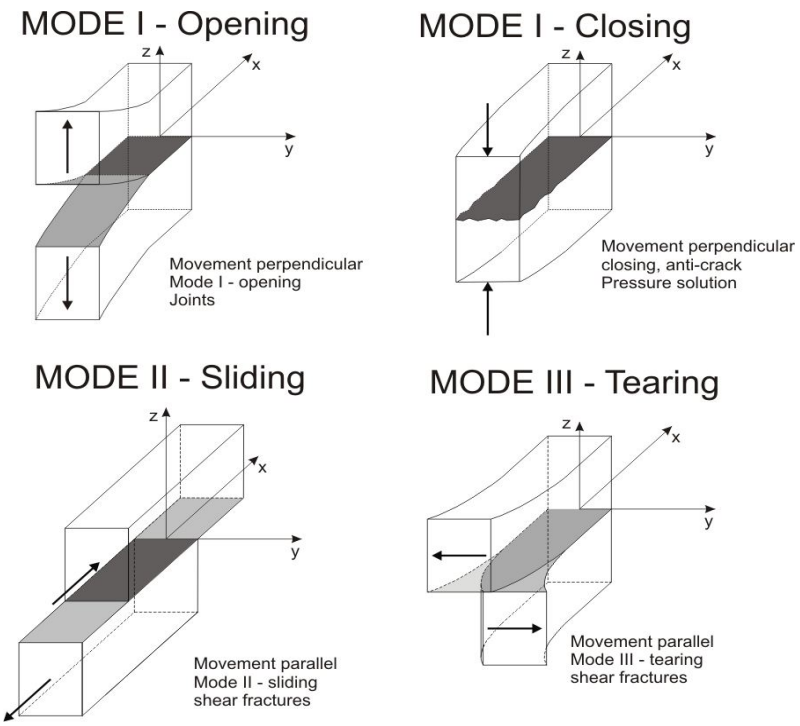

Figure 54: Different types of dislocation of brittle fracturing (Irwin, 1957; modified by Laner, 2009). Mode I – conditions result in generation of joints (opening-mode) or formation of pressure-solution-planes (closing-mode). Mode II - and mode III – conditions lead to the formation of shear zones, which are not opened.

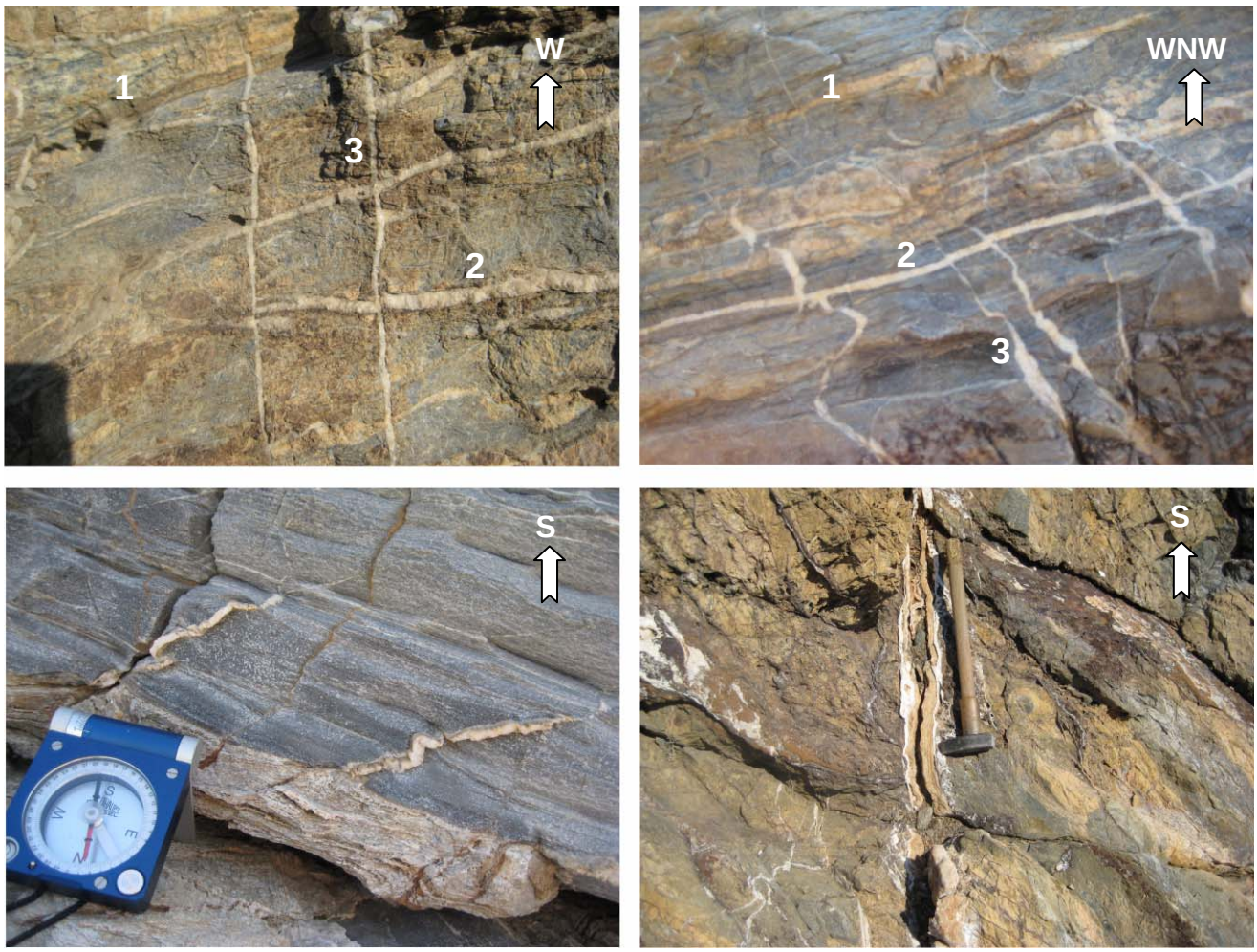

Figure 55: Top: type 1-3 veins within the marble ultramylonit unit. Down left: type 3 veins are crosscut by a type 4 vein. Down right: mode 1-open-type 4 vein containing Cal and hydrothermal Fe-mineralizations.

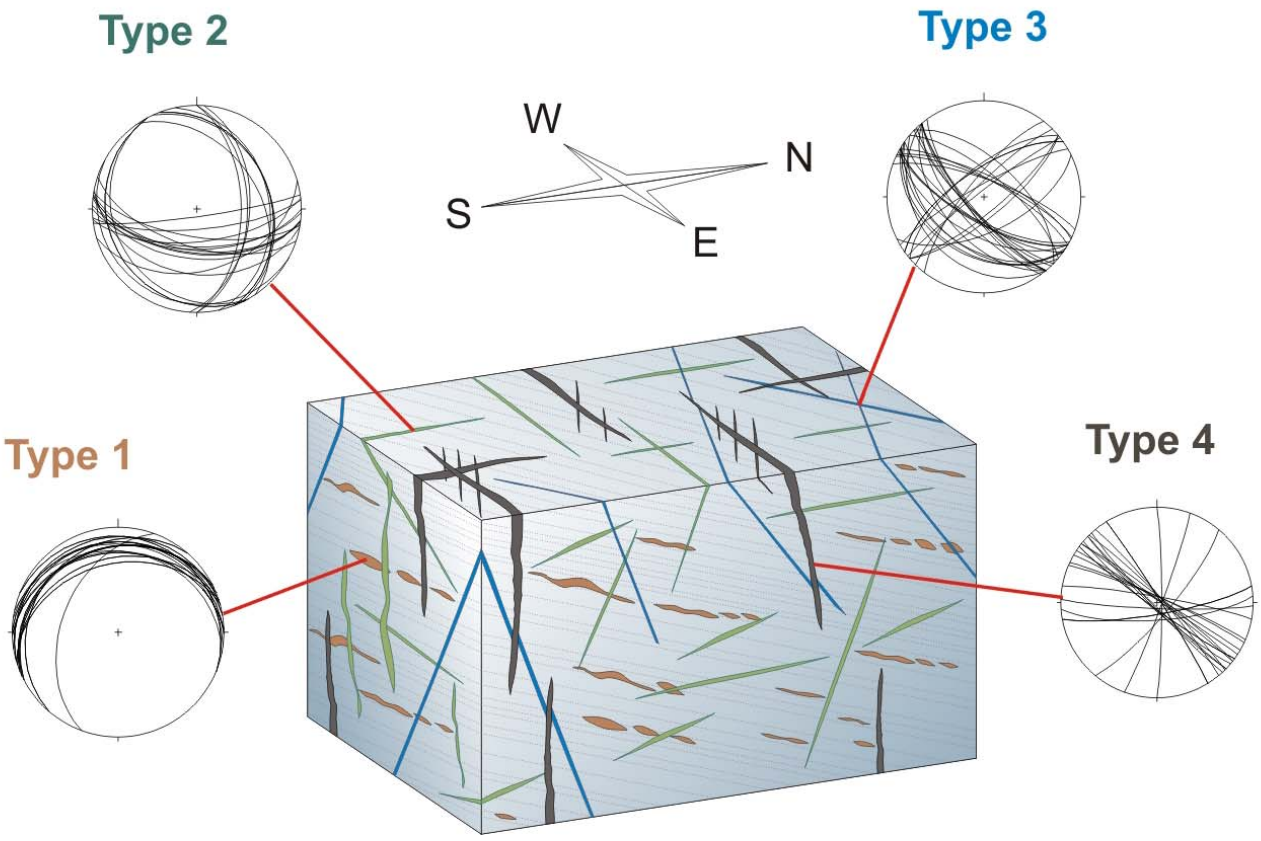

Figure 56: Synoptic plot with vein-generations.

4.4.4. Summary of deformation phases

The rocks of Kythnos Island have been affected by various stages of ductile and brittle deformation. Keither et al. (2008) described 3 ductile compressive deformation phases: Two generations of shear folding and a younger tight to isoclinal shear folding. As the younger greenschist-facies overprint was very strong, the penetrative isoclinal deformation is the dominant structure on Kythnos. According to our field observations, it is characterized by subhorizontal axial planes and NE-SW trending fold axes with SW vergence. Additionally a subordinate isoclinal folding, with subhorizontal axial planes striking NW-SE was observed. This younger folding stage, under greenschist-facies conditions, has caused a penetrative schistosity and mineral lineation trending NE-SW. According to Keither et al. (2008), the strongly compressive character of this deformation phase might be caused by an interruption in rock-exhumation with a period of reburial or renewed crustal stacking under greenschist-facies conditions in the Upper Oligocene and Lower Miocene. Deformation results in a large-scale recumbent fold.

This structure was then affected by a later upright folding, below the ductile-brittle transition. This was caused by incipient N-S extension in the Aegean Sea and therefore a strong shortening

perpendicular to the stretching direction. In the field we observed, that mineral lineation was rotated towards N, trending now NNE-SSW, with a direction of shear of top to SSW. Ongoing NNE-SSW extension caused the generation of a large scale normal fault in the south of Kythnos. Strain was localized in marbles. Therefore we assume that they acted as a kind of lubricant, also at lower temperatures. Marbles responded to high strain with grain size reduction and mylonitization. With continuing exhumation, brittle conditions were reached and further displacement results in cataclasis of the marbles.

The youngest structures observed on Kythnos are brittle normal faults and, due to ongoing NNE-SSW extension, several generations of brittle fracturing. Due to their orientations, cross cutting relationships and fillings, we were able to distiguish at least 4 generations of extension gashes (figure 56). The youngest type 1 veins have already been rotated in direction of foliation planes. Type 2 and type 3 veins are more steeply dipping and still show ductile deformation. As they have similar geochemical compositions, they might have generated from fluids of same or similar origin. Type 4 veins differ noteably from the rest. They are distinct, nearly vertical and include Fe- and Brt-mineralizations which point to hydrothermal activities.

4.5.5. Synoptic diagram

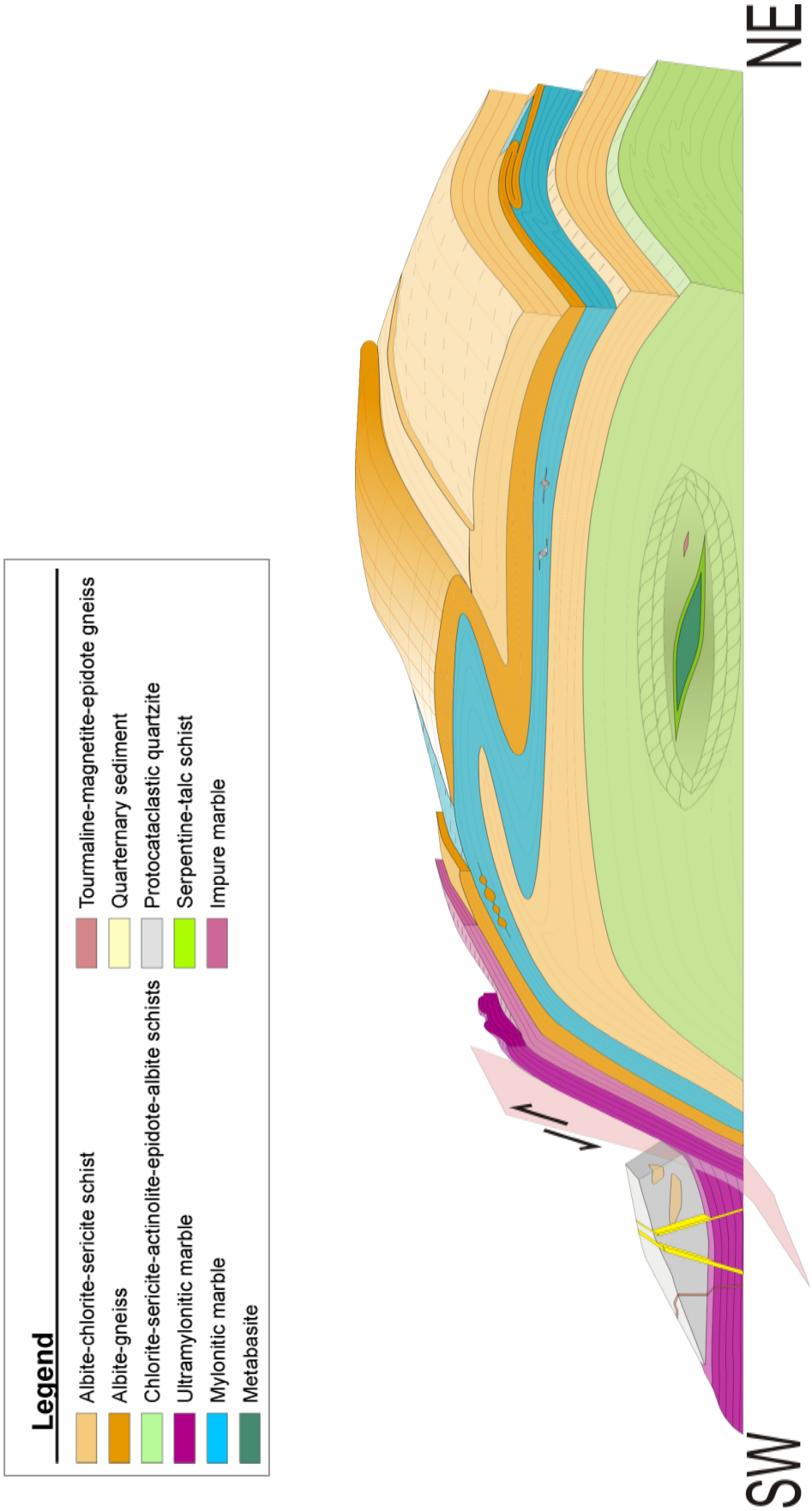

Figure 57: Synoptic diagram of major structures and lithologies on south-Kythnos after Lenauer (2009).

5. GEOCHEMISTRY OF CARBONATES

5.1. Stable Isotopes

5.1.1. Carbon

Carbon has two stable isotopes with the following abundances (Hoefs, 2004): ^{12}C: 98.89 % and ^{13}C: 1.11 %. Terrestrial carbon appears in sedimentary carbonates or organic matter. Both have two totally different isotopic abundances because of two different reaction mechanisms (Hoefs, 2004):

- Kinetic effects during photosynthesis result in a preferred incorporation of the light isotope (^{12}C) in organic materials.
- Within the inorganic carbon system (atmospheric CO_2 <-> dissolved bicarbonate <-> solid carbonate) an enrichment of the heavier isotope (^{13}C) is generated because of isotope equilibrium exchange reactions.

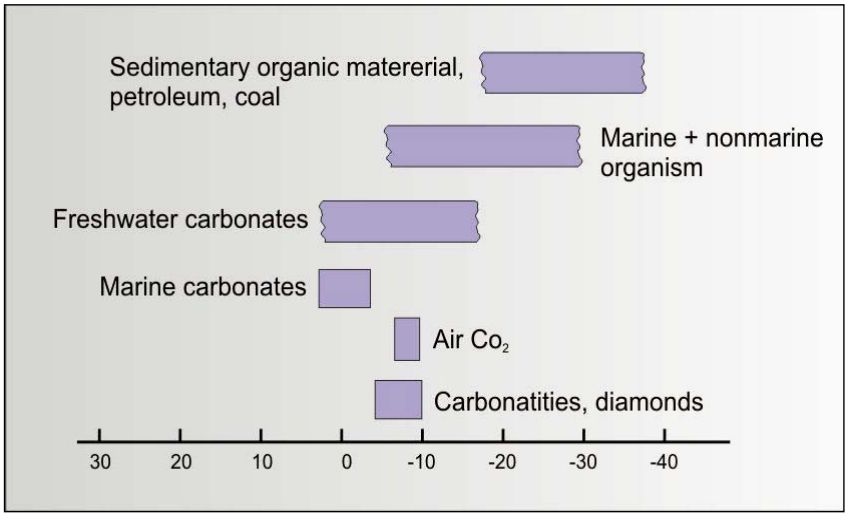

Figure 58: δ^{13} C values of carbon reservoirs (modified after Hoefs, 2004)

The $\delta^{13}C$ values (explanation of δ-value in 5.1.3.) of foraminifera can be used as a paleoceanographic tracer. It can also be applied to trace deep water circulation, since carbonates of deep water become isotopically lighter because of incremental reoxidation of the isotopically "light" (in ^{12}C enriched) organic matter (figure 58).

5.1.2. Oxygen

Oxygen has three stable isotopes with different frequencies of occurrence (Garlick, 1969):
^{16}O: 99.763 %, ^{17}O: 0.0375 %, ^{18}O: 0.1995 %. Oxygen isotope ratio analyses are very suitable for the study of fluid-rock interactions, since such interactions cause a shift of the primary isotope ratios of both rock and water. There are three possibilities to explain the exchange mechanism:

- **Solution – precipitation**: Smaller grains dissolve and recrystallize on the surface of larger ones. While the material is in solution an isotopic exchange can take place.
- **Diffusion**: Two isotopes with the same energy have different velocities due to differences in mass. So the lighter isotope will travel faster and thus will diffuse sooner.
- **Chemical reaction**: Because of great differences in chemical activity among fluid and solid, chemical reaction occurs. The new crystal is formed at or near the isotopic equilibrium with the fluid phase (Hoefs, 2004).

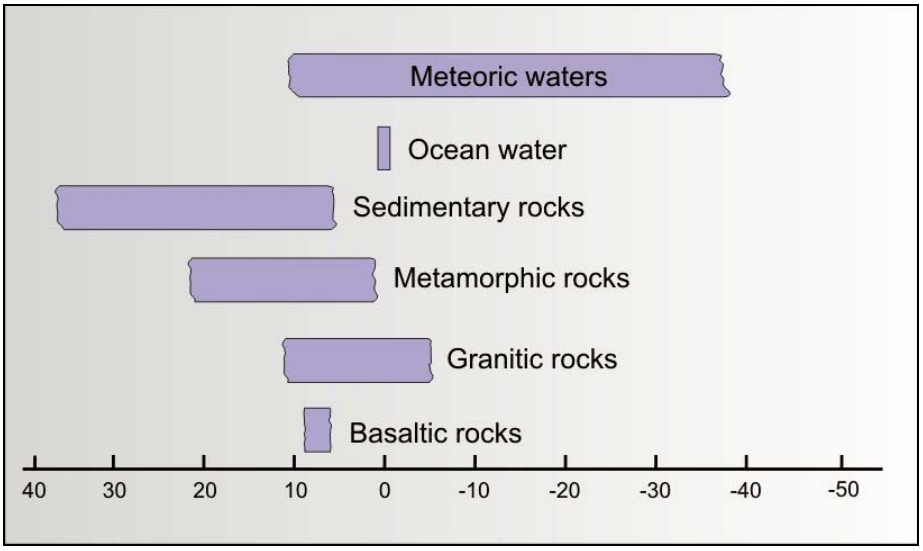

Figure 59: δ-^{18}O ratios of common geological reservoirs referred to SMOW-standard (modified after Hoefs, 2004)

Diagenesis of carbonates:

In general, effects of diagenesis increase with increasing time and depths of burial. The δ^{13}C values are usually less affected by diagenesis than the δ^{18}O values. This can be explained by the fact that fluids contain much less carbon than oxygen (Hoefs, 2004).

Diagenesis of carbonates can be split into a *meteoric* and a *burial pathway*. If carbonates are deposited in shallow marine environment they are strongly influenced by *meteoric* waters. These waters are basically rich in CO_2, which leads to the transformation of metastable aragonite and Mg-calcite to the more stable low-Mg-calcite. During processes of dissolution and reprecipitation a shift in isotopic composition towards isotopic equilibrium of the fluid phase takes place. The second diagenetic process is the extent of oxidation of organic material, which changes with increasing burial depths. Both processes result in a depletion of the heavier C-isotope. Deep sea carbonates are subjected to the *burial pathway.* The enclosed pore waters are in equilibrium with the carbonates, because they are of marine origin. Increasing diagenesis leads to a rise in temperature and pressure, so pore waters are squeezed out ascending to overlying sediment layers. In general, increasing burial results in a depletion of ^{18}O because of a raise in temperature, and a shift to lighter C-isotopes as organic material is oxidized. At greater depths, on the other hand, methane can be produced by the thermal cracking of kerogen. Methane is

enriched in ^{12}C, leaving the residue enriched in ^{13}C. So $\delta^{13}C$ values become less negative which means enriched in the heavy isotope (Faure, 1986; Hoefs, 2004).

Metamorphism

The isotope composition of metamorphic rocks is controlled by the composition of the protolith, the effects of volatilization with increasing temperature and exchange processes with infiltrating fluids or melts (Hoefs, 2004). In metamorphic rocks especially, fluids have an important role for isotope chemistry. There is a general tendency towards a decrease in ^{18}O with increasing metamorphic grade. In the absence of infiltrated fluids, the isotopic shift results from net transfer reactions, which amount only 1 ‰ or even less for an increase in temperature of about 150 °C (Kohn, 1993; Young, 1993). So, large-scale fluid transports in the crust are necessary to obtain depletions up to 10 ‰ such as being observed in marbles and especially veins in south-Kythnos. Fluid movement in rocks can be pervasive, which means that fluids move independent of structural or lithological conditions. Therefore differences in isotopic chemistry get homogenized. The channelized fluid-flow uses vein-systems, weak or shear zones or other channelways such as rock contacts or more permeable lithologic units to migrate (Baumgartner & Valley, 2001). Thereby only certain beds or units of the rock are influenced by the fluid, and thus are subjected to local equilibration. Channelized fluid flow leads therefore to chemical heterogenity, since parts of the rocks remain unaffected by fluid-interaction. If fluids are completely absent, an isotopic exchange is only possible by diffusion over very short distances of some centimetres (Bestmann, 1994; Hoefs, 2004)

The isotopic composition of metamorphic rocks is generally dependent of the composition of the protolith, processes of volatilization, the temperature and the fluid influx (Bestmann, 1994).

During metamorphism, marbles can act as a barrier to fluid flow, because they are relatively impermeable. Thus homogenization is inhibited and fluid flow only concentrates on certain channels. Massive marbles can preserve their sedimentary isotope-signatures even up to very high metamorphic grades (Valley et al., 1990). The development of fractures also facilitates an isotopic exchange in certain rock volumes. If a rock does not offer enough permeability, the isotopic composition can vary even over short distances (Faure, 1986). Thus, massive marbles are, in general, quite impermeable to the influx of fluid under moderate metamorphic conditions. But shear zones are often preferred pathways for fluids, facilitating fluid circulation also in primarily impermeable rocks. Thus the stable isotope composition of these rocks can give an inference to fluid infiltration during metamorphism (Bestmann, 2000). Within calcites especially the oxygen isotopes are very sensitive to diffusion whilst processes of fluid-rock interaction. So the original $\delta^{18}O$-ratio of the hostrock is changed by the infiltration of fluids with different isotopic compositions. The newest trends in the analysis of metamorphic rocks are the modelling of isotope discontinuities, called isotope fronts, and the numerical modelling of isotope exchange between minerals. Therefore precise micro-analytical techniques and a detailed mm sampling are required to obtain quantitative information on fluid fluxes, direction of fluid flow and duration of

infiltration events. Several authors, e.g. Abart (1995), Abart et al. (2002), Baumgartner & Rumble (1988), Ganor et al. (1988), Bickle & Baker (1990), Cartwright & Valley (1991), Dipple & Ferry (1992), Baumgartner & Valley (2001), concentrated on this topic.

5.1.3. Preface and methodology

Isotope abundances are measured by relative differences in abundances between two samples. But to be able to calculate the δ-values, it is necessary to have a reference system (standard) with known absolute isotope ratios. The δ-value (given in per mill) is calculated as shown below (Craig, 1957). The R-value is the ratio of heavy isotope relative to the lighter isotope.

$$\delta = \left(\frac{R_{Sample} - R_{S\,tan\,dard}}{R_{S\,tan\,dard}} \right) \cdot 1000$$

For the isotopic composition of carbon the PDB standard (*Belemnitella americana* from the Cretaceous Peedee formation, South Carolina) is used worldwide. The isotope ratios of oxygen are usually referred to the V-SMOW standard (Vienna-Standard Mean Ocean Water). Sometimes, like in our analyses, the PCB-standard is used for oxygen too, because with the MultiPrep™ method carbon and oxygen isotopes are measured simultaneously.
SMOW-ratios are converted to PDB-values as follows: SMOW=1.03091*PDB+30.91.

Principles of Mass Spectrometry:
Information on Mass Spectrometry was taken from McCrea (1950), Faure (1986), Sparkman (2000), Brand (2004) and Hoefs (2004).
Mass spectrometry (MS) is an analytical method to identify the chemical composition of samples due to mass-to-charge-ratio of charged particles. It is also possible to determine the isotopic composition of samples, but because of very minor differences in mass, very sensitive instruments are therefore required. These are the so called Isotopic Ratio Mass Spectrometers (IRMS).

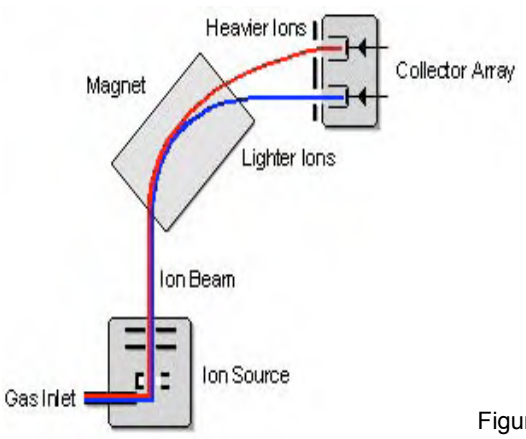

Mass Spectrometers are basically made up of an ion source, a mass analyzer and a detector (see figure 60). The *ion source* produces electrons by a thungsten or rhenium filament which is heated. The electrons are passed through two charged plates and collide with the sample-elements. Thereby electrons of the sample are removed, resulting in positively charged ions.

Figure 60: Essential modules of a Mass Spectrometer.
(Source: http://www.climatechange.umaine.edu/classes/Kreutz/ SIAnalysis.pdf)

The *mass analyzer* separates the positive ions by their masses. It contains an electromagnet which is arranged so that its magnetic field lines are positioned normal to the direction of travel of the ion beam. Thus the magnetic field deflects the ions by the rule of Lorentz into circular paths which radii are proportional to the masses. As shown in figure 60 the lighter ions get more deflected than the heavier ones.

The *detector* comprises the Farraday cups, which are positioned behind a slit plate. If an adequate beam enters the collector slit and reaches the Farraday cup, it gets neutralized and thus a voltage difference can be measured (Faure, 1986).

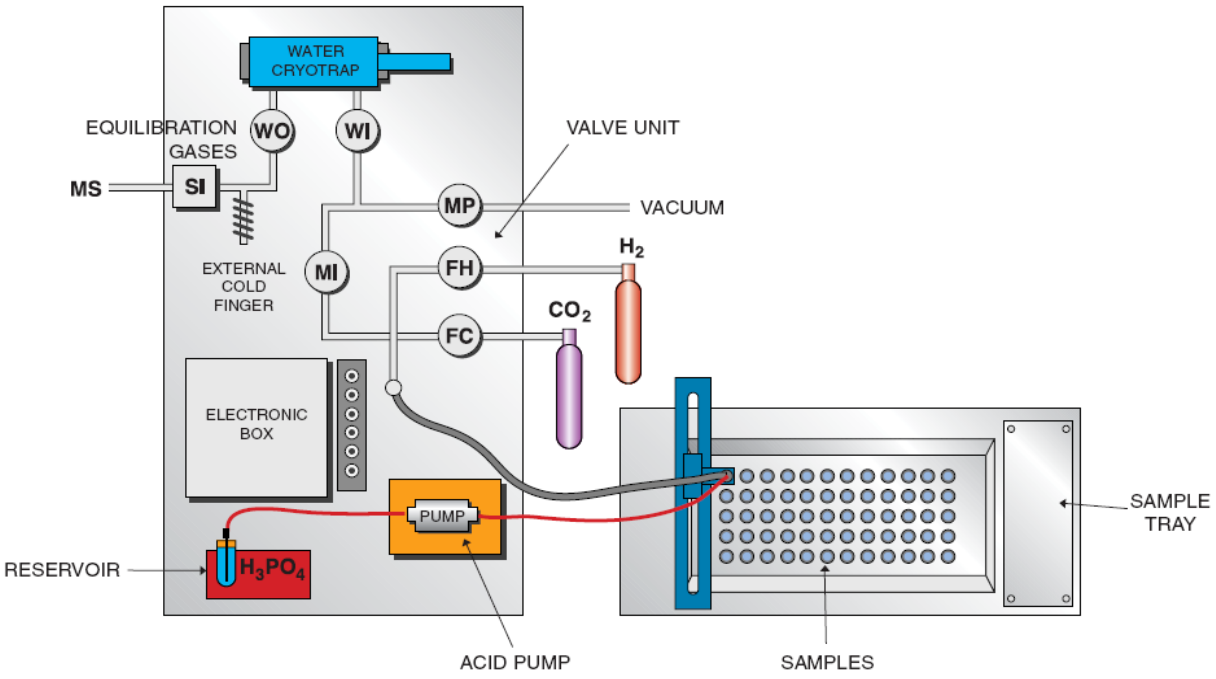

Figure 61: Schematic setup of the MultiPrep™ system of a Micromass IRMS for carbonat analyses (source: http://nytek.dev.3wstyle.ru/download/FL53V2.pdf).

Sample preparation and operations:

- Carbonate samples of extension gashes and marble layers are extracted by a micro-drill.
- An aliquot of the samples (250 to 350 µg) and the NBS19-standards is weighed into small tin-saggars and then decanted into vials.
- Samples are dried for 24 hour in the electric heater at 50 °C.
- The vials are sealed with silicone septa.
- Vials are evacuated at the MultiPrep™ (figure 61) and then dispensed with about 3 drops of pure phosphoric acid.
- Samples are heated up to 80 °C on the sample tray.
- Carbonates dissolve under release of CO_2 ($CaCO_3+H_3PO_4 \rightarrow CaHPO_4+CO_2+H_2O$)

- The envolved gas is passed through the water/cryotrap and collected in the external cold finger.
- The gas to be analysed is a trace gas in a stream of carrier gas which achieves viscous flow conditions (Hoefs, 2004).
- The CO_2 gas from the inlet system is introduced to the ion source. There the molecules are ionized via electron impact.
- The ions are separated by a magnetic field by different deflecting in terms of mass according to the Lorentzian rule.
- The separated ions are finally detected by a Multiple Farraday Cup Detector.

5.1.4. Results

Sample	Weight [µg]	δ13C [‰] (PDB)	Precision	δ18O [‰] (PDB)	δ18O [‰] (SMOW)	Precision
kg10-a2a	348	-3,54	0,12	-15,38	15,06	0,15
kg10-aa	298	-4,00	0,12	-9,14	21,49	0,15
kg10-ab	270	-5,07	0,12	-10.57	20.01	0,15
kg10-ac	318	-1,54	0,12	-9,93	20.67	0,15
kg10-ba	287	-2,47	0,12	-12,85	17,66	0,15
kg10-bb	309	-3,89	0,12	-13,45	17,04	0,15
kg10-ca	335	-2,86	0,12	-12,86	17,66	0,15
kg10-cb	333	-3,83	0,12	-13,85	16,63	0,15
kg11-9d	282	-2,35	0,12	-14,27	16,20	0,15
kg12-1	368	-5,59	0,12	-23,42	6,77	0,15
kg12-14a	340	-4,60	0,12	-20.20	10.08	0,15
kg12-14b	326	-3,37	0,12	-16,36	14,05	0,15
kg12-15a	340	-3,48	0,12	-17,19	13,19	0,15
kg12-15b	324	-3,82	0,12	-17,67	12,70	0,15
kg12-5	400	-6,56	0,12	-24,26	5,90	0,15
kg12-9v12-x	346	-4,72	0,03	-18,43	11,91	0,04
kg12-9v12-y	339	-3,66	0,03	-16,56	13,84	0,04
kg12-9v13	299	-2,52	0,03	-15,80	14,62	0,04
kg12-9v16	260	-2,30	0,03	-14,10	16,38	0,04
kg12-9v17	322	-3,56	0,03	-15,85	14,57	0,04
kg12-9v19-x	255	-3,78	0,03	-17,11	13,27	0,04
kg12-9v19-y	311	-3,72	0,03	-17,20	13,18	0,04
kg12-9v2	350	0.43	0,03	-13,93	16,55	0,04
kg12-9v20-x	287	-3,47	0,03	-15,57	14,86	0,04
kg12-9v20-y	278	-3,61	0,03	-15,83	14,59	0,04
kg12-9v21	311	-4,12	0,03	-17,77	12,59	0,04
kg12-9v23-x	304	-2,98	0,04	-14,00	16,47	0,05
kg12-9v23-y	348	-2,89	0,04	-13,88	16,60	0,05
kg12-9v24	310	0.63	0,04	-5,89	24,84	0,05
kg12-9v25	385	-3,54	0,04	-12,15	18,39	0,05
kg12-9v26a	302	-3,38	0,04	-16,26	14,15	0,05
kg12-9v3	265	0.00	0,04	-15,04	15,40	0,05
kg12-9v4-x	254	-0.38	0,04	-14,68	15,77	0,05
kg12-9v4-y	295	-0.20	0,04	-14,57	15,89	0,05
kg12-9v7-x	291	-6,77	0,04	-6,90	23,80	0,05
kg12-9v7-y	344	-6,72	0,04	-6,74	23,96	0,05
kg12-9v8-x	310	-3,19	0,04	-13,32	17,18	0,05
kg12-9v8-y	308	-3,00	0,04	-13,44	17,05	0,05
kg13-3a	328	-2,89	0,04	-14,30	16,17	0,05

kg13-3b	337	-3,34	0,04	-15,06	15,38	0,05
kg13-6	410	-3,52	0,04	-17,76	12,60	0,05
kg13-9v1	254	-3,08	0,04	-12,46	18,07	0,05
kg13-9v10	345	-3,21	0,04	-11,31	19,25	0,05
kg13-9v2	318	-3,18	0,04	-11,56	19,00	0,05
kg13-9v4	300	-2,99	0,04	-12,50	18,03	0,05
kg13-9v5a-x	273	-3,24	0,04	-14,44	16,03	0,05
kg13-9v5a-y	302	-3,11	0,04	-14,43	16,04	0,05
kg13-9v5b	262	-3,25	0,04	-14,72	15,73	0,05
kg13-9v9-x	290	-2,18	0,04	-10.25	20.34	0,05
kg13-9v9-y	330	-2,00	0,04	-10.32	20.27	0,05
kg28-ab	341	0.70	0,04	-12,49	18,04	0,05
kg2-aa	339	2,64	0,04	-10.72	19,86	0,05
kg2-ac	326	0.41	0,04	-12,66	17,85	0,05
kg4-c	375	-8,17	0,04	-10.39	20.20	0,05
kg-11-aa	296	2,32	0,02	-9,37	21,25	0,06
kg-11-ab	354	2,76	0,02	-9,58	21,03	0,06
kg-11-c	306	-3,01	0,02	-13,85	16,63	0,06
kg-11-da	348	-2,07	0,02	-13,50	17,00	0,06
kg-11-db	310	-2,00	0,02	-12,96	17,55	0,06
kg-11-e	284	-1,13	0,02	-13,44	17,06	0,06
kg-1-9aa	309	3,24	0,02	-2,08	28,77	0,06
kg-1-9ab	308	3,03	0,02	-3,12	27,69	0,06
kg-28-8aa	287	-4,05	0,02	-8,06	22,60	0,06
kg-29-8ab	284	1,93	0,02	-10.90	19,67	0,06
kg-29-8ba	296	1,90	0,02	-6,57	24,14	0,06
kg-29-8bb	306	1,24	0,02	-6,35	24,37	0,06
kg-2-9aa	294	2,83	0,02	-6,68	24,03	0,06
kg-2-9ac	301	-0.16	0,02	-18,37	11,97	0,06
kg-2-ba	301	2,77	0,02	-3,85	26,94	0,06
kg-2-bb	295	2,59	0,02	-3,80	26,99	0,06
kg-4-a	320	2,25	0,02	-10.63	19,96	0,06
kg-4-ba	331	1,13	0,02	-10.71	19,87	0,06
kg-4-bb	320	1,19	0,02	-14,99	15,45	0,06
kg-4-d	291	1,75	0,02	-9,90	20.70	0,06
kg-4-ea	354	0.52	0,02	-11,25	19,32	0,06
kg-4-eb	312	0.44	0,02	-12,75	17,77	0,06
kg-4-f	313	-2,56	0,02	-12,80	17,72	0,06

Table 1: Isotope-ratios of various marbles and calcitic veins of Kythnos Island.

5.1.4.1. Isotopic composition of marbles

As already mentioned in 5.1.2., massive marbles are quite impermeable to the fluid-influx. However, in such a case fluid circulation can be concentrated to shear zones, which are the preferred pathways for fluids even in non-permeable rocks. Infiltrated fluids, in general, will shift the isotope composition of the ambient rock away from its initial value. To get indications of the influence and the importance of fluid infiltration and fluid flow in the shear zone, respectively, during deformation in S-Kythnos, several marbles, mylonitic marbles and marble ultramylonites, all of them calcitic, were sampled and analyzed in terms of ^{13}C and ^{18}O. Across the major shear zone complex, two complete profiles were sampled and analyzed, to get information about the isotopic distribution with respect to the distance from “detachment”.

Figure 62 gives a general view of the specific isotope compositions of different marble units of our research area and the adjacent islands of Kea and Serifos as well as marbles of the north Aegean island of Thassos, which have already been analyzed by Bestmann (1994, 2000). Results of both carbon and oxygen isotope ratios are referred to the PDB-standard. For a better reproducibility and the calculation of the deviation, samples were measured alternately with the international NBS 19 calcite standard. The extraction of sample-powders from marbles was made by a micro-drill with diamond-head. If the marble-samples had visible differences in term of colour, grain size or mineralogy, the different layers were sampled and analyzed individually.

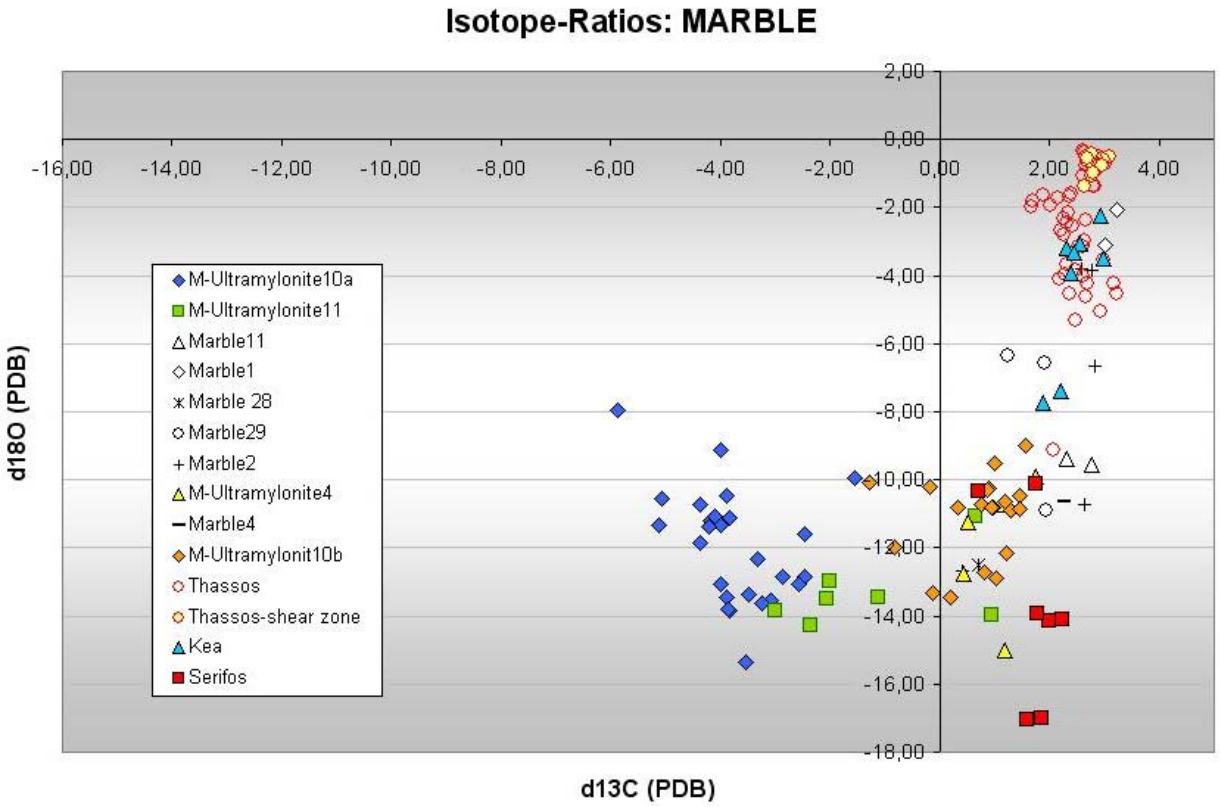

Figure 62: δ^{13}C- and δ^{18}O-ratios of different marble units of Kythnos compared to marbles of the adjacent islands Kea and Serifos and to marbles of the north Aegean island of Thassos. Isotope ratios are given in per mill [‰].

Figure 62 represents a general overview of all results of the analyzed marble-samples. The δ^{13}C-ratios of all samples range from -5.88 to 3.24 ‰, whereas the δ^{18}O-ratios vary between -17.04 and -0.34 ‰. It is obvious that different marble units plot in certain C-O-isotope-arrays. Compared to the highly strained marble-ultramylonites of Kythnos, marbles show, in general, less depletion in the heavy isotopes of carbon. δ^{18}O-ratios, however, display broad variations. The isotope composition of Kythnos-marbles, however, is rather similar to that of Kea and Serifos, especially in terms of ^{13}C. By contrast, the marbles of Thassos-island are characterized by relatively high ^{18}O- and ^{13}C-values. Also the mylonitic and ultramylonitic marbles of the Thassos shear zone complex show no depletion but rather enrichment in heavy isotopes compared to the NBS 19

calcite-standard which is assigned to a value of 1.95 ‰ for $\delta^{13}C$ and -2.20 ‰ in respect of $\delta^{18}O$, both PDB-scale (Coplen, 1996). So oversimplified spoken, the higher strained marbles of Kythnos can be characterized by strong depletions in ^{18}O as well as lower ^{13}C-ratios to some extent.

To obtain possible trends in isotope studies within the different marble-ultramylonite units with respect to distance from “detachment” and therefore varying influence of deformation conditions, two profiles were sampled. The first profile (10a) was sampled in the northern part of the major shear zone, southwest of Aghios Dimitrios (see figure 63). Altogether nine samples of these extremely fine grained marble ultramylonites were taken over a total distance of 120 cm to the shear zone. Therefrom twentysix isotope analyses were carried out, because marbles partly show intense layering and variation in colour from red, to dark grey, yellow and light grey. In principle, the marble-ultramylonites of 10a are characterized by the strongest depletion in ^{13}C, up to -5.88 ‰, and distinct variations in ^{18}O-ratios of more than 7 ‰.

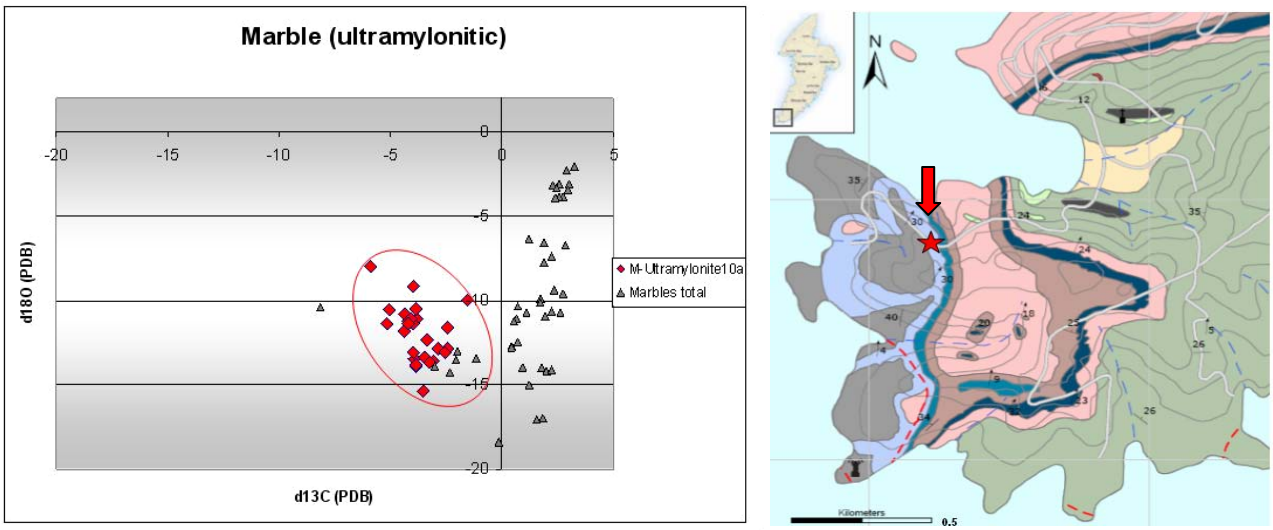

Figure 63: Left: $\delta^{13}C$- and $\delta^{18}O$-ratios of marble-ultramylonites in profile 10a (in red) compared to the isotope composition of all other analyzed marbles (grey symbols). Right: Position of profile 10a (red star) in geological map.

The graphs in profile 10a show a strong impact on isotope composition within the first 15 cm from the fault plane (see figure 64). ^{13}C and ^{18}O-ratios seem to behave the opposite way. In the central field isotopy remains relatively stable, whereas at the end of the profile, close to the contact to the impure marbles and schists of the footwall, isotope ratios of carbon and oxygen fluctuate again.

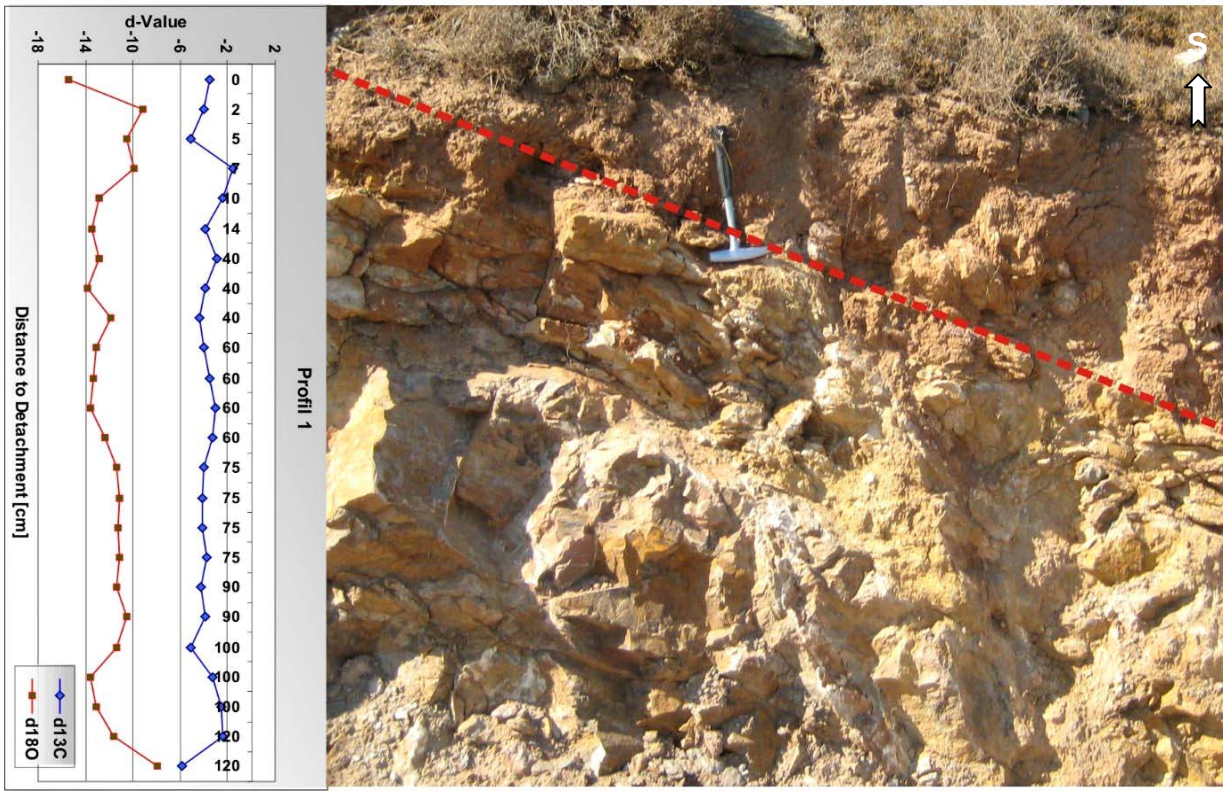

Figure 64: Profile of δ^{13}C- and δ^{18}O-variations in marble-ultramylonites of 10a. Blue graph shows the δ^{13}C-ratios, red graph is related to δ^{18}O. The photo on the right shows the situation at the outcrop, “detachment”-horizon is marked in red. The substratum is built up by ultramylonitic marbles; the top of the shear zone comprises ultra-cataclasites.

The second profile (10b) is situated in the north-western section of the shear zone just next to the coast (figure 65). The overall thickness of this profile is roughly 140 cm. 10 samples were taken from these ultramylonitic marbles from which twenty isotope-analyses have been carried out. Marble-ultramylonites in 10b are also fine grained, but not as much as marbles of 10a. As shown in figure 67, the marbles have a layering in terms of colour.

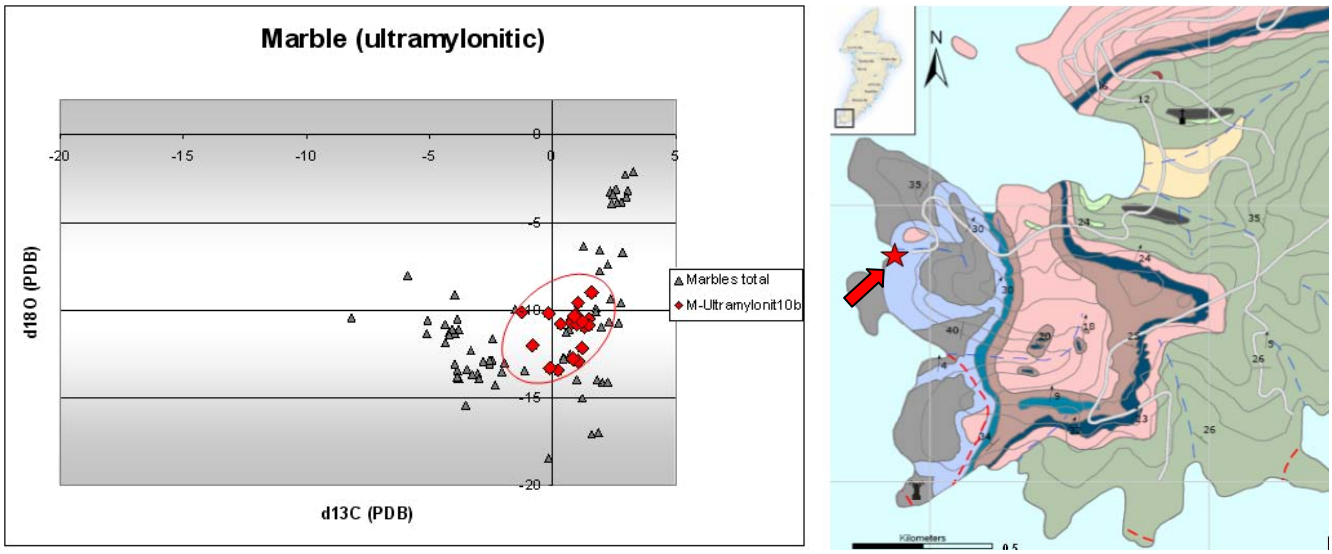

Figure 65: Left: δ^{13}C- and δ^{18}O-ratios of marble-ultramylonites in profile 10b (red symbols) compared to isotope composition of all other analyzed marbles (grey symbols). Right: Position of 10b (red star) in geological map.

The ultramylonitic marbles of profile 10b are not strongly depleted in ^{13}C with ratios ranging from -1.29 to 1.57 ‰ (figure 66). The oxygen data from -13.48 to -8.98 ‰ is quite similar to the marble of the profile 10a (figure 64).

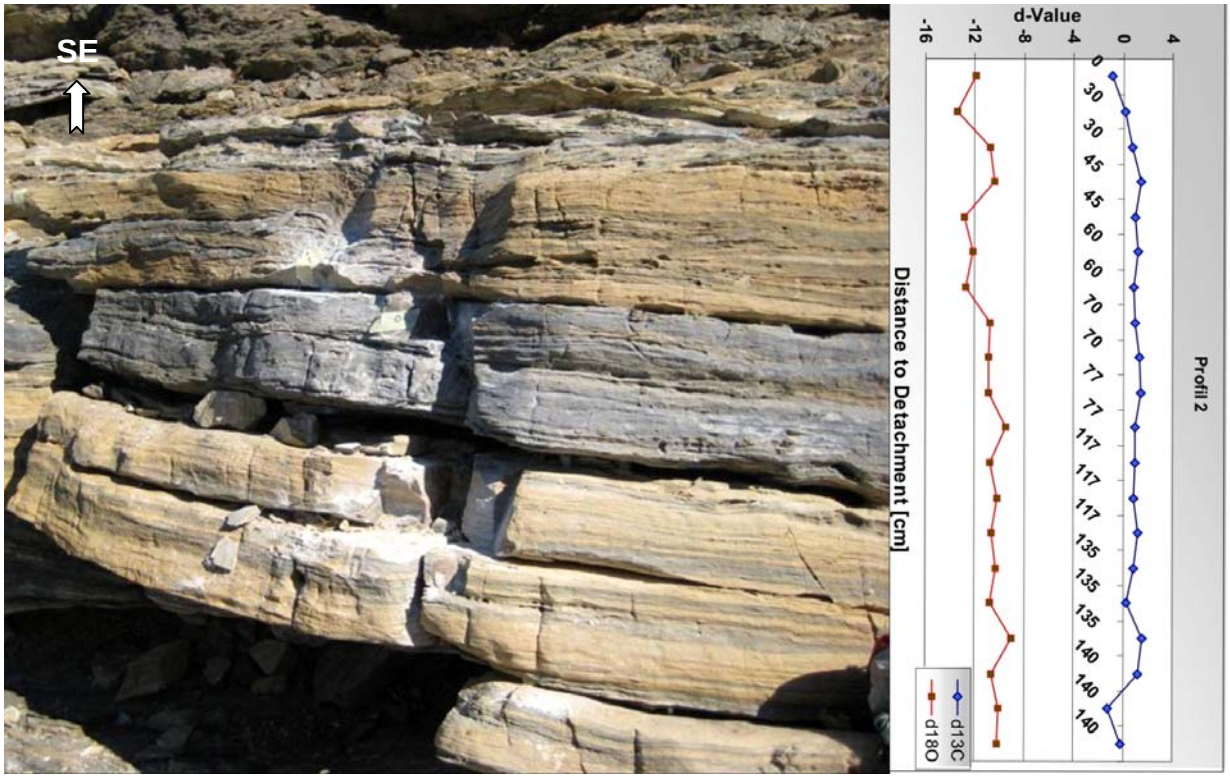

Figure 66: Profile of $\delta^{13}C$- and $\delta^{18}O$-variations in marble-ultramylonites of 10g. Blue graph again shows the $\delta^{13}C$-ratios, red graph is related to $\delta^{18}O$. The photo on the left shows the situation at the outcrop, the shear zone is situated on top of the marble-ultramylonite unit.

The graphs in figure 66 show a relatively consistent trend of the $\delta^{13}C$-ratios, with a slight increase in ^{13}C close to the centre of the shear-zone and some fluctuations at the end of the profile. The $\delta^{18}O$-values seem to be more influenced by the shear zone, showing variations especially within the first 50 cm away from “detachment”. Fluctuations in isotope composition within one sample are due to the intense layering of the marbles. Therefore the isotopy is not homogeneous across an individual sample, which indicates a variable fluid-rock-interaction. As marbles are, in general, very impermeable, fluid flow is either concentrated only in certain “channels” or is predominant only in certain layers.

Figure 68 displays the connection between purity of marble layers and their variation in isotopy. It seems that pale marble layers, which are obviously the purer domains, are not that resistant to isotopic diffusion with respect to the impure, darker layers. One explanation for this phenomenon might be the

Figure 67: Ultramylonitic marble with pale and impurer dark layers, which were sampled separately.

concentration of fluid-flow to predominantly darker layers, which causes an isotopic homogenization of affected marble layers.

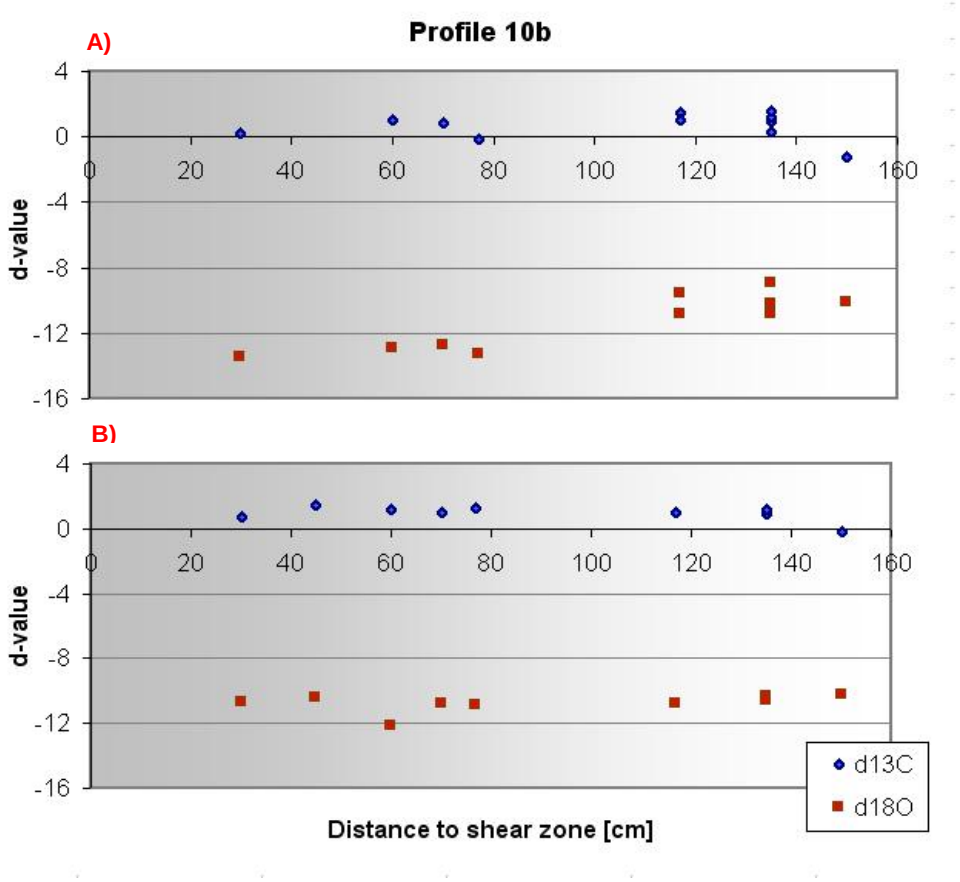

Figure 68: δ^{13}C- and δ^{18}O-ratios of ultra-mylonitic marbles of profile 10b plotted against the distance to the shear zone. Diagram A) shows the isotopic composition of exclusive bright layers, B) displays the isotope-ratios measured in the dark marble-layers. Dark layers evidence more stability in terms of isotopic composition relative to shear-zone-distance.

In addition to the Kythnos marbles, 5 marble-ultramylonites from the detachment zones of the neighbouring islands Kea, in the north and Serifos, in the south, have been analyzed. As shown in figure 69, the Kea-marbles are characterized by relatively high δ^{18}O- and also δ^{13}C-ratios. The oxygen-ratios of marbles sampled in north-Kea reach values of about -2 ‰, whereas marbles of south-Kea have slightly lower values of about -7 ‰. They are situated roughly in the range of the Thassos-marbles, as analyzed by Bestmann in 1994 and 2000.

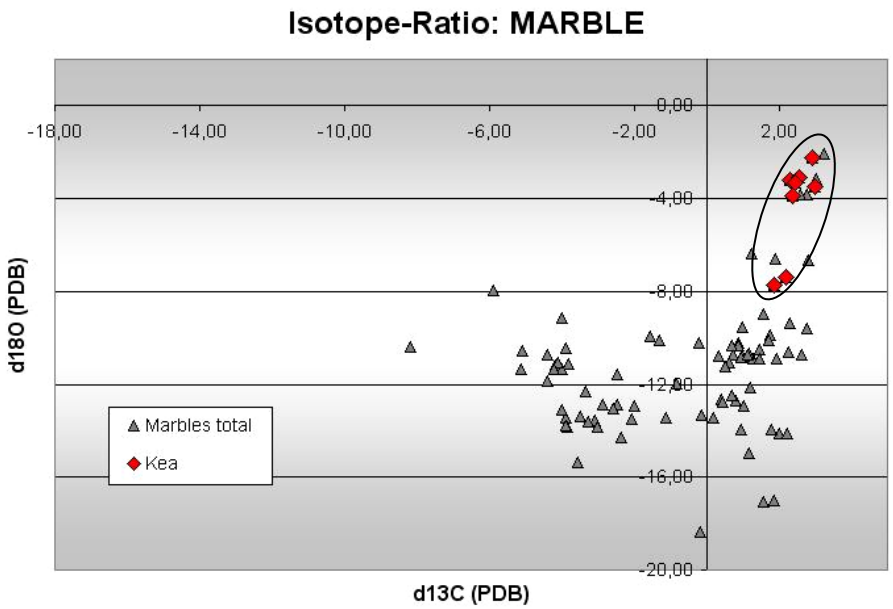

Figure 69: δ^{13}C and δ^{18}O-variations of ultramylonitic Kea-marbles (symbols in red) compared to all other analyzed marbles (symbols in grey).

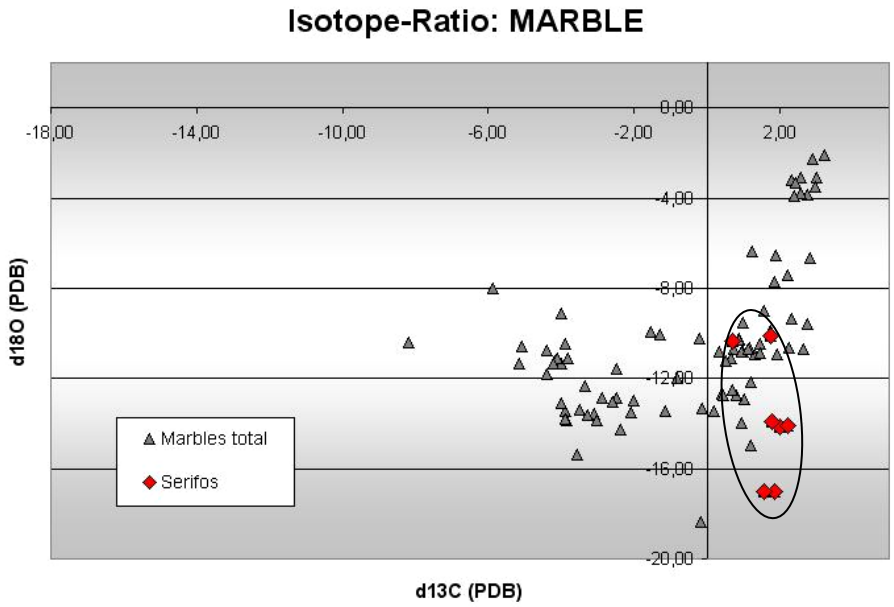

Figure 70: δ^{13}C- and δ^{18}O-ratios of marble-ultramylonites of Serifos-detachment (symbols in red) compared to all other analyzed marbles (symbols in grey).

Marble-ultramylonites of the Serifos-detachments are, in part, strongly depleted in the heavy oxygen isotopes, ranging down to -17 ‰. The ^{13}C-ratios do not show such great variations, with data scattering around 1 ‰. Considering the ^{13}C/^{12}C-ratios, the ultramylonitic marbles of Kea and Serifos show similarities to the grey, lower strained marble-mylonites of Kythnos (compare figure 71).

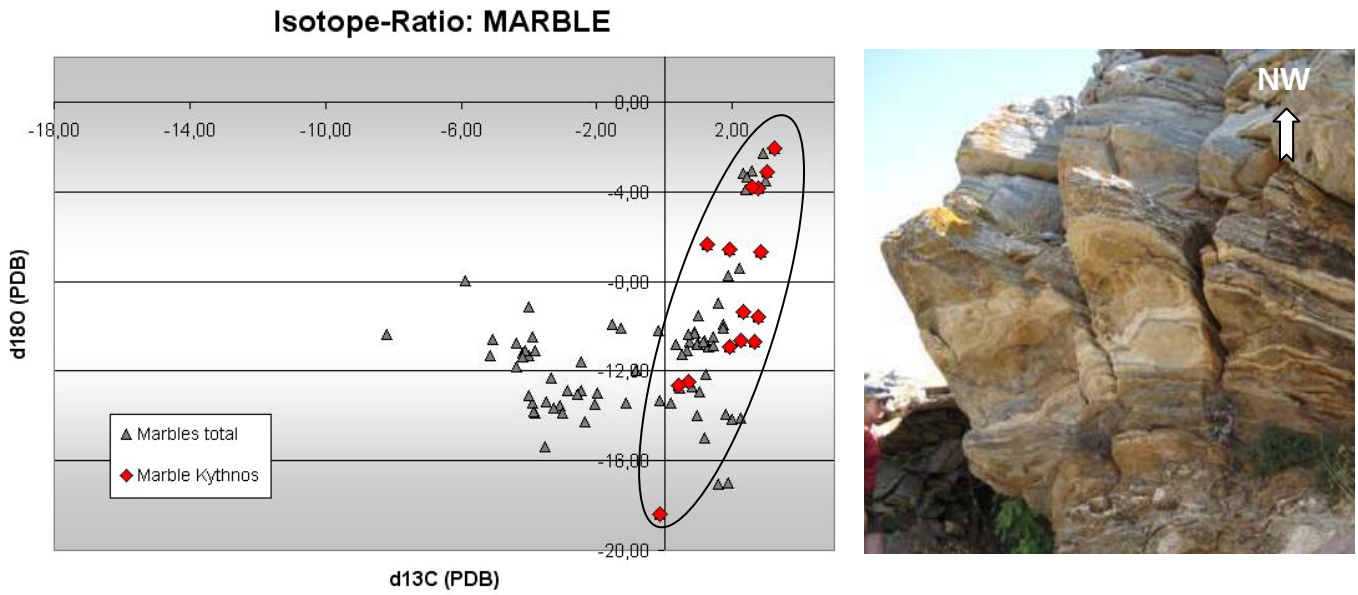

Figure 71: δ^{13}C- and δ^{18}O-ratios of the grey, mylonitic marble-units of Kythnos (symbols in red) compared to all other analyzed marbles (symbols in grey). Picture on the right shows an outcrop of the grey marble-unit.

5.1.4.2. Isotopic composition of vein-cements

The determination of isotope ratios can provide information about the origins of fluids as well as temperatures of mineralization.

The water or fluid which can be found in pore space or fractures of buried rocks may originate from different sources (Jeary & Spencer, 2001). The three principal sources of waters are meteoric water, seawater and juvenile water. *Juvenile waters* are formed chemically within the upper mantle of the earth and come to the surface by volcanic eruptions. *Meteoric water* arises from precipitation and crustal weathering. This type of water has a comparatively low δ^{18}O-ratio, which means a strong depletion of the heavier isotope, due to isotope fractionation during evaporation and precipitation. Waters which are trapped during sedimentation are called *connate waters*. They are left without contact to the atmosphere from the time they were deposited and thus keep the primary oxygen-isotope-ratio of the seawater. *Dehydration waters* are generally enriched in the heavier oxygen-isotope. They emerge from dehydration processes of water-bearing solids like gypsum during diagenesis (Jeary & Spencer, 2001). *Residual evaporate brines* also show a strong enrichment in ^{18}O-isotopes which results from the constant evaporation of the lighter isotopes and thus accumulation of the heavier isotope in the residual liquid. These very hypersaline brines are very dense and therefore they can seep downward through permeable rocks by displacement of connate waters. Finally *hydrothermal brines* feature a significant increase in δ^{18}O-ratio because of the decrease in isotope-fractionation with increasing temperature. Thus the isotope ratio of the water will exchange with that of the host rock much more intensely at elevated temperatures (Faure, 1986; Jeary & Spencer, 2001; Hoefs, 2004).

Sampe	Weight	d13C (PDB)	d18O (PDB)	d18O (SMOW)	Orient.		Typ	Lok
kg12-9v12-x	346	-4,72	-18,43	11,91	210	69	**3**	L
kg12-9v12-y	339	-3,66	-16,56	13,84	210	69	**3**	L
kg12-9v13	299	-2,52	-15,80	14,62	330	80	**3**	L
kg12-9v16	260	-2,30	-14,10	16,38	320	85	**3**	M
kg12-9v17	322	-3,56	-15,85	14,57	325	85	**3**	M
kg12-9v19-x	255	-3,78	-17,11	13,27	020	75	**3**	M
kg12-9v19-y	311	-3,72	-17,20	13,18	020	75	**3**	M
kg12-9v2	350	0.43	-13,93	16,55	008	17	**1**	L
kg12-9v20-x	287	-3,47	-15,57	14,86	025	75	**3**	M
kg12-9v20-y	278	-3,61	-15,83	14,59	025	75	**3**	M
kg12-9v21	311	-4,12	-17,77	12,59	-	-	**3**	M
kg12-9v23-x	304	-2,98	-14,00	16,47	210	89	**4**	M
kg12-9v23-y	348	-2,89	-13,88	16,60	210	89	**4**	M
kg12-9v24	310	0.63	-5,89	24,84	194	84	**4**	M
kg12-9v25	385	-3,54	-12,15	18,39	208	87	**4**	M
kg12-9v26a	302	-3,38	-16,26	14,15	201	85	**4**	M
kg12-9v3	265	0.00	-15,04	15,40	262	85	**1**	L
kg12-9v4-x	254	-0.38	-14,68	15,77	094	80	**1**	L
kg12-9v4-y	295	-0.20	-14,57	15,89	094	80	**1**	L
kg12-9v7-x	291	-6,77	-6,90	23,80	224	85	**4**	L
kg12-9v7-y	344	-6,72	-6,74	23,96	224	85	**4**	L
kg12-9v8-x	310	-3,19	-13,32	17,18	230	77	**3**	L
kg12-9v8-y	308	-3,00	-13,44	17,05	230	77	**3**	L
kg13-9v1	254	-3,08	-12,46	18,07	315	80	**3**	M
kg13-9v10	345	-3,21	-11,31	19,25	317	26	**1**	H
kg13-9v2	318	-3,18	-11,56	19,00	210	57	**3**	M
kg13-9v4	300	-2,99	-12,50	18,03	140	73	**2**	M
kg13-9v5a-x	273	-3,24	-14,44	16,03	242	15	**2**	M
kg13-9v5a-y	302	-3,11	-14,43	16,04	242	15	**2**	M
kg13-9v5b	262	-3,25	-14,72	15,73	242	15	**2**	M
kg13-9v9-x	290	-2,18	-10.25	20.34	272	41	**2**	H
kg13-9v9-y	330	-2,00	-10.32	20.27	272	41	**2**	H
kg12-9-v1	368	-5,59	-23,42	6,77	359	24	**1**	L
kg12-9v14a	340	-4,60	-20.20	10.08	090	24	**1**	M
kg12-9v14b	326	-3,37	-16,36	14,05	090	24	**2**	M
kg12-9v15a	340	-3,48	-17,19	13,19	270	10	**2**	M
kg12-9v15b	324	-3,82	-17,67	12,70	270	10	**2**	M
kg12-9v5	400	-6,56	-24,26	5,90	335	20	**1**	L
kg13-9v3a	328	-2,89	-14,30	16,17	069	30	**2**	M
kg13-9v3b	337	-3,34	-15,06	15,38	069	30	**2**	M
kg13-9v6	410	-3,52	-17,76	12,60	061	10	**1**	H
kg7-11v1a	-	-5,83	-7,21	24,90	030	87	**4**	L
kg7-11v1b	-	-6,25	-6,91	24,47	030	87	**4**	L
kg7-11v2a	-	-6,94	-4,98	23,75	030	88	**4**	L
kg7-11v2b	-	-8,17	-7,36	22,49	030	88	**4**	L
kg7-11v2c	-	-9,91	-6,86	20.70	030	88	**4**	L

Table 2: Isotope ratios of carbonatic vein-cements and orientation of associated extension gashes. F (footwall), H (hanging wall) and M (ultramylonitic marble of the shear zone) specify the position of sampling in the stratigraphic column. Numbers 1 - 4 describe the type of vein-generation.

As already mentioned in 4.4.3.2., cross-cutting relationships and orientations of extension gashes enable a first classification into four different vein types. As shown in figure 72 below, the results of the stable isotope analysis of carbon and oxygen in carbonatic cements also display remarkable differences in isotopic character. The combination of both structural and geochemical results permits the differentiation of four major vein generations.

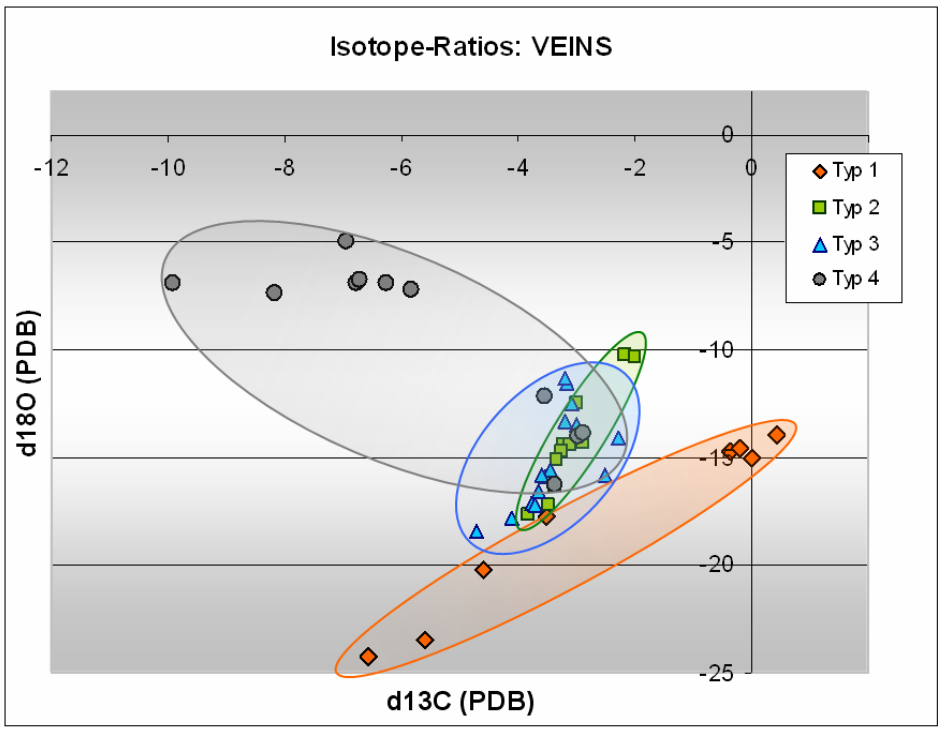

Figure 72: Graphic chart of oxygen- and carbon-isotope-ratios and classification of veins.

5.1.5. Interpretation

Type 1 veins show distinct variations of δ^{13}C-values ranging form -6.56 ‰ to + 0.63 ‰. The δ^{18}O-ratios show strong depletion in the heavier isotope to some extent. In general the oxygen-ratios of calcitic type1-cements are rather low, ranging from -24.26 ‰ to -11.31 ‰. Altogether the $^{13}C/^{12}C$ and $^{18}O/^{16}O$ ratios show a positive correlation-trend. It can be assumed that this type of vein is formed at the base of the shear zone where the system is subjected already to ductile conditions of deformation. Field evidence for these ductile conditions is the subsequent partial “folding” of the extension gashes (see figure 42 and 55) which are filled with quartz or calcite. At these greater depths there are no longer open-system-conditions and only rock-buffered fluids can pass the rocks. So the fluids of these regions are strongly influenced by the wall rock (Famin et al., 2004).

Type 2 and *type 3* veins have quite similar isotope ratios, whereas the type 3 veins show both (1) lower δ^{18}O-ratios, between -18.43 and -11.56 ‰, and (2) a stronger depletion in ^{13}C, ranging from -4.72 to -2.30 ‰. The isotope-ratios of type 2 veins vary between -16.36 and -10.25 ‰ for δ^{18}O and between -3.82 and -2.00 ‰ for δ^{13}C. Type 2 veins are mostly calcite but sometimes include also parts of iron-rich fluids. Type 3 veins have about the same composition. Because of the minor differences in isotopic composition, the conditions of formation likely are quite similar for type 2 and type 3 extension gashes. Both show a consistent depletion in ^{13}C and ^{18}O. The

positive correlation between $\delta^{13}C$ and $\delta^{18}O$ can be explained by calcite precipitation due to the mixing of two fluids of different salt-concentrations or by the precipitation from a H_2CO_3-dominant fluid due to temperature effect together with either CO_2 degassing or fluid-rock interaction (Hoefs, 2004). Our field observations show that a few of these veins also have indications of ductile deformation. It can be assumed, however, that they are generated at the transitional zone between the ductile and brittle regimes. Therefore the cements of these extension gashes already show an input of external fluids which implies a changeover to a gradually opening system.

Extension gashes of *type 4* completely differ from the other types. They show a strong variation in $\delta^{13}C$ of roughly 7 ‰. With reference to oxygen isotopes, the veins can be subdivided into two groups. The first one shows high variations in ^{13}C with relatively consistent $\delta^{18}O$-ratios around -6 ‰. The second subgroup, which is more depleted in ^{18}O, is located around the field of the type 2 and type 3 veins, also showing a positive correlation. It is not certain whether they still belong to the formerly established veins of the transitional zone. They may also have been formed at greater depths in the brittle crust. As some extension gashes feature several generations of calcitic cements, we assume that the already-existing veins have been partially reactivated over the period of brittle deformation. Besides calcite, veins also comprise quartz or iron and barite mineralizations, which may be a sign for hydrothermal activity. Towards the top of the shear zone, veins become more open (see figure 55: Mode I open-veins). We can assume that type 4 extension gashes had already opened in the brittle crust, and meteoric fluids were able to infiltrate down to depths of around 10 kilometres, or even more, reaching the brittle-ductile transitional zone (Mulch et al., 2004).

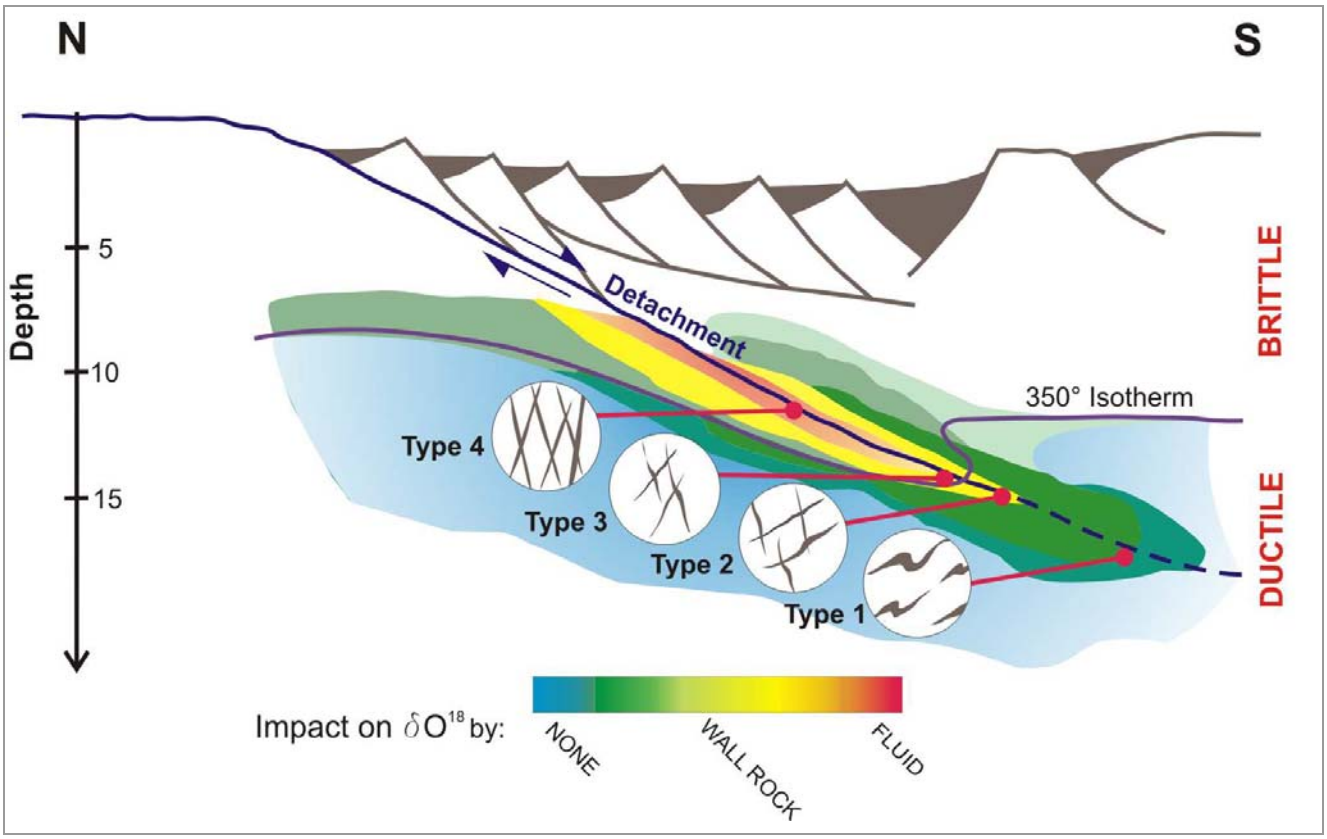

Figure 73: Influence of fluids or wall rock on the δ^{18}O-ratio of vein-cements at certain depths within a major shear zone. Schematic diagram also shows the assumed zones, where the different types of extension gashes may originate. Graph shows the isothermal line of 350 °C, separating brittle from ductile regime. Redrawn and modified after Famin (2003) and Famin et al. (2004).

5.2. Radiogenic Isotopes

5.2.1. Geochemistry of Rubidium and Strontium

Rubidium is an alkali metal with an ionic radius that is quite similar to that of potassium. Therefore it is able to substitute for potassium in all K-bearing minerals and therefore it is enriched in micas, K-feldspar, certain clays and evaporites. Rubidium has two naturally occurring isotopes (^{85}Rb, ^{87}Rb). The radioactive ^{87}Rb decays to stable ^{87}Sr by the emission of a negative beta particle.

Strontium belongs to the alkaline earths. Its ionic radius is similar to that of calcium which enables its substitution in calcium carbonates, plagioclase and apatite. Strontium has four naturally occurring isotopes which are all stable. According to Faure (1986), their approximate abundances are 82.53 % (^{88}Sr), 7.04 % (^{87}Sr), 9.87 % (^{86}Sr) and 0.56 % (^{84}Sr). Because of the persistent decay of rubidium to radiogenic strontium with a half-life 4.88×10^{10} a (Steiger & Jäger, 1977), the isotopic abundances are variable, and the precise isotopic composition of strontium in rubidium-bearing minerals or rocks is controlled by the Rb-Sr-ratio and the age (Faure, 1986).

	Upper crust	**Carbonates**	**Mudstone**	**Seawater** [3.5 % salinity]	**River water**
Sr [ppm]	350	610	300	7.6	0.071
Rb [ppm]	112	3	140	0.12	0.001
Ca [ppm]	42000	300000	22000	400	19.7
K [ppm]	34000	2700	27000	416	2,3
Sr/Ca	8.3	2	13.6	19.5	3.6
Rb/K	3.3	1.1	5.2	0.3	1.4

Table 3: Average frequencies of Sr, Rb, Ca and K in lithosphere and hydrosphere (modified after Mudroch, 2001). Sr/Ca and Rb/K ratios are referred to weight.

Strontium-salts have a high solubility in water. The residence time for strontium in the hydrosphere averages 10^6 years. The time for intermixture of oceans is only about 1000 years (Mudroch, 2001). So the ^{87}Sr/^{86}Sr ratio of seawater is quite constant over all oceans. The variation in the overall Sr concentration is controlled by two parameters, the annual influx by rivers and by Sr-exchange reactions with basalts at the MORs. According to analysis of marine carbonates, Veizer and Compston (1976) demonstrated the Sr isotope evolution of Precambrian seawater which shows a substantial rise in Sr isotope ratio during the Proterozoic. Throughout

Phanerozoic time the Sr isotope evolution shows strong variations. Currently the mean $^{87}Sr/^{86}Sr$ ratio of recent global seawater is 0.709175 (considering the 95% confidence limit) (Howarth & McArthur, 2001 and 1997). As shown in figure 74 below, the $^{87}Sr/^{86}Sr$ isotope ratio varies between 0.7067 and 0.7092 during the Phanerozoic (Mudroch, 2001). Thus, in principle, Sr-isotope-ratios lend the possibility for approximately constraining the age of marine carbonatic rocks. The concentration and the isotopic ratio of Sr in surface and subsurface waters generally reflects the isotopic composition and age of the host rocks that have interacted with the fluids. Thus, the isotopic composition of fluids can provide information about the origin, mixing and movement of waters.

The $^{87}Sr/^{86}Sr$ ratio of seawater is controlled by their mixing with the following sources, providing different isotopic signatures: a) old rocks of the continental crust, b) young volcanic rocks and c) marine carbonates of Phanerozoic age (Faure et al., 1965). Variations of the $^{87}Sr/^{86}Sr$ ratio in carbonatic rocks can arise from alteration during diagenesis or metamorphism. If the carbonates comprise detrital silicates from old cratonic sources (e.g. white mica), the ratio may increase. If they contain young volcanic detritus, the isotopic ratio will be lowered, however (Faure, 1986).

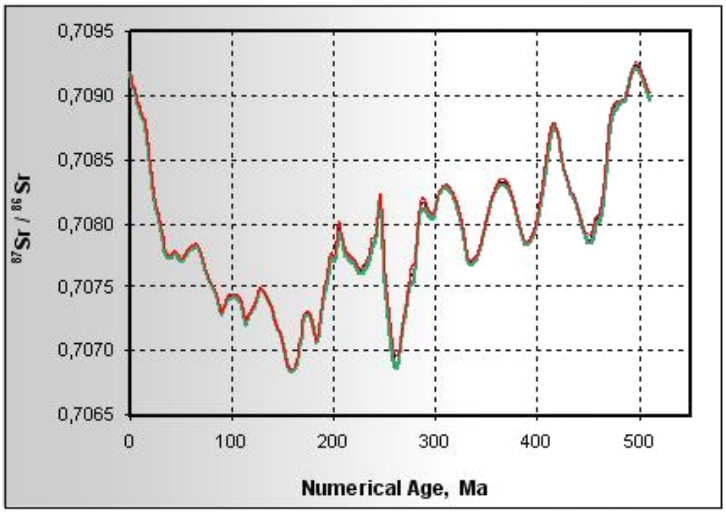

Figure 74: Variation of $^{87}Sr/^{86}Sr$ ratio of marine carbonates during Phanerozoic times (McArthur et al., 2001), modified.

5.2.2. Methodology

Thermal ionization mass spectrometry (TIMS)

TIMS is used to carry out high-precision measurements of isotope ratios which is important for radiometric dating. The sample material has to be dissolved and purified by means of chromatography and is then loaded onto a degassed U-shaped filament, which is a small piece of ultrapure (99.999%) metal (usually rhenium or tantalum) around 1 mm wide and with a thickness of about 0.03 mm. The filament is heated at ultrahigh vacuum conditions which results in ionization of the material as it evaporates from the hot filament. Using slits and charged plates, the ions are focussed into a beam and pass through a magnetic field. There, the ions are deflected according their mass-to-charge-ratio (cf. 5.1.3. figure 60) and finally detected by collector (generally Faraday) cups.

(sources: Faure, 1986 ; http://www.sahra.arizona.edu/programs/isotopes/methods/ionization.html)

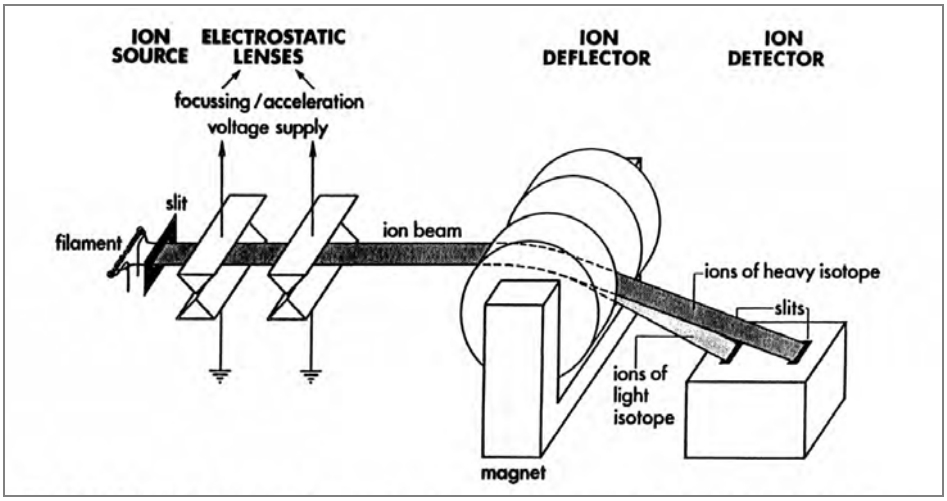

Figure 75: Schematic diagram of a Thermal Ionization Mass Spectrometer, after Geyh & Schleicher (1990).

5.2.3. Results and interpretation

To get a general idea of the isotopic composition of the different marble units and veins, a few representative samples of each category were analyzed for $^{87}Sr/^{86}Sr$-ratio (table 4). In addition, two samples (out of a total of twelve) were also analyzed for Rb and Sr concentration by ID-TIMS (Isotope Dilution-TIMS), see table 4.

Sample	Rb [ppm]	Sr [ppm]	$^{87}Rb/^{86}Sr$	$^{87}Sr/^{86}Sr$	+/-2sm	$^{87}Sr/^{86}Sr$ (180 Ma)
KG7-11D R WR	3.4	363	0.027	0.708191	0.000021	0.708122
KG7-11D R WR IC				0.708147	0.000004	
KG7-11D L WR				0.708194	0.000003	
KG7-4F WR				0.708854	0.000003	
KG7-4F	18.3	246	0.215	0.708847	0.000005	0.708298
KG7-4D WR				0.707543	0.000008	
KG7-11C WR				0.708585	0.000007	
KG7-11E WR				0.708100	0.000014	
KG7-1A				0.707295	0.000004	
KG7-2B				0.707220	0.000004	
KG7-11A				0.707318	0.000004	
KG7-11V3a				0.708971	0.000007	
KG7-11V3b				0.708977	0.000005	
KG7-13-V1				0.708483	0.000004	
KG7-13-V5				0.708437	0.000004	
NBS987 (n=13)				0.710251	0.000004	

Table 4: Results of Rb and Sr analyses of selected ultramylonitic marbles (marked in purple), marbles (grey) and calcitic veins (yellow) on Kythnos Island.

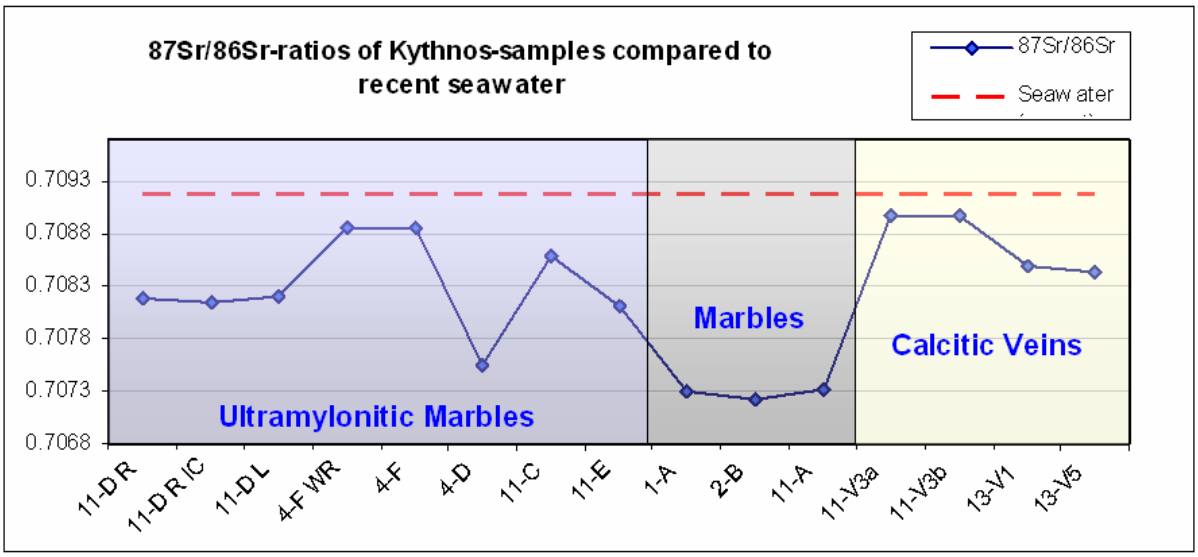

Figure 76: Variation of the $^{87}Sr/^{86}Sr$-ratio of the selected Kythnos-samples (see table 4), ranging from 0.707220 to 0.708977 compared to recent seawater with a Sr-ratio of 0.709175 (dashed red line). Ultramylonitic marbles marked in purple, marbles marked in grey and calcitic veins marked in yellow.

Figure 76 shows the variation of the $^{87}Sr/^{86}Sr$-ratios compared to the composition of present-day seawater. As the $^{87}Sr/^{86}Sr$-ratio in seawater increased in the course of the Cenozoic for a maximal value (0.7092), all analyzed carbonate-samples are expected to yield lower values. The analyzed samples feature quite strong variations, ranging from 0.707220 up to 0.708977. This indicates secondary influencing. Generally, lowering of $^{87}Sr/^{86}Sr$-ratios is expected to be unlikely, as this would need a secondary impact by fluids generated from basic rocks or volcanic activity. Since the concentration of Sr in seawater is rather high, large quantities of fluids with low $^{87}Sr/^{86}Sr$ would be necessary to cause a significant shift towards lower isotope ratios in the carbonates. We assume that the lowest $^{87}Sr/^{86}Sr$-ratio of 0.70722, measured in the marble sample KG7-2B, closely reflects the primordial Sr-isotope composition in seawater during genesis of the carbonates. By the use of this sample, compared to the Sr-seawater curve, we can define a possible age of the carbonates (see figure 79).

Comparable with KG7-2B, all other samples show, to a greater or lesser extent, higher $^{87}Sr/^{86}Sr$-ratios. (a) A rise in ^{87}Sr is caused by an increased input of Rb, as the radioactive ^{87}Rb decays to stable ^{87}Sr. Thus, if carbonates comprise detrital silicates (e.g. micas) from old cratonic sources, the $^{87}Sr/^{86}Sr$-ratio will increase. (b) An additional shift in $^{87}Sr/^{86}Sr$-ratio can be caused by the interaction of the carbonates with fluids that were generated in crustal regions, “contaminated” with Sr of “radiogenic” isotope composition. This might account for the higher $^{87}Sr/^{86}Sr$-ratio in sample KG7-4F compared to KG7-11D, where the $^{87}Rb/^{86}Sr$-ratio is about ten times lower (table 4). To resolve these assumptions, it would be necessary to determine the $^{87}Rb/^{86}Sr$-ratio of all samples. In any case, back-calculation of the “initial” Sr isotopic composition for the two samples with known Rb/Sr (KG7-11D and KG7-4F, table 4) clearly demonstrates that input of fluids containing “radiogenic” Sr played a major role compared with in-situ ingrowth of ^{87}Sr from

inherited (detrital) Rb-bearing phases in this case. As an approximation, we assume that the lowest $^{87}Sr/^{86}Sr$-ratio is the most pristine value, most likely approaching seawater composition during genesis of the carbonates, while all others have been variously influenced by the same secondary events.

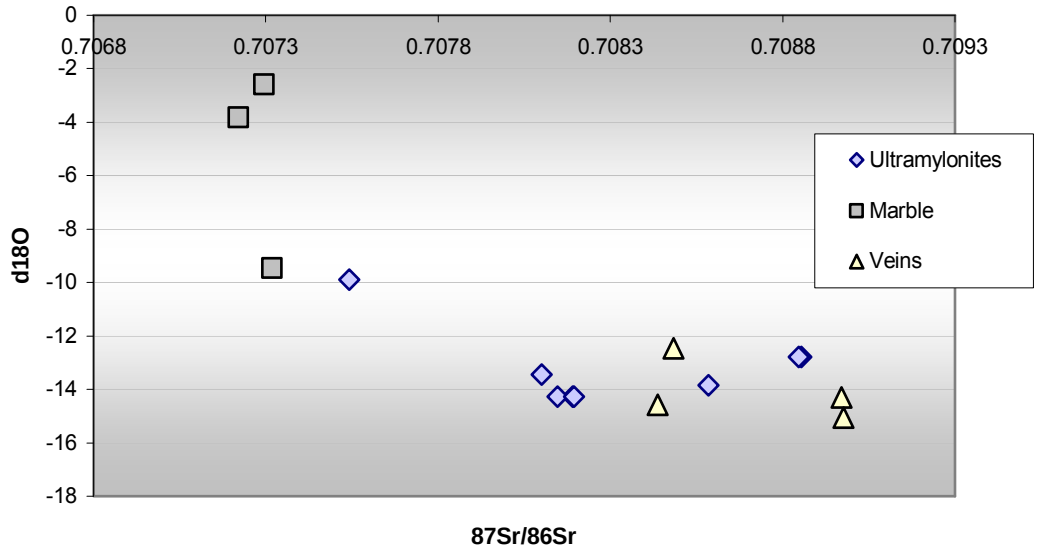

Figure 77: Correlation of $\delta^{18}O$-ratios and $^{87}Sr/^{86}Sr$-ratios of distinct samples of marble-ultramylonites from the ductile shear zone, the grey-blue marble unit and brittle veins.

Figure 77 shows the variations of the $^{87}Sr/^{86}Sr$-ratios measured in the Kythnos-samples, correlated with their $\delta^{18}O$-values. In principle they show a negative correlation. The graph illustrates, that the lesser deformed marbles of the grey-blue marble units feature the lowest Sr-isotope-ratios, whereas most of the higher strained marbles show higher $^{87}Sr/^{86}Sr$-values but also higher depletion in the heavier oxygen isotope. A similar behaviour can be observed in the late, hydrothermally affected vein-fillings. Therefore fluids of the late brittle deformation phase may have derived from rocks which basically have higher Sr-isotope ratios or comprise older detrital silicates.

The ultramylonitic marbles show a large spread in the Sr-isotope-values. The sample KG7-4D, for example, with a $^{87}Sr/^{86}Sr$-ratio of 0.707543, features similar values to the grey-blue marbles. KG7-4F, on the other hand, which is situated only about 150 cm away in the footwall of the pale marbles of KG7-4D (figure 78), has a $^{87}Sr/^{86}Sr$-value of 0.708847. This is one of the highest Sr-isotope ratios of our samples. Considering this fact, we can assume that fluid flux was concentrated only (or at any rate, mainly) in preferential domains. The high penetration of the grey marble in the range of KG7-4F by veins testifies an intensified fluid activity.

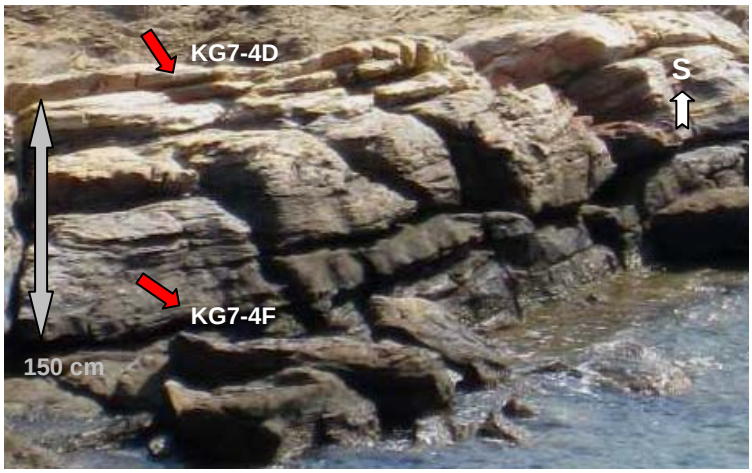

Figure 78: Ultramylonitic marble unit with the approximate positions of sample KG7-4F, which is relatively enriched in ^{87}Sr in the footwall, and the depleted sections of KG7-4D in the hanging wall.

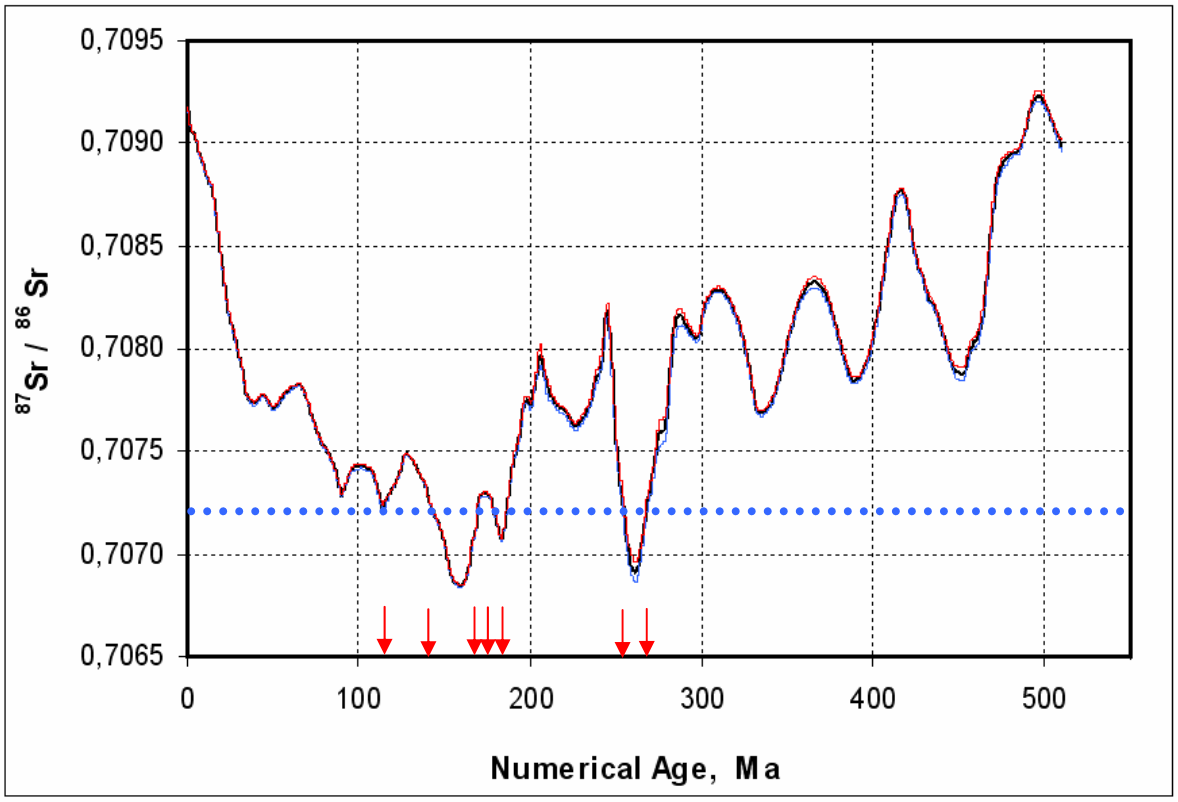

Figure 79: Sr-seawater curve from 0-509 Ma with possible ages of the analyzed marbles of Kythnos, assuming that Sr-ratios have not been secondary altered (McArthur et al., 2001), modified.

Assuming that the $^{87}Sr/^{86}Sr$-ratio of sample KG7-2B (0.70722) reflects the primordial Sr isotopic composition of the seawater during formation of the carbonates, the possible ages for the carbonate-marbles can be determined by comparison of the measured ratio with the global Sr-seawater curve. Figure 79 shows, that the seawater reached a ratio of 0.70722 at least 7 times

during the Phanerozoic Eon. The youngest possible age occurs within the Early Cretaceous, around 114 Ma or 143 Ma B.P. In the Early and Middle Jurassic there are 3 possibilities, ranging from 169 Ma to 178 Ma or 186 Ma. The period of the Permian around 254 Ma or 267 Ma B.P. represents one further possibility. However, since there was no significant carbonate production in Permian times, we can exclude such early ages. Age suggestions for marbles of the Cycladic Blueschist Unit in Naxos agree with Jurassic ages. Feenstra (1985) describes Jurassic meta-bauxite units within the carbonates of Naxos, which mark periods of uplift, exposure and chemical weathering of the Mesozoic carbonate platform. In conclusion, the lowest $^{87}Sr/^{86}Sr$-ratios obtained in my study suggest a Jurassic or Lower Cretaceous age for the carbonates.

6. CONCLUSIONS

- Structural investigations show the existence of a hitherto unrecognised large-scale ductile-brittle shear zone in the southernmost part of Kythnos Island which is probably due to Miocene extensions in the Aegean region.

- The shear zone consists of two distinct horizons of extremely fine grained, calcitic marble ultramylonites and ultracataclasites that generally plunge SW.

- Probably associated with high extension in NE-SW direction, a strong shortening perpendicular to the stretching lineation was observed, reflected in the bending and buckling of the shear zone with fold axes striking ca. NE-SW.

- The stretching and mineral lineations of all lithologies trend NE-SW, shallowly plunging towards the NE in northern parts and towards SW in the southern part. Shear sense indicators show consistent top to SW- respectively top to SSW-directed kinematics.

- Within the greenshist-facies rocks that build up the footwall of the shear zone, there are lenses of metagabbros, showing relicts of their original magmatic fabric. They form relative rigid blocks; these are coated with Srp-Tlc-schist and are positioned in the core of a km-scale recumbent fold.

- Structural investigations show evidence for an earlier phase of tight to isoclinal folding with subhorizontal axial planes and a later upright folding with nearly vertical axial planes and also NEE-SSW striking fold axes.

- Due to ongoing extension, rocks were subjected to brittle high-angle normal faulting and fracturing.

- By way of crosscutting relationships, orientation and geochemistry four different generations of ductile to brittle extension gashes can be distinguished.

- Stable isotopes of carbon and oxygen, measured in the mylonitic marbles, the marble-ultramylonites of the shear zone and in the calcitic extension gashes, all give evidence of a strong interaction with fluids in the shear zone. Variation in isotope ratios implies a transition from a ductile, closed system to an opened regime with infiltration of surface waters.

- $^{87}Sr/^{86}Sr$-ratios of marbles and calcitic vein-fillings show quite dramatic fluctuations compared to current seawater data.

- Assuming that the Sr-isotope data of the marble-sample with the lowest $^{87}Sr/^{86}Sr$-ratio was not secondarily influenced by fluids, possible ages of these rocks can be defined. Accordingly, carbonates may have been generated either during Early Cretaceous or Early to Middle Jurassic times.

7. REFERENCES

Abart R. (1995): Phase equilibrium and stable isotope constraints on metasomatic vein formation, Contrib.Mineral.Petrol., 122, 116-133.

Abart R., Badertscher N., Burkhard M., Povoden E. (2002): Oxygen, carbon, and strontium isotope systematics in two profiles across the Glarus Thrust: implications for fluid flow. Contrib.Min.Pet., 143, 192-208.

Aubouin J. (1959) : Contribution à l´étude géologique de la Grece septentrional: les confins de L`Epire et de la Thessalie. Annales Geologiques des Pays Helleniques, 9, 1-484.

Armijo R., Meyer B., King G.C.P., Rigo A., Papanastassiou D. (1996): Quarternay evolution of the Corinth Rift and its implications for the Late Cenozoic evolution of the Aegean. Geophysical Journal International, 126, 1, 11-53.

Bartsch V. (1993): Die grünschieferfazielle Überprägung im Norden von Kithnos (Kykladen, Griechenland): Geologie, Petrographie und Geochemie. – Diploma thesis, Universität Hannover, 163 p, unpubl.

Baumgartner L.P. & Rumble D. (1988): Transport of stable isotopes. I. Development of a kinetic continuum theory for stable isotope transport. Contrib Mineral Petrol 98:417 – 430.

Baumgartner L.P. & Valley J.W. (2001): Stable isotope transport and contact metamorphic fluid flow. Rev Min Geochem 43:415–467.

Bestmann M. (1994): Untersuchungen zur Petrographie und Strukturgeologie nördlich des Rachoni-Tals und zur Isotopengeochemie (δ^{13}C, δ^{18}O) an Marmoren (Thassos, Nordgriechenland). Diplomarbeit, Institut für Geologie und Mineralogie der Friedrich-Alexander-Universität Erlangen-Nürnberg.

Bestmann M. (2000): Evolution of a shear zone in calcite marble on Thassos Island, Northern Greece: results from microfabrics and stable isotopes. In: Erlanger geol. Abh. 131, 1-127.

Bestmann M., Kunze K. & Matthews A. (2000): Evolution of a calcite marble shear zone complex on Thassos Island, Greece: microstructural & textural fabrics and their kinematic significance. In: *J. Struct. Geol.* 22, 1789-1807.

Bickle M.J. & Baker J. (1990): Migration of reaction and isotopic fronts in infiltration zones: assessments of fluid flux in metamorphic terrains. Earth Planet Sci Lett 98:1 - 13.

Brand W.A. (2004): Mass Spectrometer Hardware for Analyzing Stable Isotope Ratios. - In: De Groot P.A. (ed): Handbook of Stable Isotope Analytical Techniques. Elsevier Science & Technology.

Carl M. (1993): Petrographische, geochemische und mineralchemische Untersuchungen an Metamorphiten von Süd-Kithnos (Kykladen, Griechenland). – Diploma thesis, Universität Hannover, 148 p., unpubl.

Cartwright I. & Valley J.W. (1991): Steep oxygen isotope gradients at marble-metagranite contacts in the NW Adirondacks Mountains, N.Y. Earth Planet Sci Lett 107:148 – 163.

Chrysanthaki A.I. & Baltatzis E.M.M. (2003): Geochemistry and depositional environment of ferromanganoan metasediments on the Island of Kythnos, Cyclades, Greece. N. Jb. Miner. Mh., 1:1-17.

Coney P.J., Jones D.L. & Monger J.W.H. (1980): Cordilleran suspect terranes. Nature, 239, 329-333.

Coplen T. B. (1994): Reporting of stable hydrogen, carbon, and oxygen isotopic abundances, Pure Appl. Chem., 66, 273-276.

Coplen T.B. (1996): Guidelines for the Reporting of Stable Hydrogen, Carbon and Oxygen Isotope-Ratio Data. Paleoceanography, 11:369-370.

Craig H. (1957): Isotopic standards for carbon and oxygen and correction factors for mass-spectrometric analysis of carbon dioxide. Geochim Cosmochim Acta, 12:133-149.

Dermitzakis M.D. (1984): A Guide to the Geology of Greece. University of Athens, Subfaculty of Earth Sciences, Department of Stratigraphy-Geography-Climatology. Athens.

De Smeth J.B. (1975): Geological Map of Greece 1:50 000. Kythnos Island. IGME, 1975.

Dipple G.M. & Ferry J.M. (1992): Fluid flow and stable isotope alteration in rocks at elevated temperatures with applications to metamorphism. Geochim Cosmochim Acta, 56:3539 – 3550.

Duermeijer C.E, Nyst M., Meijer P.Th., Langereis C.G. & Spakman W. (2000): Neogene evolution of the Aegean arc: paleomagnetic and geodetic evidence for a rapid and young rotation phase. Earth and Planetary Science Letters 176, 509-525.

Dürr S., Altherr R., Keller J., Okrusch M., Seidel E. (1978): The Median Aegean Belt: Stratigraphy, Structure, Metamorphism. - in: Closs H., Roeder D., Schmidt K. (eds.): Alps,

Apennines, Hellenides; Geodynamic Investigations along Geotraverses by an International Group of Geoscientists. E. Schweizerbart´sche Verlagsbuchhandlung, Stuttgart, pp. 455-474.

Edwards M. A. & Grasemann B. (in press): Mediterranean snapshots of accelerated retreat and geodynamic instability in continental orogenesis. In: van Hinsbergen D., Edwards M. A. and Govers R. (eds) Collision and collapse at the Africa-Arabia-Eurasia subduction zone. Geological Society, London, Special Publication, accepted pending revisions.

Endrun L.T.C., Meier M., Bohnhoff M. & Harjes H.-P. (2005): Modelling the influence of Moho topography on receiver functions: a case study from the central Hellenic subduction zone. Geophysical Research Letters, L12311.

Exner U., Mancktelow N.S. & Grasemann B. (2004): Progressive development of s-type flanking folds in simple shear. Journal of Structural Geology, 26, 12, 2191-2201.

Famin V. (2003): Incursion de fluids dans une zone de cisaillement ductile (Tinos, Cyclades, Grece) : Mecanismes de circurlation et implications tectoniques. Thèse de Doctorat de l´Úniversité Paris VI.

Famin V., Philippot P., Jolivet L. & Agard L. (2004): Evolution of hydrothermal regime along a crustal shear zone, Tinos Island, Greece. Tectonics, 23, TC5004.

Faure G., Hurley P.M., Powell J.L. (1965): The isotopic composition of strontium surface water from the North Atlantik Ocena. Geochim. Cosmochim. Acta, 29, 209-220.

Faure G. (1986): Principles of isotope geology. Second Edition, John Wiley & sons, New York, Chichester, Brisbane, Toronto, Singapore, 589 pp.

Feenstra A. (1985): Metamorphism of bauxites on Naxos, Greece. Geologica Ultraiectina, 39. Offsetdrukkerij Kanters B.V., Alblasserdam, Netherlands.

Ganor J., Matthews A., Paldor N. (1989): Constraints on effective diffusivity during oxygen isotope exchange at a marble-schist contact, Sifnos (Cyclades), Greece. Earth Planet Sci Lett 94:208 – 216.

Garlick G.D. (1969): The stable isotopes of oxygen. In: Wedepohl KH (ed) Handbook of geochemistry, 8B. Springer, Berlin Heidelberg New York.

Geyh M. A. & Schleicher H. (1990): Absolute Age Determination, Springer Verlag, Berlin, Heidelberg, New York, London, Paris, Tokyo, Hong Kong, Barcelona.

Grasemann B., Stüwe K. & Vannay J.K. (2003): Sense and non-sense of shear in flanking structures.- Journal of Structural Geology, 24/1, 19-34.

Grasemann B., Wiesmayr G., Draganits E. & Fusseis F. (2004): Classification of refold structures.- Journal of Geology, 112/1, 119-126.

Hoefs J. (2004): Stable Isotope Geochemistry. 5th, Resvised and Updated Edition, Springer Verlag, Berlin, Heidelberg.

Howarth R.J. & McArthur J.M. (1997): Statistics for strontium isotope stratigraphie. A robust LOWESS fit to the marine Sr-curve for 0-206 Ma, with look up table for the derivation of numerical age. Journal of Geology, 105, 441-465.

Iglseder C. (2005): Fold-structures in the tectono-metamorphic evolution of the Serifos Metamorphic core complex, Cyclades, Greece. Diploma thesis. University of Vienna, Vienna.

Irwin G.R. (1957): Analysis of stresses and strains near the end of a crack traversing a plate. Journal of Applied Mechanics, 24: 361-364.

Jackson J. A., Haines J. & Holt W. E. (1992): The horizontal velocity field in the deforming Aegean Sea region determined from the moment tensors or earthQ15 quakes. Journal of Geophysical Research, 97.

Jacobshagen V. (1986) : Geologie von Griechenland. Borntraeger, Berlin Stuttgart.

Jeary V. & Spencer R.J. (2001): Isotopic and fluid inclusion evidence for hydrothermal alteration: Mississippian Rival Subinterval, Indian Hill Reservoir, North Dakota. Rock the Foundation Convention, June 18-22, Canadian Society of Petroleum Geologists, 019-1 – 019-9.

Jolivet L., Faccenna C. (2000): Mediterranean extension and the Africa - Eurasia collision, Tectonics, 19, 6, 1095-1106.

Jolivet L. (2001): A comparison of geodetic and finite strain pattern in the Aegean, geodynamic implications. Earth and Planetary Science Letters, 187, 95-104.

Jolivet L., Famin V., Mehl C., Parra T., Aubourg R., Hébert R. & Philippot P. (2004): Progressive strain localisation, boudinage and extensional metamorphic complexes, the Aegean Sea case, in

Gneiss domes in orogeny, in: C.T.a.C.S.S. D.L. Whitney, (Ed) 380. Geological Society of America Special Paper, Boulder, Colorado, pp. 185-210.

Keiter M., Tomaschek F. & Ballhaus C. (2008): The structural evolution of Kythnos Island (Cyclades, Greece) - a reconnaissance. Zeitschrift der Deutschen Gesellschaft für Geowissenschaften, 159:513-520.

Kohn M.J., Valley j.W., Elsenheimer D., Spicuzza M. (1993): Oxygen isotope zoning in garnet and staurolite; evidence for closed system mineral growth during regional metamorphism. Am Mineral 78:988 – 1001.

Kretz R. (1983): Symbols for rock-forming minerals. American Mineralogist, 68, 277-279.

Laner R. (2009): Deformation Bands in neogenen Kalksandsteinen des Eisenstädter Beckens (St. Margarethen, Burgenland). Bachelor thesis, unpubl.

Lenauer I. (2009): Structural and petrological investigations along a low angle normal fault on Kythnos, Greece. Master´s thesis. University of Vienna, Vienna.

Lenauer I., Mörtl G., Iglseder C., Grasemann B., Edwards M. (2008): Field evidence for a major normal fault on Kythnos Island (Western Cyclades, Greece).- Geophysical Research Abstracts, Vol. 10, EGU2008-A-03218.

Lenauer I., Mörtl G., Grasemann B. and Iglseder C. (2008): Structural investigations along a low angle normal fault zone (Kythnos, Greece). YORSGET 2008, Oviedo, Spain.

Lister G.S. & Davis G.A. (1989): The origin of metamorphic core complexes and detachment faults formed during Tertiary continental extension in the northern Colorado River region, Journal of Structural Geology, 11, 65-94.

Lister G.S., Etheridge M.A. & Symonds P.A. (1986): Detachment faulting and the evolution of passive continental margins. Geology, 14, 246-250.

Malavieille J. (1993): Late orogenic extension in mountain belts: Insights from the Basin and Range and the Late Paleozoic Variscian Belt. Tectonics 12 (5): 1115-1130.

McArthur J.M., Howarth R.J. & Bailey T.R. (2001): Strontium isotope stratigraphy: LOWESS Version 3. Best isotope curve for 0 to 509 Ma and accompanying look-up table for deriving numerical age. Journal of Geology, 109, 155 – 169.

McClusky S., Balassanian S., Barka A., Demir C., Ergintav S., Georgiev I., Gurkan O., Hamburger M., Hurst K., Kahle H., Kastens K., Kekelidze G., King R., Kotzev V., Lenk O., Mahmoud S., Mishin A., Nadariya M., Ouzounis M., Paradissis D., Peter Y., Prilepin M., Reilinger R., Sanli I., Seeger H., Tealeb A., Toksöz M. N., Veis G. (2000): Global Positioning System constraints on plate kinematics and dynamics in the eastern Mediterranean and Caucasus, Journal of Geophysical Research, 105, 5695-5719.

McClusky S., Reilinger R., Mahmoud S., Ben Sari D., Tealeb A. (2003): GPS constraints on Africa (Nubia) and Arabia plate motions. Geophysical Journal International, 155, 126-138.

McCrea J.M. (1950): On the isotopic chemistry of carbonates and paleotemperature scale. J Chem Phys 18:849-857.

Mudroch A.(2001): Fischzähne aus dem Oberjura Nordwesteuropas – Systematic, Biogeochemie und Palökologie. Dr. Thesis, Universität Hannover, 142 pp., unpublished.

Mörtl G., Grasemann B., Lenauer I., Edwards M., Iglseder C., Thöni M., Mader D. (2008): Fluid-rock interaction in a low-angle-normal fault (Kythnos, Western Cyclades, Greece). – Geophysical Research Abstracts, Vol. 10, EGU2008-A-04585.

Mulch A., Teyssier C., Cosca M.A., Vanderhaeghe O. & Vennemann T.W. (2004): Reconstructing paleoelevation in eroded orogens. Geology, 32, 525-528.

Okrusch M. & Bröcker M. (1990): Eclogites associated with high-grade blueschists in the Cyclades archipelago, Greece: a review. – European Journal of Mineralogy (2): 451 – 478, Stuttgart.

Papazachos B. C. (1973): Distribution of seismic foci in the Mediterranean and surrounding area and its tectonic implication. Geophysical Journal of the Royal Astronomical Society, 33, 419–428.

Passchier C.W. (2001): Flanking structures. Journal of Structural Geology, 23, 951-962.

Passchier C.W. & Trouw R.A.J. (2005): Microtectonics. Springer, Berlin Heidelberg.

Pe-Piper G., Piper D.J.W. (2002): The igneous rocks of Greece - The anatomy of an orogen. Berlin, Gebrüder Bornträger, 316 p.

Rambousek C. (2007): Quantitative Tectonic Studies of a Miocene Low Angle Normal Fault (Serifos, Greece). Master's thesis, University of Vienna.

Ramsay J.G. (1967): Folding and Fracturing of Rocks. McGraw-Hill Book Company, New York, 568 pp.

Ring U., Gessner K., Gungor T. & Passchier C.W. (1999): The Mendcres Massif of western Turkey and the Cycladic Massif in the Aegean-do they really correlate? Journal of the Geological Society, London, 156, 3-6.

Schliestedt M., Barsch V., Carl M., Matthews A. & Henjes-Kunst F. (1994): The P-t path of Greenschist-Facies Rocks from the Island of Kithnos (Cyclades, Greece). – Chemie der Erde 54: 281-296, Jena.

Sodoudi F. (2000): Lithospheric structure of the Aegean obtained from P and S receiver functions. Dissertation, University of Berlin.

Sparkman O.D. (2000): Mass Spectrometry Desk Reference. Global View Pub.

Steiger R. H. & Jager E. (1977): Subcommission on geochronology: convention on the use of decay constants in geo- and cosmochronology.- Earth and Planetary Science Letters, 36: 359 - 362.

Taymaz T., Yilmaz Y. & Dilek Y. (2007): The geodynamics of the Aegean and Anatolia: introduction. Geological Society, London, Special Publications, 291:1–16.

Valley J.W., Bohlen S.R., Essene E.J. & Lamb W. (1990): Metamorphism in the Adirondacks.II.J Petrol 31:555 – 596.

Van der Maar P.A. & Jansen J.B.H. (1983): The geology of the polymetamorphic complex of Ios, Cyclades, Greece and its significance for the Cycladic Massif. – Geologische Rundschau 72: 283-299, Stuttgart.

Van Hinsbergen D.J.J., Langereis C. G. & Meulenkamp J. E. (2005): Revision of the timing, magnitude and distribution of Neogene rotations in the western Aegean region. Tectonophysics, 396, 1-34.

Veizer J. and Compston W. (1976): 87Sr/86Sr in Precambrian carbonates as an index of crustal evolution. Geochim. Cosmochim. Acta 40, 905-14.

Voit K. (2008): Structural Geology and Geomorphology of Northern Kea - A crustal scale viscous frictional Shear Zone (Western Cyclades, Greece). Master's thesis, University of Vienna.

Wiesmayr G. & Grasemann B. (2005): Sense and non-sense of shear in flanking structures with layer-parallel shortening: implications for fault-related folds. Journal of Structural Geology 27(2), 249-264.

Young E.D. (1993): On the $^{18}O/^{16}O$ record of reaction progress in open and closed metamorphic systems. Earth Planet Sci Lett 117:147–167.

Zamolyi A. (2006): Tectonic Geomorphology of Serifos (Cyclades, Greece). Diploma thesis. University of Vienna, Vienna.

8. APPENDIX

Geological map of S-Kythnos on a scale of 1:10,000.

Geological Map of S-Kythnos, M 1:10000

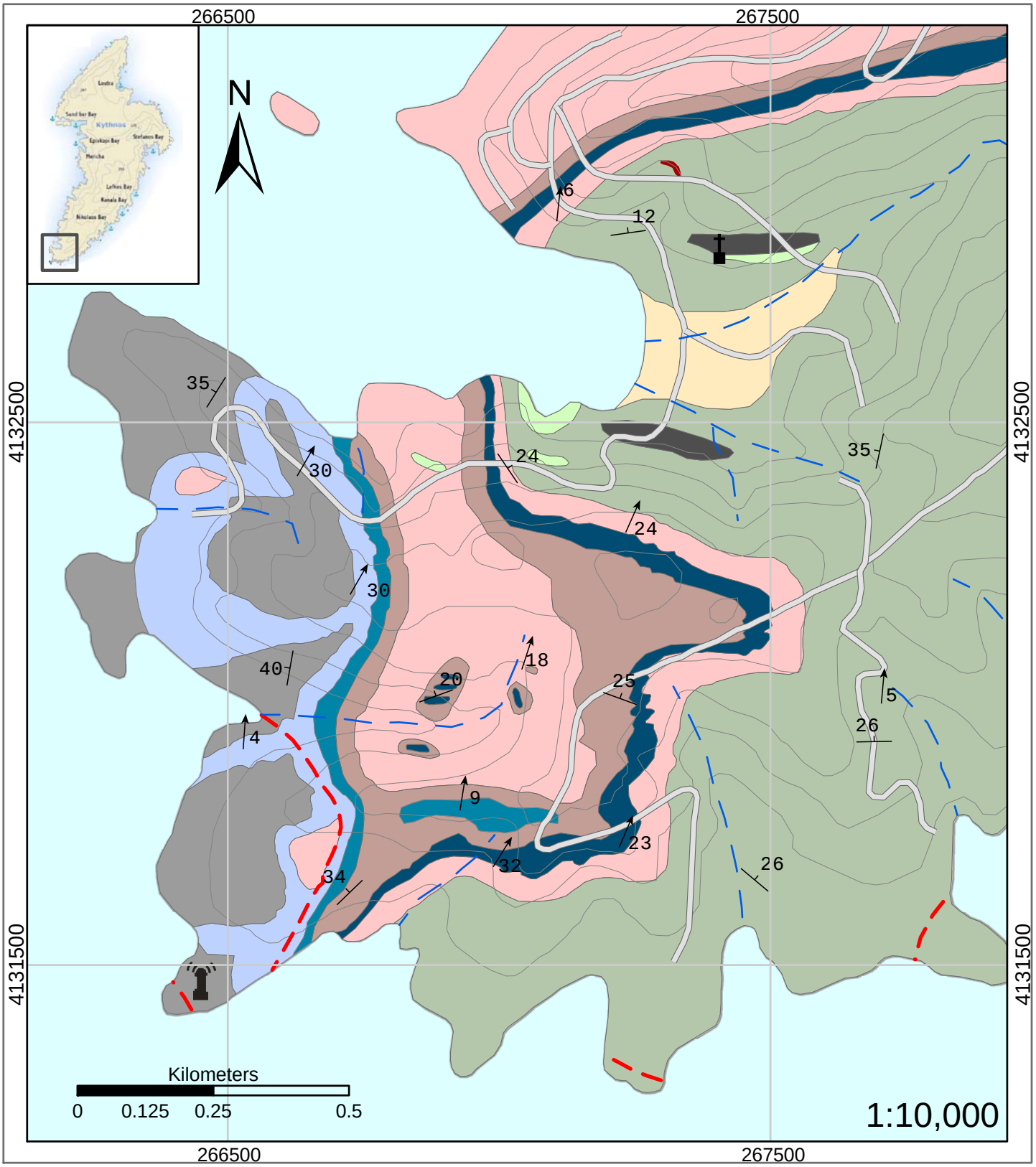

Legend

- Church
- Dip of Planes
- Lineation
- Lighthouse
- Water Channels
- Faults
- Roads
- Contour Lines 20 m
- Ab-Chl-Ser-schist
- Ab-gneiss
- Chl-Ser-Act-Ep-Ab-schist
- Marble impure
- Marble ultramylonitic
- Marble mylonitic
- Metabasite
- Tur-Mag-Ep-quartzite
- Quartzite
- Quaternary
- Srp-Tlc-schist

Author: Gariele Laner

Date: January 2009